

Massive Star Formation Rates and Radial Distributions from $H\alpha$ Imaging of 84 Virgo Cluster and Isolated Spiral Galaxies

Rebecca A. Koopmann

Union College

Department of Physics, Schenectady, NY 12308

`koopmanr@union.edu`

Jeffrey D. P. Kenney

Astronomy Department

Yale University, P.O. Box 208101, New Haven, CT 06520-8101

`kenney@astro.yale.edu`

ABSTRACT

The massive star formation properties of 55 Virgo Cluster and 29 isolated S0-Scd spiral galaxies are compared via analyses of R and $H\alpha$ surface photometry and integrated fluxes as functions of Hubble type and central R light concentration. The total massive star formation rates in Virgo Cluster spirals have been reduced by factors up to 2.5 in the median compared to isolated spirals. The inner disk star formation rates of most Virgo Cluster spirals are similar or enhanced by factors up to 2.5 in the median, while outer disk star formation rates are reduced by factors up to 7.1 in the median. Thus the reduction in total star formation of Virgo Cluster spirals is caused primarily by truncation of the star-forming disks. The star formation morphologies of Virgo Cluster spirals compared to isolated spirals can be divided into four categories: normal (27%), anemic (6%), enhanced (15%), and truncated (52%). Several galaxies with truncated star-forming disks have anemic inner disks, but the majority have normal-enhanced inner disks. Some of these galaxies have undisturbed stellar disks, and are likely the products of ICM-ISM stripping, but others have disturbed stellar disks, and are likely the products of recent tidal interactions or minor mergers, possibly in addition to ICM-ISM stripping. Several intermediate mass Virgo galaxies (M_B between -18.2 and -19) have global star formation rates higher than any isolated sample galaxy. Low-velocity tidal interactions and perhaps HI accretion seem to be the triggers for the enhanced rates of star formation in most of these galaxies. ICM-ISM interactions also appear to enhance the SFR of some Virgo galaxies, but only modestly and locally.

Subject headings: galaxies: spiral, galaxies: star formation, galaxies: clusters: general, galaxies: clusters: individual name: Virgo, galaxies: fundamental parameters, galaxies: peculiar, galaxies: structure

1. Introduction

What role does the environment play in the evolution of cluster galaxies? The observation that the morphological mix of galaxies varies in different nearby environments was qualitatively noted even in the early studies of the Virgo Cluster by Hubble and Humason (1931) and has been

confirmed in many studies (e.g., Oemler 1974; Dressler 1980; Postman & Geller 1984; Dressler et al. 1997). In addition, many studies of nearby galaxies have detailed how cluster galaxies differ from field galaxies within the same Hubble type, including redder colors (Kennicutt 1983a; Oemler 1992), less HI gas (Chamaraux, Balkowski, & Gérard 1980; Giovanelli & Haynes 1983), and

truncated outer HI gas disks (Giovanelli & Haynes 1983; Warmels 1988; Cayatte et al. 1990). Studies of higher redshift cluster galaxies show that evolution in cluster galaxy morphology and star formation properties has occurred over the last several billion years. Butcher & Oemler (1978) showed that distant clusters of galaxies have a higher proportion of blue galaxies. More recently, Dressler et al. (1997) found an excess of spirals and a lack of S0 galaxies in about the same proportion in dense clusters at redshifts of 0.5 compared to local dense clusters. These results suggest that many of the S0's in local clusters were actively star-forming spirals at $z=0.5$.

The rate of ongoing star formation is an important measure of the evolutionary state of a galaxy, and a sensitive indicator of some types of environmental interactions. The star formation rates of cluster galaxies have often been studied, with varying and sometimes opposite conclusions. Some authors have found reduced star formation rates in clusters (Kennicutt 1983a; Bica & Giovanelli 1987; Kodaira et al. 1990; Moss & Whittle 1993; Abraham et al. 1996; Balogh et al. 1998; Koopmann & Kenney 1998; Hashimoto et al. 1998), others similar rates (Kennicutt, Bothun, & Schommer 1984; Donas et al. 1990; Gavazzi, Boselli, & Kennicutt et al. 1991, Gavazzi et al. 1998), and others enhanced rates (Moss & Whittle 1993, 2000; Bennett & Moss 1998). This confused situation on cluster galaxy star formation rates is one of the motivations for the present work. In addition, many previous studies of star formation rates have been based on aperture or whole galaxy spectral observations. Spatial studies of star formation can probe the types of environmental interactions at work in nearby clusters, therefore revealing what may have influenced galaxies in richer clusters earlier in the history of the Universe.

The types of environmental processes which could influence the evolution of cluster galaxies have been extensively described in the literature. Processes which tend to affect the gas content of the galaxy, but not the existing stellar content, include (i) ICM-ISM interactions (Gunn & Gott 1972; Nulsen 1982; Valluri & Jog 1990; Schulz & Struck 2001; Vollmer et al. 2001) which selectively remove ISM gas from galaxies and might also compress the ISM and trigger star forma-

tion, (ii) gas accretion, which would presumably occur in the cluster outskirts, and (iii) starvation, or the stripping of gas from a galaxy's surroundings which might otherwise have accreted onto the galaxy (Larson, Tinsley, & Caldwell 1980; Balogh, Navarro, & Morris, et al. 2000). Tidal or gravitational effects (Toomre & Toomre 1972; review by Struck 1999), which affect both stars and gas, are also likely to be important, and include (i) low-velocity tidal interactions and mergers, which can occur both inside and outside of clusters, (ii) high-velocity tidal interactions and collisions, which occur almost exclusively in clusters, and (iii) tidal interactions between galaxies and the cluster as a whole, or sub-units within clusters (Byrd & Valtonen 1990). There have been a number of recent studies of environmental processes in nearby and distant cluster galaxies with authors reaching a variety of conclusions (see also a review by O'Connell 1999) concerning star formation histories and lenticular formation. Some of these studies find that the optical and spectral properties of the cluster members can be explained mainly by a decrease in star formation, caused presumably by ICM-ISM stripping (Abraham et al. 1996; Bravo-Alfaro et al. 2000, 2001; Jones, Smail, & Couch 2000; Couch et al 1998; Balogh et al. 1999). Other studies strongly suggest that a significant and strong bursting star formation history is required. The bursts would be caused mainly by tidal interactions with the cluster and/or other member galaxies (Moss & Whittle 2000; Caldwell, Rose, & Dendy 1996; Henriksen & Byrd 1996; van Dokkum et al. 1999; Rose et al. 2001). Some studies indicate that at least two processes, e.g., ICM-ISM stripping in addition to tidal interactions, may be required to explain the properties of different galaxies (Poggianti et al. 1999). The results of these studies indicate that the properties of cluster galaxies may be determined by a variety of environmental interactions over a Hubble time (e.g., Miller 1988; Oemler 1992; Moore, Lake, & Katz 1998) and may vary between clusters.

This work describes results from an imaging survey of Virgo Cluster and isolated spiral galaxies in both broadband R and the H α emission line. The intent of this study is to compare the amounts and distributions of massive star formation in Virgo Cluster galaxies to those of a relatively undisturbed isolated sample of galaxies.

Differences in the massive star formation characteristics between the two samples provide clues to the types of environmental effects which have influenced the gas content of cluster galaxies. We base our comparisons on the $H\alpha$ emission from galaxies, which is a good tracer of the massive star formation rate (Kennicutt 1983b) in relatively dust-free regions. It can be used to estimate the total star formation rate by making standard assumptions for the initial mass function. We use the $H\alpha$ surface brightness and the $H\alpha$ flux normalized by the R flux as distance-independent tracers of the massive star formation rate. The data we have gathered thus allow a quantitative radial comparison of massive star formation rates in the two environments. The Virgo Cluster is a particularly good laboratory to study environmental effects on star formation since it is the nearest moderately rich cluster, it has significant ICM, it is dynamically young with a current infall of spirals (Tully & Shaya 1984), and its galaxies are subject to a variety of environmental effects.

An important consideration in addressing these issues is the objective comparison of galaxies with different morphologies. van den Bergh (1976) made the very important observation, based on visual inspection of images on plates, that many cluster spiral galaxies have low rates of star formation relative to field spirals, and that the traditional Hubble classification did not work well in nearby clusters because the bulge-to-disk ratio was not well correlated with the disk star formation rate. Koopmann & Kenney (1998) confirmed and quantified this effect, using objective measurements from CCD images, showing that a one-dimensional classification scheme such as the Hubble classification is not applied in the same way to field and cluster galaxies, and that it is not adequate to describe the wider range in morphologies of cluster galaxies. For example, Koopmann & Kenney find that a significant fraction ($\sim 50\%$) of Virgo Cluster spirals classified as Sa are small-to-intermediate concentration (bulge-to-disk) galaxies with reduced global star formation rates, presumably due to environmental effects. This effect contributes to the excess of ‘early-type’ spiral galaxies in the Virgo Cluster and therefore to the local morphology-density relationship.

This paper presents the main results of a program which is published in separate papers. We

present the observational data for the Virgo galaxies in Koopmann et al. (2001) and that for the isolated galaxies in Koopmann & Kenney (2003, in prep). These papers include $H\alpha$ and R images for all galaxies, as well as radial profiles, and the derivation of the disk scalelengths. Koopmann & Kenney (1998) present comparisons of Hubble type and central R concentration for isolated and Virgo galaxies. The present paper gives a fuller discussion of the results presented in the short 1998 paper, and also concentrates on the massive star formation properties, with comparisons between integrated $H\alpha$ fluxes, $H\alpha$ radial profiles, and the relative concentrations of $H\alpha$ emission. Environmental effects are discussed in light of the differences between isolated and Virgo samples.

2. The Sample

The 55 Virgo S0-Scd galaxies have $B_T^0 < 13$ ($M_B < -18$ for an assumed distance of 16 Mpc) and inclinations less than 75° . The Sa-Scd sample is 95% complete for $M_B \leq -19$ and 76% complete for $M_B \leq -18$, which is about 2 magnitudes fainter than L^* .

The S0 galaxies observed are 13% of the population to $M_B \leq -18$. Since this study was not designed to focus on S0’s, the results for these galaxies will not be extensively discussed. There is a slight bias toward galaxies with higher IRAS fluxes in our sample, since a subset of these galaxies (75%) were obtained as part of a study of star formation rates and efficiencies in a larger sample of spiral galaxies (Young et al. 1996). Observational and reduction details are discussed in Koopmann et al. (2001).

Isolated galaxies were chosen from the Nearby Galaxies Catalog (Tully 1987) and Gourgoulhon, Chamaraux, & Fouqué (1992) to be as similar as possible to the Virgo Cluster sample galaxies in B luminosity, inclination, and distance, but are located in the least dense regions as defined by parameters from Tully (1987). The search criteria produced 140 Sa-Scd galaxies. Our 24 Sa-Scd galaxies comprise 18% of this sample to $M_B \leq -19$ and 17% for $M_B \leq -18$. S0 galaxies are observed to a higher completeness than in the Virgo Cluster: 46% to $M_B \leq -18$. Details of the selection of isolated galaxies are given in Koopmann & Kenney (2003, in prep.).

All R observations are calibrated to the standard Kron-Cousins R filter. Images were flux-calibrated using spectrophotometric standard stars (Massey et al. 1988). Extinction coefficients were obtained from Landolt standards or from standard extinction curves at KPNO and CTIO. Continuum-free $H\alpha$ images were derived by subtracting scaled R images from the line images. $H\alpha$ in this paper should be read as $H\alpha+[N II]$, since two [N II] lines ($\lambda\lambda$ 6584, 6548) are included in the filter and we make no correction.

3. Surface Photometry Methods

Surface photometry of the R and $H\alpha$ images of sample galaxies was performed using an IDL-based program (Koopmann et al. 2001). R and $H\alpha$ profiles were measured assuming a fixed center, inclination, and position angle, with inclination and position angle derived primarily from the outer R isophotes. Identical elliptical annuli were applied in the $H\alpha$ and R surface photometry for each galaxy. Isophotal radii, isophotal fluxes, and central light concentrations are calculated from the derived profiles within the IDL program. Exponential R disk scalelengths were measured from the profiles using the decomposition routines in the *fitting* programs in IRAF/STSDAS. Profiles and fitted parameters for individual galaxies are presented in Koopmann et al. (2001) and Koopmann & Kenney (2003, in prep).

For comparison between galaxies, all surface brightness profiles were corrected to face on assuming complete transparency in the disk, i.e., by applying the correction $2.5 \log(a/b)$ to the surface brightness, where a/b is the major-to-minor axis ratio and is approximately equal to $\cos^{-1}(\text{inclination angle})$. All future references to isophotal radii or fluxes integrated within an isophotal radius refer to quantities derived from the profiles corrected to face-on. The assumption of complete transparency is obviously incorrect, especially at inner radii, but since extinction values for other galaxies are poorly known, no corrections were attempted. If the extinction properties of Virgo Cluster and isolated galaxies are similar, there should be no systematic error due to inclination since the Virgo Cluster and isolated samples span similar inclination ranges. The most serious errors in $H\alpha$ integrated fluxes and radial profiles

will occur for highly inclined galaxies. For example, Young et al. (1996) find that the $H\alpha$ surface brightness significantly decreases in the mean with inclination for galaxies with inclinations greater than $\sim 70^\circ$. All galaxies discussed in this paper have an inclination of 75° or less, and we find that the measured quantities do not depend on inclination in this range.

3.1. Radial Normalization of Profiles

The outer isophotal radii at 24 R mag arcsec⁻² were measured in order to normalize the profiles of galaxies of different sizes and distances. Outer isophotal radii are direct tracers of the size/luminosity of high surface brightness galaxies and depend relatively little upon disk extinction, since the outer parts of galaxy disks are nearly transparent (Giovanelli et al. 1994, 1995). The radius at the 24 mag arcsec⁻² isophote in R was selected because the signal at this radius dominates the uncertainty in the sky background for most of the sample galaxies. (The uncertainty in the sky level includes uncertainties due to scattered light, background gradients, and, in some cases, the effects of small frame size.) The values of r_{24} in R are similar to r_{25} in B.

Disk scalelengths were also used to normalize radial profiles, and comparisons based on the disk scalelength rather than the isophotal radius produced no significant difference in the results. We chose to use the isophotal radius instead of the disk scalelength primarily because of the difficulty of fitting B and D models to sample galaxies, particularly in the Virgo Cluster, which has proportionately more galaxies with complex profiles. 23% (13/55) of Virgo Cluster galaxies have derived disk scalelengths which are uncertain by $> 20\%$, compared to 7% (2/29) of the isolated sample galaxies (Koopmann et al. 2001; Koopmann & Kenney 2003, in prep.). These numbers include 4 galaxies for which we were unable to derive disk scalelengths due to dominant bulge components (the Virgo galaxy NGC 4383 and the isolated NGC 3414) and/or complex profiles (the Virgo galaxy NGC 4586, which has a brighter outer disk component and the isolated NGC 2090, which has a lower surface brightness outer disk component). Of the remaining 11 Virgo galaxies with scalelengths more than 20% uncertain, eight have a higher surface brightness inner disk compared to

the fit to the outer disk (in 3 cases, this appears to be related to a star formation enhancement) and three have a higher surface brightness outer disk.

4. Galaxy Morphology

4.1. Hubble Types

In order to compare properties of the two samples, we initially binned galaxies as a function of Hubble type. Types were extracted from Binggeli, Sandage, and Tammann (1985), hereafter BST, who give classifications for Virgo members based on high resolution plates, the Revised Shapley-Ames Catalog of Bright Galaxies (Sandage & Tammann 1987, hereafter RSA), the Carnegie Atlas (Sandage & Bedke 1994, hereafter CA), and the Third Reference Catalog of Bright Galaxies (de Vaucouleurs et al. 1991, hereafter RC3).

An examination of the cataloged types indicates problems in the application of the Hubble system to Virgo Cluster galaxies. Three Virgo sample galaxies were classified by BST as Sc/Sa or Sc/S0. Several Virgo sample galaxies were classified as Sc by BST, but Sa or S0 by RC3. Two galaxies (NGC 4383, NGC 4694) are classified as amorphous by RSA/BST, but as Sa and S0 by the RC3. Figure 1 shows a comparison between the BST/RSA/CA and RC3 classifications, with the three Sc/Sa and Sc/S0 Virgo Cluster galaxies plotted as Sc on the RSA scale. There is good agreement between the two systems for isolated galaxies. Three galaxies, or 12% of isolated galaxies with cataloged RSA types, differ in classification by more than a half type. This is due in two cases to a disagreement between the Sc and Sd/Sm classes and in one case to a disagreement between the Sc and Sb classes. In the Virgo Cluster, 30% of Virgo galaxies vary in type by more than a half type. This is caused in part by the Sc/Sd disagreement, which affects Virgo Cluster Sc galaxies in the same proportion as isolated galaxies. However, the remaining discrepancy is caused by a disagreement between *early- and late-type* spiral classifications.

Figure 1 illustrates the problem of subjectivity in the application of a one-dimensional system to galaxy classification, particularly in the classification of galaxies which most obviously do not fit the system. However, it does not show cases of galaxies which have *consistent* classifications in the two catalogs, but which do not fit the Hubble system.

In particular, several of the galaxies consistently classified as Sa and Sab in the Virgo sample are not large B/D systems, as shown in Koopmann & Kenney (1998) and Sections 4.2 and 5).

4.2. R Profiles

The bias in Hubble types for cluster galaxies is also illustrated by a comparison of the radial R profiles of isolated and cluster galaxies.

Radial R profiles, binned according to Hubble type and environment, are shown in Figure 2 as a function of r_{24} and in Figure 3 as a function of disk scalelength. Median profiles were derived for each bin as a function of r_{24} and are overplotted as solid lines in Figure 2.

The extrapolated central surface brightnesses of the disks of the sample galaxies differ in surface brightness by a factor of 4-16 for different bins, with no statistically significant dependences on either Hubble type or environment. This is consistent with previous results (e.g., Bothun 1982, Kent 1985) for central disk surface brightnesses derived from model fits.

S0-Sc median R profiles are compared for each environment in Figure 4. Isolated median profiles have the expected increase in relative B/D from Sc to S0, unlike the Virgo Cluster sample, in which the median Sa profile has a smaller B/D than the median Sb profile! A direct comparison between Virgo and isolated median profiles for S0-Sc morphological types is given in Figure 5. First and third quartiles of the radial profile ranges are indicated in the graph with shading. Virgo Sa's are less centrally concentrated in the median than isolated Sa's. The S0 plot also suggests a smaller B/D for Virgo S0's compared to isolated S0's; however this comparison is based on only 3 Virgo S0 galaxies. The plot also shows that the Sc galaxies in the Virgo Cluster tend to have a higher surface brightness than those in the isolated sample.

The comparison between R radial light profiles indicates that Hubble classifications are not always an indicator of bulge-to-disk ratio when applied to the complexity of morphologies in a cluster environment. Similar conclusions were drawn by van den Bergh (1976), Bothun (1982), and Koopmann & Kenney (1998). Koopmann & Kenney (1998) find a number of galaxies which deviate from the Hubble scheme: these galaxies have

small-to-intermediate B/D, but are either classified as Sa due to reduced star formation or as Sa or peculiar due to active star formation within $0.3r_{24}$, but no star formation at larger radii. These galaxies are further discussed in section 6.3.

Figure 5 also shows that the Virgo Sc galaxies tend to have a higher surface brightness inner disk than the isolated galaxies. While Virgo and isolated Sc galaxies span the same range in surface brightness, there are proportionally more Virgo Sc’s with higher inner disk surface brightness, as can also be seen in Figure 3.

4.3. Central R Light Concentration

Given the biases in Hubble type for cluster galaxies, we also compare galaxies as a function of the objective central R light concentration parameter. The central R light concentration parameter is a quantitative indicator of bulge-to-disk ratio for galaxies of similar surface brightness. It is ideally independent of the star formation characteristics of a galaxy (unless the star formation characteristics have significantly contaminated a galaxy’s R radial profile; see below). The central light concentration used in this work is similar to the parameter used by Abraham et al. (1994):

$$C30 = \frac{F_R(0.3r_{24})}{F_R(r_{24})},$$

where $F_R(r_{24})$ is the total flux in R measured within the r_{24} isophote and $F_R(0.3r_{24})$ is the flux within the $0.3r_{24}$ isophote. The C30 values are computed directly from the surface photometry calculated using fixed center, inclination, and position angle. Therefore the measurement uncertainty is due mainly to uncertainties in the center, inclination, and position angle of the elliptical apertures. For most of the galaxies, these uncertainties are less than 5%, which causes a negligible error in C30 (Koopmann et al. 2001).

B/D is correlated to C30 in a non-linear fashion (see also Graham 2001). For our isolated sample, we find the following mean [C30, B/D] pairs: [0.3,0.1], [0.4,0.3], [0.5,0.8], [0.6,1.0]. These numbers are meant only to suggest a rough scale for C30 in terms of B/D, which may be a more familiar quantity to some readers. The scatter of these numbers is at least ± 0.1 , which is due mainly to the uncertainty in the determination of B/D (see

also Koopmann et al. 2001) and a smaller uncertainty due to the mild surface brightness dependence of C30 (Abraham et al. 1994).

While attractive and useful because of its objective nature, C30 can be influenced by any phenomenon which changes the shape of a galaxy’s R surface brightness profile. For example, rings or dust or bright star formation regions which dominate the light from old stars can affect its value. Half a magnitude of enhancement or extinction in the integrated R flux of the inner disk can result in an increase or decrease in C30 of 0.1. Similarly, half a magnitude of fading in the outer disk can increase C30 by 0.1. In addition, C30 has a mild dependence on surface brightness (see also Abraham et al. 1994), which causes higher surface brightness galaxies to have a higher C30. This is due to the use of the isophotal radius, which is not a perfect indicator of relative galaxy size when galaxies have different surface brightnesses. Since most of our bins span similar ranges in R surface brightness, these effects do not seriously influence most of the galaxies in our sample, and do not explain the presence of low bulge-to-disk ratio galaxies with early-type Hubble classifications. However, since the Virgo sample contains proportionally more high surface brightness galaxies classified Sc than the isolated sample (section 4.2), there may be a systematic effect causing some of these Sc galaxies to have higher C30. Several galaxies classified as Sc and with B/D less than 0.15 do have C30 values more similar to isolated Sb or even Sa, including NGC 2090 (isolated), NGC 4303 (Virgo), NGC 4651 (Virgo) and NGC 4567 (Virgo). All of these galaxies also have active star formation within $0.3r_{24}$, which may influence their C30 values.

In comparisons between galaxies with different C30 values, we bin into four C30 ranges. These ranges were chosen based on comparisons between Hubble type and C30 for the isolated sample, since C30 correlates well with Hubble type for the isolated galaxies (Koopmann & Kenney 1998) and field galaxies in general (e.g., Kent 1985). The C30 bins correspond roughly to isolated S0 ($0.61 \leq C30 \leq 0.72$), Sa ($0.51 \leq C30 \leq 0.60$), Sb ($0.38 \leq C30 \leq 0.50$), and Sc ($0.24 \leq C30 \leq 0.37$) galaxies. Note that the approximately even distribution in Hubble type and C30 for the isolated galaxies is due to the selection of galaxies, which was moti-

vated by the need to obtain adequate numbers for statistical comparison of S0-Sc galaxies, and not to trace the actual relative field populations, in which Sc galaxies far outnumber S0-Sa. In contrast, the Virgo sample galaxies are not evenly distributed in C30, but primarily fall toward lower concentrations. This is a combined effect due (i) to a more complete sample of Sc relative to Sa galaxies compared to the isolated sample, but also (ii) to the fact that several Virgo galaxies classified as Sa or mixed type have lower central concentration than isolated Sa galaxies.

5. Total Normalized H α Fluxes

Total H α fluxes were computed from cleaned, sky-subtracted H α images, by summing the total flux within an elliptical aperture including all HII regions. Uncertainties in integrated H α fluxes due to sky background noise, calibration errors, continuum subtraction errors are typically 20-30%. The dominant component of this uncertainty is the continuum subtraction error. Error bars given in this paper include a 3% typical uncertainty in the continuum subtraction factor, which corresponds to a much larger error in the calculated H α flux, especially for galaxies dominated by faint, diffuse emission. S0 galaxies have the most uncertain H α fluxes, since few contain obvious HII regions, and we therefore do not place much emphasis on the analysis of their H α properties, although we include them in the plots.

H α fluxes derived from 50 of the Virgo Cluster sample galaxies have been published in Young et al. (1996). As discussed in Koopmann et al. (2001), an adjustment was made to the Young et al. H α calibration for consistency with the Massey et al. (1988) spectrophotometric standard system used for the isolated galaxy observations. Therefore the H α fluxes are \sim 11-20% lower in our system, and are in good agreement with those measured by Kennicutt & Kent (1983).

To compare total H α fluxes between galaxies, we normalized by the flux in R contained within r_{24} to obtain the normalized massive star formation rate (hereafter NMSFR or $\frac{F_{H\alpha}}{F_{R24}}$). This quantity is a measure of the total H α luminosity per unit red luminosity and is analogous to an equivalent width. It correlates well with the H α equivalent widths measured by Kennicutt and Kent

(1983) for galaxies in common. This quantity is weakly anti-correlated with the total R magnitude within r_{24} (i.e., the total luminosity). Kennicutt et al. (1984) also find a weak trend for galaxies of lower luminosity to exhibit higher H α equivalent widths. There is no dependence on the inclination of the galaxy.

Figure 6 shows $\frac{F_{H\alpha}}{F_{R24}}$ plotted vs. C30. Symbols indicate the RSA Hubble types of the galaxies, with three Sc/Sa and Sc/S0 galaxies indicated by asterisks. The dotted lines provide the bounds of isolated star-forming galaxies. As a function of Hubble type or C30, galaxies in both samples show a large spread in total NMSFR's. Within a Hubble type, $\frac{F_{H\alpha}}{F_{R24}}$ ranges by a factor of 10, which is similar to measurements in previous surveys of galaxy star formation rates as a function of Hubble type (Kennicutt 1998 and references therein). Within concentration bins, however, the $\frac{F_{H\alpha}}{F_{R24}}$ of Virgo Cluster galaxies ranges by factors up to 20-40. While the distributions are non-Gaussian and span a large range, the larger spread in star formation rates in Virgo is mostly due to galaxies with reduced star formation, but is also partially due to *enhancements* in the NMSFR's by factors of up to 2 for several galaxies.

Figure 6 shows how reduced NMSFR's can cause misleading Hubble classifications, as discussed by Koopmann & Kenney (1998). Note in the figure how low-intermediate concentration Virgo galaxies with reduced star formation are systematically classified as Sa galaxies. Thus, the Hubble type of these galaxies is more representative of their reduced star formation than the stellar mass distribution.

Median total normalized H α fluxes with standard deviations for Virgo Cluster and isolated galaxies are listed in Table 1 as a function of type and central light concentration. In both samples, the typical NMSFR's decrease as a function of earlier Hubble type and of greater central concentration.

For the isolated galaxies, the median NMSFR's for spiral galaxies of different Hubble types and concentrations are similar within a factor of 4, consistent with other studies of globally averaged H α surface brightness for larger samples of field galaxies (Young et al. 1996). Thus many early-type/high concentration spirals have significant amounts of star formation (see also Hameed

& Devereux 1999). However, the tendency for these ($0.51 \leq C30 \leq 0.60$; approximately Sa) isolated galaxies to have lower NMSFR's compared to the lowest concentration galaxies is significant ($> 99\%$) when the binned samples are compared via Mann-Whitney tests.

In the median, Virgo galaxies have reduced star formation with respect to isolated galaxies as a function of either Hubble type or C30. The larger spread in the Virgo NMSFR's is evident in the larger standard deviations from the median, particularly in the C30-binned results. Table 1 also provides the factor by which Virgo normalized star formation is reduced in the median with respect to the isolated. The error associated with the scatter in normalized star formation rates is given in parentheses.

It can be seen in Table 1 that the reductions in the median NMSFR's in the sequence Sc to Sa are larger than in the low C30 to high C30 sequence. This is true for the isolated sample and partly true for the Virgo sample because several actively star-forming galaxies which are classified as Sb or Sc fall in the high C30 bin (As mentioned in Section 4.3, some of these galaxies may have higher C30 due to higher surface brightness disks or enhanced inner star formation.) In the Virgo sample, the difference between the Sc to Sa and the low C30 to high C30 sequences is also partly due to several low C30, weakly star-forming galaxies which are classified as Sa.

The trend for Sc galaxies within the 6° projected distance to M87 to have lower star formation rates compared to field galaxies, first noticed by Kennicutt (1983a), is apparent in our sample. Compared to the isolated Sc galaxies, the 20 Virgo Sc galaxies within 6° of M87 have NMSFR's reduced by a factor of 1.5 in the median with respect to isolated galaxies.

6. Radial $H\alpha$ Distributions

In the previous section, we found that Virgo Cluster galaxies typically have less total star formation than isolated counterparts, but that there is a large range in total star formation rates among cluster galaxies, which includes both reductions and enhancements. In this section, we investigate where in the disks the star formation has been enhanced or reduced. In particular, we seek to deter-

mine whether those galaxies with reduced global star formation have truncated star-forming disks or whether the star formation has been depressed across the disk.

Figure 7 shows all $H\alpha$ profiles normalized by r_{24} as a function of Hubble type and environment. All profiles extend to the radius of the last visible HII region. Figure 8 shows all $H\alpha$ profiles plotted as a function of C30 and environment. The concentration bins are the same as in section 4.1, roughly tracing Hubble type for the isolated galaxies. Errors in individual profiles are discussed in Koopmann et al. (2001); in general, the largest error bars occur where star formation is the weakest.

Median $H\alpha$ profiles for each Hubble type and C30 bin were derived by calculating the median of the surface brightness at numerous radii across the disk for galaxies within a given C30 or Hubble type bin. Outside of the radius of the outermost HII region, the surface brightness was assumed to drop to 0 and was counted in subsequent radial bins as 0. Hence, the median profiles include the effect of truncated $H\alpha$ surface brightness profiles. The median profiles are overplotted as solid lines in each bin in Figures 7 and 8.

Figures 7 and 8 show that the $H\alpha$ surface brightnesses of different galaxies in each Hubble class or concentration bin span a factor 10 to 100 range at different radii in the disk. This range is in contrast to the R surface brightness, which spans a factor 4 to 16 range at any given radius (Section 4.1) and to global star formation rates which vary by about a factor of 10 within a given Hubble type (see Section 5; Kennicutt 1998). The much larger range in $H\alpha$ surface brightness is probably associated with variations in the surface density and critical density of gas as a function of radius in galaxies (Kennicutt 1989). The $H\alpha$ surface brightness distribution within an individual galaxy can vary due to bars, rings, spiral arms, circumnuclear regions, and the truncation of the star-forming disk.

6.1. Massive Star Formation Rates in the Inner and Outer Disks: Radial Profiles

The relative ranges in $H\alpha$ surface brightnesses across the disk for isolated and Virgo galaxies are

directly compared in Figures 9 and 10, which show the $H\alpha$ profiles overplotted as a function of Hubble type and C30, respectively. Isolated galaxies are plotted with solid lines, while Virgo Cluster galaxies are plotted with dotted lines.

It is evident in these figures that many Virgo Cluster galaxies have truncated $H\alpha$ disks compared to isolated counterparts. The smaller $H\alpha$ disks of Virgo Cluster galaxies are plainly seen as the emergence of dotted lines, many steeply declining, below the solid lines beyond about $0.4r_{24}$ in the plots. Truncated profiles are seen in all Hubble type and C30 bins. 46% (24/52) of Virgo Cluster spirals have $H\alpha$ disks truncated within $0.9r_{24}$, compared to 17% (4/24) of isolated spirals.

Within the truncation radii, the Virgo Cluster galaxies have star formation rates which are typically similar or enhanced compared to isolated counterparts. Few Virgo Cluster galaxies have star formation which is reduced across the disk below isolated rates. These few exceptions can be seen in the 0.24-0.37 and 0.51-0.60 C30 bins in Figure 10 as the dotted profiles which lie below the solid lines over large parts of the disk.

There is a significant population of galaxies, however, for which star formation has been enhanced above isolated values, particularly within the inner half of the optical disk. This is particularly noticeable in Figure 9 for Virgo Cluster galaxies classified as Sc. These galaxies are spread over a number of C30 bins in Figure 10.

To compare profiles in the two samples in a more statistical way, median profiles were derived for each bin (Section 6). Median radial profiles of different Hubble types and C30 are shown for each environment in Figure 11. In Figure 12, the median profiles for Virgo and isolated galaxies are overplotted for each Hubble type or C30 bin.

Figure 11 shows that despite the range of 1-2 orders of magnitude in $H\alpha$ surface brightnesses, at a given radius, the medians of isolated spirals as a function of Hubble type and C30 agree to within a factor of 3-4 over most of the disk. The agreement of median radial profiles within a factor of 4 is similar to the agreement between the total median $H\alpha$ fluxes (Section 5, Young et al. 1996) and emphasizes that even early-type/high C30 isolated galaxies typically have substantial amounts of ongoing massive star formation across the disk (see

also Hameed & Devereux 1999). Figures 11 and 12 show that in the Virgo Cluster, a similar trend is seen for the median $H\alpha$ surface brightnesses of Sb and Sc, which are within a factor of 3 of each other and of the isolated median profiles, except in the outer parts of the disk.

The smaller $H\alpha$ disks of Virgo Cluster spirals compared to isolated spirals can be seen in the median profiles, which are truncated for Virgo Cluster galaxies in all bins in Figure 12. The inner star formation rates tend to be similar or enhanced compared to the isolated. Note again that the inner disks of Virgo spirals show a tendency to enhancement compared to the isolated.

Quantitative differences between medians in different radial bins will be given based on integrated fluxes in the next section.

6.2. Massive Star Formation Rates in the Inner and Outer Disks: Integrated Fluxes

The radial dependence of massive NMSFR's can also be studied by deriving integrated $H\alpha$ fluxes normalized by R over several radial bins. Figure 13 shows the integrated NMSFR's per unit R luminosity as a function of environment and C30 over the whole disk (a,b) and the inner 30% of r_{24} (c,d), and the outer 70% of r_{24} (e,f). Figure 14 shows the integrated rates for five smaller radial bins: within $0.1r_{24}$, $0.1r_{24} < r < 0.3r_{24}$, $0.3r_{24} < r < 0.5r_{24}$, $0.5r_{24} < r < 0.7r_{24}$, and $< 0.7r_{24} < r < 1.0r_{24}$. In both figures, the dotted lines indicate the approximate bounds of isolated Sa-Sc galaxies for each bin.

Median NMSFR's were calculated for each radial bin and are presented in Tables 1 and 2. Table 1 gives the median, standard deviations (based on the median), and the isolated-to-Virgo ratio for the $r < 0.3 r_{24}$ and $0.3r_{24} < r < 1.0r_{24}$ outer bins. A comparison of the standard deviations shows that the inner Virgo NMSFR's have similar or enhanced values compared to the isolated sample. In the outer disk, however, the Virgo NMSFR's are reduced by factors of 1.6 - 7.1 for galaxies of similar C30 or Hubble type. Note especially the values of 2.8 - 7.1 for early Hubble type or high C30. The difference between the Sa and the $0.51 \leq C30 \leq 0.60$ bins is due to (i) the shifting of several galaxies classified as Sa to lower C30 bins and

(ii) the presence of a few galaxies classified as Sc with active star formation and higher C30.

Table 2 gives the median isolated-to-Virgo ratios and standard deviation (based on the median) for the five smaller bins shown in Figure 14. Where necessary in the outer two bins, the values are given as upper limits, based on the level of the background sky error. From the table and the figure, the integrated NMSFR's of Virgo Cluster spirals are progressively lower in progressively outer radial bins. Significant reductions appear first for Sa and high C30 in the 0.3-0.5 r_{24} radial bin, and increase to factors greater than 5 in the outermost bin. Reduction becomes significant for Sb and smaller C30 galaxies in the 0.5-0.7 r_{24} bin. In the outermost bin, all ratios are > 2.8 .

The results for the outer disk are in contrast to the inner disk. Within $0.3r_{24}$, 94% of Virgo Cluster spirals have NMSFR's similar to or enhanced compared to isolated galaxies of similar type or C30 (Figure 13). In Table 2, the two inner bins show isolated-to-Virgo ratios which are less than or about 1 within the scatter for all type and C30 bins. Note in particular the 0.38-0.50 C30 inner bins, where star formation in Virgo galaxies is enhanced by a factor of 1.7 - 2.

Thus many galaxies which have reduced global and outer disk star formation have normal or enhanced inner disk star formation rates. These results show that the primary mechanism of reduction in star formation for intermediate-low C30 galaxies is the truncation of the outer disk rather than significant reductions across the disk.

6.3. H α Concentration

The tendency for Virgo Cluster galaxies to have truncated star-forming disks and/or enhanced inner star formation rates means that the concentrations of H α light for these galaxies will be systematically different than those of isolated galaxies. We define a quantitative measure of the H α concentration as the ratio of the flux in H α within $0.3r_{24}$ to the total H α flux. The value will be higher for galaxies with truncated star forming disks and/or enhanced inner star formation rates. In contrast, we would not expect to find a high value for a galaxy with anemic star formation, in which the H α is distributed at low surface brightness over much of the disk.

The H α concentration is plotted as a function of the R light central concentration in Figure 15. The dashed lines indicate the boundaries for galaxies which contain three-quarters, half, and one-quarter of their H α emission within $0.3r_{24}$. Examination of the plot shows Isolated galaxies typically have much of their star formation outside $0.3r_{24}$, while Virgo galaxies more typically have most of their star formation within $0.3r_{24}$. For example, only 4% of isolated spirals compared to 25% of Virgo Cluster spirals have at least three-quarters of their H α emission within $0.3r_{24}$. This effect is largely due to the truncated star forming disks in Virgo Cluster galaxies. This is NOT due to a morphological effect, since the isolated sample contains proportionately *more* Sa than Virgo.

The H α concentration does not reveal the relative level of star formation of a galaxy. In Figure 15, for example, S0 galaxies with reduced star formation have high H α concentration values and therefore fall in similar locations as galaxies with active inner star formation and truncated disks. By plotting the H α concentration versus the level of inner normalized H α flux, as in Figure 16, it is apparent that a large proportion of Virgo Cluster galaxies have inner star formation rates similar to those of isolated Sb-Sc galaxies, but have much higher H α concentration. Thus the Virgo galaxies tend to have inner disks with normal to enhanced star formation combined with truncated outer disks.

7. Star formation morphologies in the Virgo Cluster

The radial profiles, integrated fluxes, visual inspection of the H α images, and the H α concentration plots can be used to group Virgo Cluster galaxies into several star formation morphology classes:

- (A) **Normal:** *galaxies with star formation rates which are similar to isolated counterparts in all parts of the disk within r_{24}* (14 galaxies, 27% of Virgo Cluster sample).
- (B) **Anemic:** *galaxies with total, inner, and outer rates reduced below that of isolated galaxies* (3, 6%).
- (C) **Enhanced:** *galaxies with enhanced inner and global star formation rates and normal outer rates* (8, 15%).

(D) **Truncated:** *galaxies with smaller star-forming disks than isolated counterparts.* (27, 52%). The severity of the truncation in the star-forming disk and the level of star formation within the truncation radius varies for these galaxies. We therefore subdivide galaxies with truncated star-forming disks into several subcategories:

(D1) **Truncated/Normal:** galaxies with truncated star-forming disks and normal or enhanced star formation interior to the truncation radius (18).

(D2) **Truncated/Anemic:** galaxies with truncated star-forming disks and anemic star formation interior to the truncation radius (5).

(D3) **Truncated/Compact:** galaxies with only circumnuclear non-axisymmetric HII complexes (4). For 2 of these galaxies, the integrated normalized circumnuclear H α fluxes of these complexes are similar, though on the low end, to those of isolated galaxies. The other two have circumnuclear (within $0.1r_{24}$) NMSFR enhanced over those of isolated spirals.

These groups were initially defined by inspection of Figures 13 and 14. Figure 17 shows the location of each type of galaxy in the inner CH α -NMSFR plot. While there is some overlap, the types are well-separated, suggesting that this type of approach may be useful in identifying trends in star formation morphologies in large samples of galaxies.

Figure 18 shows the radial profiles of sample galaxies, grouped according to the star formation category, along with the median profile derived for each class. Figures 19 and 20 provide comparisons between the median of normal Virgo spirals and the other categories. Figure 20 also provides a comparison between isolated low-C30 spirals. The normal Virgo spiral median is given as a solid line, with vertical lines denoting the range of the 1st and 3rd quartile, while the comparison class is given as a dashed line and shading to indicate the 1st and 3rd quartile ranges. The normal Virgo spiral median is significantly different from the other classes, except the low-C30 isolated spirals (although there is a clear tendency toward truncation at radii beyond r_{24} for the Virgo normal spirals).

The 'St' or 'severely truncated' galaxies identified in Koopmann & Kenney (1998) are galaxies with star formation contained only within $0.3-$

$0.4r_{24}$, but with rates within this region similar to those of isolated Sc galaxies. In Figure 16, these galaxies are located at $\log(\text{inner NMSFR's})$ greater than -2.5 , and CH α greater than 0.75 . The star formation morphologies of these galaxies are however heterogeneous, so that they fall in either the truncated/normal category or the truncated/compact category.

No normal Virgo spiral is found within a distance of 3 degrees from M87. Other types of morphologies are found at all radii from M87.

There is little correlation with star formation type and C30, as shown in Figure 21. The galaxies in each category show a range in C30. Anemic galaxies show the least range, with all three anemic galaxies at higher C30 of $0.42 - 0.52$. Three out of five of the truncated/anemic galaxies also have higher C30 values of about 0.5 , but the other two have low C30. Enhanced galaxies tend to be lower in C30. While higher C30 Virgo galaxies tend to have higher CH α , they have a variety of star formation morphologies. The fact that the star formation morphology is largely independent of C30 is in contrast to the result for Hubble types, where the Virgo Sa and mixed types are all either truncated/compact, truncated/anemic, or anemic (see Figure 16).

Each of the star formation categories is discussed in the following sections. Given the large sample, we briefly discuss selected galaxies which may have undergone recent environmental effects or are otherwise especially interesting. It is important to note that while we have grouped galaxies together due to similarities in their integrated inner and outer NMSFR's, not all galaxies within each group necessarily have experienced the same type of interactions. For example, among the galaxies with strongly truncated H α disks, there are galaxies with features consistent with ICM-ISM stripping, and others with features suggestive of galaxy interactions, perhaps in addition to ICM-ISM stripping.

Following the discussion of the star formation categories, we discuss two other interesting subsets of galaxies: galaxies with star formation enhanced locally near the truncation radius and several apparent pairs in the Virgo Cluster.

7.1. Virgo Spirals with Normal Star Formation Rates Within r_{24}

27% (14) of Virgo Cluster sample spirals have star formation rates similar to those of isolated spirals within r_{24} . The galaxies can be identified as those which do not have outer disks truncated within r_{24} and/or enhanced inner disks in Figure 14. These galaxies range in concentration, and are classified as Sb (3) and Sc (11) galaxies. A number of these galaxies do have smaller star-forming disks than isolated spirals, as can be seen in Figures 7 - 10, with truncation radii outside of r_{24} . (Because not all the profiles extend significantly beyond r_{24} , we chose to define our classes only within r_{24} .)

Apparently these galaxies have not experienced a strong and/or recent environmental interaction. Some may be recent arrivals in the cluster. Although these galaxies do not show significant differences in star formation rates from the isolated spirals, some do display peculiarities. For example, NGC 4654 has a peculiar $H\alpha$ distribution and an HI tail and may be experiencing an ICM-ISM encounter (Phookun & Mundy 1995). NGC 4651 appears as a relatively normal Sc within r_{24} , but deep optical images reveal a peculiar linear feature and several shell-like features at large radii (Schneider & Corbelli 1993; Malin 1994). These features are probably caused by a minor merger. Some of these galaxies also show asymmetric outer arcs of star formation, possibly indicating ICM pressure (Section 7.5).

7.2. Virgo Anemic Spirals

Anemic galaxies were first defined based on the arm-interarm contrast in the disk, which is related to star formation activity. We define 'anemia' to mean low $H\alpha$ surface brightness *across the disk*. To fall in this class, a galaxy must show measurable star formation across most of the disk but with a lower intensity than *typical* isolated spirals. Note that, historically, the term 'anemia' has sometimes been used to refer to any galaxy with a reduced global star formation rate. The spatial resolution of our study allows us to use a more specific definition.

Anemic galaxies should not be confused with low surface brightness galaxies. Anemic galaxies have low $H\alpha$ surface brightness with respect to the

continuum, while low surface brightness galaxies have low $H\alpha$ and low continuum surface brightnesses. Because we normalize the $H\alpha$ emission by the R continuum brightness, the NMSFR's of low surface brightness galaxies fall in regions of our plots similar those of high surface brightness galaxies.

Anemic galaxies tend to fall in the lower left-hand corner of the $H\alpha$ concentration plot, with low inner star formation rates and normal to low $H\alpha$ concentration. The boundary for anemic galaxies is difficult to quantify, especially since some isolated galaxies also fall in this region. We take as a rough boundary $H\alpha$ concentration ≤ 0.4 and NMSFR within the inner 30% of the disk ≤ -2.3 . This category includes only 3 Virgo galaxies: NGC 4394, NGC 4548, and NGC 4698. In addition, the spirals NGC 4293, NGC 4380, NGC 4450, NGC 4419, and NGC 4772 are anemic galaxies which also have truncated outer disks (see Section 7.4.2). NGC 4192 falls close to the boundaries for anemic galaxies, but it has a high inclination and is more properly classified as a normal galaxy.

The paucity of anemic galaxies shows that global anemia alone does not play a dominant role in reduction of total star formation rates among the Virgo spirals. While the star formation of some Virgo galaxies may indeed appear weak across the disk, isolated galaxies can have equally weak disk star formation (as also pointed out for a sample of nearby galaxies by Bothun & Sullivan 1980). The isolated spirals IC 356, IC 5240, NGC 7098, NGC 2196, and NGC 3673 fall in the anemic region of the plot.

It is illustrative of the past approach of anemic classification to compare the classifications of van den Bergh (1976) and van den Bergh, Pierce, & Tully (1990). They classify NGC 4548 as anemic, but NGC 4394 as a normal spiral. They list a number of other galaxies in our sample as anemic, including (i) NGC 4457, 4424, 4569, and 4580, which we find to be severely truncated, (ii) NGC 4293 and NGC 4450 which are truncated/anemic (iii) NGC 4522, 4579, and 4689, which are mildly truncated, (iv) NGC 4651, which is normal, and (v) NGC 4643, 4710, and 4429, which do not have detectable HII regions. We reemphasize that the term anemic, as used in the past, has been applied to a variety of star formation morphologies.

7.3. Virgo galaxies with enhanced inner and total star formation rates

15% of Virgo Cluster galaxies have global and inner star formation rates significantly higher than those in the isolated sample. Most of these galaxies are intermediate mass galaxies with M_B between -19 and -18.2, and most are found projected near the M49 area, the Southern Extension, or the cluster outskirts.

The 3 Virgo sample galaxies with the highest normalized massive star formation rates are NGC 4299, NGC 4383, and NGC 4532. NGC 4299 and NGC 4532 have global rates 2.5 - 3 times higher the median star formation rates and 2 - 2.5 times higher than the upper envelope of isolated galaxies of similar Hubble type or central concentration in the isolated sample. It is harder to quantify the enhancement in the global star formation rate of NGC 4383, which is a high C30 galaxy classified as amorphous, because most of the isolated galaxies of similar concentration are S0 galaxies without significant HII regions. Its global star formation rate is enhanced by a factor of 5 compared to isolated galaxies in the 0.51-0.60 bin. Each of these galaxies is described in more detail in the following paragraphs.

NGC 4299 has a very small bulge. The $H\alpha$ image shows numerous bright HII regions throughout the disk. The outer extent of the $H\alpha$ distribution is irregular, except in the southwest, where it forms a well-defined ridge extending over 90 degrees, perhaps suggesting ongoing ICM pressure. The most luminous HII complex in the galaxy is located at the southern end of this ridge. NGC 4299 is in an apparent pair with NGC 4294, which is projected $5.8'$ (27 kpc) away, and has a similar line-of-sight velocity (232 km s⁻¹ and 355 kms⁻¹). NGC 4294 is similar to NGC 4299 in mass, luminosity, and morphology, and also has a normal HI content (HI def = -0.08 and 0.05). Its global star formation rate is a bit lower than NGC 4299, but a bit higher than the isolated galaxies, and the star formation rate within $0.3r_{24}$ is much higher than the isolated galaxies. Unlike NGC 4299, there is no clear ridge of HII regions at the outer edge of the $H\alpha$ disk. The high rates of star formation in these galaxies might be due a tidal interaction, perhaps enhanced in NGC 4299 due to an ongoing ICM-ISM interaction. The lo-

cation of this pair, only 2.4° from M87, makes an ICM-ISM interaction plausible.

NGC 4532 is an Sm/Im galaxy located 6° south of M87, in between the M49 group and the Southern Extension. The $H\alpha$ image shows vigorous star formation throughout this irregular galaxy, and there is no indication in the $H\alpha$ morphology of ICM pressure. The galaxy is HI-rich (HI def=-0.30), and both NGC 4532 and the nearby DDO137 are associated with a large extended, bilobal, HI cloud (Hoffman et al. 1993). Much of the HI is concentrated around the 2 optical galaxies, but about one-third seems kinematically and spatially distinct from the individual galaxies (Hoffman et al. 1999). The starburst in NGC 4532 might therefore be caused by a combination of tidal forces and gas accretion.

NGC 4383 is an HI rich (HI def = -0.39) galaxy with a large bulge-to-disk ratio, located 4.3° from M87. It is classified as amorphous by Sandage, presumably because any disk component is weak, and there is starburst activity and irregular dust lanes. The $H\alpha$ image shows a biconical filamentary structure strongly suggestive of a starburst outflow, numerous HII regions in the central 2 kpc, and an irregular string of bright HII regions extending into the outer galaxy. The dS0 galaxy UGC 7504 (VCC 794), 3.3 magnitudes fainter than NGC 4383, is very nearby in projection ($2.5'=12$ kpc), with a line-of-sight velocity difference of 800 km s⁻¹. UGC 7504 shows no $H\alpha$ emission, although its wavelength shift was within the filter transmission curve for the image. There is no evidence of an ICM-ISM interaction, and it is likely that a tidal interaction and/or gas accretion is responsible for the starburst in NGC 4383.

There are an additional 4 Virgo galaxies with normalized massive star formation rates 20-50% higher than any of those observed in the isolated sample.

NGC 4713 is an Sc galaxy in the Southern Extension of Virgo, with flocculent spiral structure. Luminous HII complexes occur throughout the disk. Although NGC 4713 is relatively isolated within Virgo, its nearest bright neighbor, NGC 4808, projected 1.8° (500 kpc) away, has a similar line-of-sight velocity (653 km s⁻¹ and 766 kms⁻¹). NGC 4808 is similar to NGC 4713 in mass, luminosity, and morphology. Whereas NGC 4713 has a normal HI content (HI def = -

0.13), NGC 4808 is HI rich (HI def = -0.68), with 5 times the "normal" amount of HI. VLA HI mapping of NGC 4808 reveals a highly warped, disturbed, extended HI distribution (Kenney et al., in prep.). Its global star formation rate is a bit lower than NGC 4713, and comparable to the isolated galaxies with the highest SFRs. The HI properties of NGC 4808 suggest that HI accretion, either directly or through the associated tidal effects, may be responsible for its enhanced SFR. There is little direct evidence for what caused the enhanced SFR of NGC 4713, but the similarities with its distant neighbor NGC 4808 might suggest a common explanation.

NGC 4561 is a Sc or Sdm galaxy with bright HII regions located along a bar and spiral arms. It is in the northern outskirts of the Virgo cluster. The galaxy is HI-rich (HI def = -0.33), with 2 peculiar, extended, symmetric HI arms beginning at the optical edge of the galaxy (Kenney et al., in prep.). There is no bright galaxy near NGC 4561, and we postulate that the enhanced SFR in this galaxy may be due to HI accretion or a tidal interaction with a low surface brightness object.

NGC 4303 (M61), a classic Sc spiral observed at a low inclination angle, is the largest galaxy among the Virgo systems with enhanced SFRs. Most of its bright HII regions are located in the 30-90'' annular zone beyond the end of the bar. There is no obvious cause for the galaxy's modestly enhanced SFR, except for the possibility of a tidal interaction with the nearby spiral NGC 4301 = NGC 4303A, which is 3 magnitudes fainter and projected 9.5'=44 kpc away, with a line-of-sight velocity difference of only 300 km s⁻¹.

NGC 4519 is a Sc galaxy, whose H α distribution shows strong emission along a bar and along a double spiral arm beginning near the western end of the bar. This morphology resembles the "ocular" morphology described by Elmegreen et al. (1991), which can be produced by tidal interactions. A plausible explanation for the ocular morphology and enhanced SFR in NGC 4519 is a tidal interaction with the nearby small galaxy NGC 4519A, which is 2.7 magnitudes fainter and projected only 2.4'=11 kpc away, with a line-of-sight velocity difference of 200 km s⁻¹. (We detected no H α emission from NGC 4519A.)

All those galaxies with enhanced NMSFR's are HI normal to HI rich. All except NGC 4303 are

lower luminosity, with $18.2 > M_B > -19$. Most have apparent nearby companions, which suggests that low-velocity tidal interactions may play a role in the enhancement in SFR. Some of them are not only HI rich, but are associated with large, extended clouds of HI, suggesting that HI accretion, perhaps combined with tidal forces, may play a role in the enhancement in SFR. NGC 4299 has an H α morphology suggestive of an ongoing ICM-ISM interaction, so perhaps ICM pressure combined with tidal effects is responsible for its starburst.

There is evidence that ICM-ISM interactions enhance the SFR of some Virgo galaxies, but the enhancements appear to be local and globally modest. NGC 4522, which exhibits strong evidence of an ongoing ICM-ISM interaction (Kenney & Koopmann 1999; Kenney et al. 2002), has a modestly enhanced inner disk SFR, possibly attributable to the ICM-ISM interaction. As discussed in Section 7.5, there are a number of other Virgo galaxies whose H α morphologies are suggestive of locally enhanced SFR due to ICM pressure. However these local enhancements do not cause the star formation rates to be enhanced either globally or in any of the radial bins shown in Figure 14.

7.4. Virgo Spirals with Truncated Star-Forming Disks

52% or 27 spirals in this Virgo Cluster sample show truncation in the star-forming disk within r_{24} . This type of star-formation morphology is therefore by far the most common in the Virgo Cluster. The severity of truncation in the star-forming disk varies for the galaxies in this sample, from relatively mild truncation in the outer half of the disk (17), to relatively severe truncation at radii less than 0.3-0.4 r_{24} (11). The star formation morphology within the truncation radius also varies, from normal-enhanced (18) to anemic (5) to compact (4).

The group of 11 severely truncated galaxies were referred to as 'St' by Koopmann & Kenney (1998). In this paper, we give these galaxies a more detailed designation according to their star formation morphology, which is either truncated/normal or truncated/compact. The properties of these galaxies and their star formation morphology classes are listed in Table 3.

The following three sections discuss each type of truncation and several examples.

7.4.1. *Truncated Spirals with Normal Inner Disks*

The largest subclass of truncated galaxies are those which have normal or enhanced inner star formation rates compared to isolated spirals. We discuss galaxies with the most severe truncation in the most detail, then summarize galaxies with less truncated star-forming disks.

Six galaxies, NGC 4405, NGC 4580, IC3392, NGC 4457, NGC 4351, and NGC 4569 have normal-to-enhanced star formation within $0.3-0.4r_{24}$, but have no star formation outside this radius.

NGC 4580, NGC 4405, and IC 3392 are the three galaxies with 'mixed' Hubble-type classifications of Sc/Sa and Sc/S0. R and H α images and radial profiles of these galaxies are shown in Figure 24. The R images show regular stellar isophotes for all three galaxies. The stellar disks beyond the edge of the star-forming disk are mostly featureless, except for NGC 4580, which shows 2-3 spiral arms. The H α morphologies of NGC 4580 and IC 3392 are dominated by symmetric rings of star formation near the truncation radius. These rings contain a large fraction of the H α emission. NGC 4405 shows a knottier and asymmetric HII region distribution, with an arc or partial ring to the southwest. H α major axis spectra of all three galaxies show a regular, rising rotation curve for the ionized gas (Rubin, Waterman, & Kenney 1999; Koopmann, Kenney, & Rubin, in prep.). The truncated H α distribution, combined with the regular stellar isophotes and regular gas kinematics, strongly suggest that these galaxies are victims of ICM-ISM stripping. The ring morphology of the gas may be consistent with this scenario. Gas rings at the outer edges of truncated gas disks are seen in the simulations of ICM-ISM interactions by Schulz & Struck (2001). Their Figure 2 shows simulated gas distributions strikingly similar to the H α morphology of these galaxies. NGC 4405 at 4 degrees and IC 3392 at 2.7 degrees from M87 have heliocentric velocities of 1747 and 1680 km/s, which are consistent with orbits with large radial components. NGC 4580 is located 7.2 degrees from M87, with a heliocentric velocity of 1034 km/s, so that its orbit could be

highly radial, with a significant component parallel to the plane of the sky.

NGC 4351, shown in Figure 25, is strongly asymmetric in H α . In R, it has a nucleus offset by about 10" (0.8 kpc) from the center as judged from the outer isophotes. The H α emission has a patchy distribution, with a higher surface brightness in the circumnuclear regions. Most originates from the eastern side of the nucleus. The HI emission is highly asymmetric in the same direction as the H α emission (Warmels 1988). The ionized gas has regular kinematics (Rubin et al. 1999). NGC 4351 is one of the galaxies closest to the cluster center, with an angular separation of 1.7° from M87, and it has a line-of-sight velocity of 2310 km s $^{-1}$. The location of the galaxy and the combination of more regular R isophotes and asymmetric H α and HI emission make this galaxy a good candidate for a recent or possibly ongoing ICM-ISM interaction.

NGC 4457 is located in the Southern Extension region in the Virgo Cluster. Its R morphology is regular and the nearly circular outer ring suggests we are viewing the galaxy close to face-on. Figure 25 provides the R and H α images and radial profile. The galaxy has a relatively strong but truncated H α disk with much of the H α emission arising from one peculiar spiral arm. One-arm morphologies are seen in the disturbed ISMs in the ICM-ISM simulations of Schulz & Struck (2001) and Vollmer et al. (2001). However NGC 4457 is located 9 degrees from M87, so it seems unlikely that the galaxy is presently experiencing a strong ICM-ISM interaction.

NGC 4569 has been frequently studied because of its smooth, 'soft', outer spiral arms and its very bright, blue, pointlike nucleus. Barth & Shields (2000) review the properties of this nucleus, which is usually classified as a composite starburst/LINER (e.g., Ho, Filippenko, & Sargent 1997), although most properties suggest nuclear starburst activity rather than a true AGN (Keel 1996; Tschoke et al. 2001). Its global H α morphology shows a ring of star formation at a radius of $1' \sim 0.3 r_{24}$ and a detached arm of HII regions, which may be extraplanar, perhaps like those in the ICM stripped galaxy NGC 4522 (Kenney & Koopmann 1999). The Ha "rotation curve" of Rubin et al. (1999) does not appear unusual, but the CO kinematics show large linewidths and

disturbed motions in the central arcminute, resembling the motions in a disturbed bar (Jogee 1999). This suggests that an ICM-ISM interaction may have even disturbed the kinematics in the central region.

Two additional galaxies NGC 4522 and NGC 4689, are almost as severely truncated as the galaxies discussed above.

The highly inclined NGC 4522, described in Kenney & Koopmann (1999), has an H α disk truncated beyond $0.4r_{24}$, combined with extraplanar HII regions which appear to lie within filamentary structures ≥ 3 kpc long above one side of the disk. Ten percent of the H α emission arises from these extraplanar HII regions. In contrast, the stellar disk appears relatively undisturbed. HI images show a displacement in emission in the same direction as the H α (Kenney, van Gorkom, & Vollmer 2002, in prep.). Together, the truncated H α disk and extraplanar H α and radio continuum are reminiscent of a bow shock morphology, which strongly suggests that the interstellar medium (ISM) of NGC 4522 is being stripped by the gas pressure of the intracluster medium (ICM). The galaxy has a line-of-sight velocity of ~ 1300 km s $^{-1}$ with respect to the mean Virgo cluster velocity, and thus could be experiencing a strong interaction with the intracluster gas.

The disk of NGC 4689, shown in Figure 26, is truncated within a radius of $0.55 r_{24}$. The R distribution appears regular and the HII regions follow the flocculent arm segments. The galaxy is projected at 3.7 degrees from M87 and has a line-of-sight velocity of 1616 km s $^{-1}$. Given the undisturbed R, it is likely that the galaxy has been affected by ICM-ISM stripping.

The remaining ten galaxies are: NGC 4212, NGC 4237, NGC 4298, NGC 4321, NGC 4413, NGC 4501, NGC 4571, NGC 4567, NGC 4568, and NGC 4579. They have less severely truncated star-forming disks, with truncation radii of $0.5-0.9r_{24}$. They also have more HI than galaxies with severely truncated H α disks, with HI deficiencies ranging from 3-10x. They range from luminous galaxies, such as NGC 4501 ($B_T = 10.27$) to faint galaxies, such as NGC 4413 ($B_T = 12.97$). All lie within 4.5 degrees from M87. Their line-of-sight velocities range between -81 km s $^{-1}$ and 2281 km s $^{-1}$. Three, NGC 4567, NGC 4568, and NGC 4298, are members of apparent pairs (see

section 7.6). NGC 4321 is tidally interacting with several dwarf companion galaxies. NGC 4579, a Seyfert galaxy, has complex circumnuclear H α morphology, featuring a loop parallel to the stellar bar (e.g., González-Delgado et al. 1997). NGC 4413 (shown in Figure 26), NGC 4212, and NGC 4237 are lower luminosity galaxies ($B_T = 12.97$, 11.86 , and 12.37 , respectively). NGC 4413 has an asymmetric HI distribution (Warmels 1988) and NGC 4237 shows an outer kinematic asymmetry (Rubin et al. 1999). NGC 4571, shown in Figure 26, has a regular R distribution and an unusual H α morphology, in that the HII regions have an almost random-appearing distribution. It may be significant that NGC 4571, NGC 4212, and NGC 4522 have unusually blue colors for moderately HI deficient galaxies (e.g., Vollmer et al. 2001).

We note that several isolated galaxies have H α profiles truncated within r_{24} , including NGC 613 ($0.8r_{24}$), NGC 986 ($0.9r_{24}$), NGC 2525 ($0.88r_{24}$), and IC 5273 ($0.87r_{24}$). Only NGC 613 has been mapped in HI, and it has optical and HI disks of similar size (Kristen & Jörsäter 1996).

7.4.2. *Truncated Spirals with Anemic Inner Disks*

Five galaxies have truncated star-forming disks with anemic star formation within the truncation radius. These galaxies are NGC 4293, NGC 4380, NGC 4450, NGC 4419, and NGC 4772. All are classified as Sa by BST and/or RC3, but NGC 4293 and NGC 4380 have C30 values similar to isolated Sb or Sc galaxies.

The R and H α images of NGC 4380 are shown in Figure 27. NGC 4380 appears undisturbed in R. It has weak star formation over much of the disk within the truncation radius of $0.7r_{24}$, but there is a sharp ridge of H α emission on the northwest side, possibly suggesting ongoing ICM pressure. It is located 2.7° southwest of M87 and has a line-of-sight velocity of 967 km s $^{-1}$. NGC 4380 is a striking case of the failure of the Hubble Classification scheme to describe cluster galaxies. It is classified as Sa by both BST and RC3, probably because of its reduced star formation and tightly wound spiral arms. However, this galaxy has low C30! This galaxy might have been overlooked as a candidate for depressed inner disk star formation if we had compared radial profiles solely as a function of Hubble type. In Figure 10, the pro-

file of NGC 4380 stands out in the lowest C30 bin with low H α surface brightness compared to other galaxies. Its H α radial profile is not as striking in the Sa bin in Figure 9, compared either to other Virgo or isolated galaxies classified as Sa.

NGC 4293, shown in Figure 27, is a low C30 galaxy with a disturbed stellar morphology. BST classifies the galaxy as an Sa pec, while the RC3 classifies it as an Sb. There is a prominent higher surface brightness feature within the central 5 kpc in R, which shows a smaller axial ratio than the outer disk. The outermost isophotes are asymmetric (also seen in Sandage & Bedke 1994). In H α , there is a central emission peak coincident with the R nucleus and one additional HII complex, located at $\sim 70''$ (3 kpc) east. The rotation curve is measured within $40''$ (1.7 kpc) and is classified as irregular (Rubin et al. 1999), suggesting non-circular motions in the ionized gas.

The remaining three truncated/anemic galaxies are all moderate C30 galaxies, classified as Sa. All show evidence of disturbed gas distributions or kinematics. NGC 4419, a highly inclined (70°), HI deficient galaxy located 2.8° north of M87, has regular ionized gas kinematics (Rubin et al 1999), but a strongly asymmetric CO distribution (Kenney et al. 1990). The line-of-sight velocity of the galaxy is -261 km s^{-1} , suggesting an orbit with a strong radial component along our line-of-sight. The moderately HI deficient Southern Extension galaxy NGC 4772 shows kinematic signatures of a past minor merger (Haynes et al. 2000). The HI deficient galaxy NGC 4450, shown in Figure 27, has a LINER nucleus and a kinematically distinct circumnuclear disk (Rubin, Kenney, & Young 1997). It is projected 4.7° north of M87 with a line-of-sight velocity of 1954 km s^{-1} . It has smooth, massive arms, with multiple inner dust lanes throughout the inner part of the galaxy. One unusual dust lane ends abruptly on the brightest HII complex in the galaxy.

7.4.3. *Virgo Spirals with Compact Star-Formation*

Four Virgo Cluster spirals have extremely small H α disks, with HII complexes distributed asymmetrically and only within the central kpc. All four are HI deficient by at least a factor of 10. They all have luminosities of $M_B > -19$.

Two of these galaxies, NGC 4424 and NGC

4064, have compact H α emission from several circumnuclear HII complexes, as shown in Figure 28. The H α surface brightnesses of these two galaxies within $0.1r_{24} \sim 0.8 \text{ kpc}$ are among the highest in the Virgo and isolated samples (see Figures 19 and 20). H α major axis spectra show that the HII regions have low line-of-sight velocities inconsistent with circular motions in the plane suggested by the outer optical isophotes (Rubin et al. 1999). The peculiar properties of NGC 4424 are further described in Kenney et al. (1996). The galaxy has unusual heart-shaped inner R isophotes and shell-like features similar to those seen in simulations of mergers (e.g., Hernquist & Quinn 1988; Hernquist 1992, 1993). These characteristics suggest NGC 4424 is the product of a recent minor merging event (Kenney et al. 1996). NGC 4064 has a more regular R morphology than NGC 4424. It shows very open spiral arms and a bar in the center. The peculiar dust morphology also suggests a minor merger (Cortes & Kenney, in prep.).

The other two galaxies have fainter H α emission. NGC 4606 has ~ 3 faint HII complexes, distributed in a linear feature extending from the center towards the southwest and almost coincident with the major axis. The ionized gas extent is so small that it is difficult to judge the kinematics, although the line-of-sight velocities (Rubin et al. 1999) appear regular. It may be significant that there is another spiral galaxy, NGC 4607, projected at an apparent nucleus-nucleus separation of $4'$ (18.5 kpc) from NGC 4606 and with a velocity difference of 593 km/s (4606: 1664 km/s , 4607: 2257 km/s), so that the two galaxies may be experiencing a tidal interaction. NGC 4606/4607 are projected about 2.5 degrees from M87 and may be currently encountering the hot ICM. NGC 4607 is not in our Virgo Cluster sample due to its high inclination. Its H α emission ($\log \text{H}\alpha \text{ flux} = -12.12$) uncorrected for dust effects suggests that it has at least a typical star formation rate for a small bulge spiral. However all the star formation apparently lies within the inner half of the disk, suggesting that NGC 4607 has enhanced inner disk star formation. This would be consistent with either an ICM interaction or a tidal interaction with NGC 4606.

NGC 4694 has a high C30. Its H α morphology consists of a peak, offset from the center in R by $2'' = .15 \text{ kpc}$, and one bright HII complex lo-

cated toward the northwest at a radius of $11'' = .84$ kpc (at a PA of 115). The $H\alpha$ morphology to the southeast is partly obscured by dust. An HST snapshot (Malkan, Gorjian, & Tam 1998) obtained from NED shows complex dust morphology in this region. The major axis velocities of NGC 4694 are low for a spiral, suggesting that the ionized gas has non-circular motions (Rubin et al. 1999). NGC 4694 has a peculiar HI distribution, with a small central concentration of HI and a tail of HI extending 40 kpc, with the peak of the tail centered on the neighboring magnitude dwarf irregular galaxy VCC 2062 (van Driel & van Woerden 1989; see also Hoffman et al. 1996). We detect $H\alpha$ emission of $\log(H\alpha \text{ flux}) = -14.15$. from this dwarf. van Driel & van Woerden (1989) discuss several possible scenarios for the HI morphology of this galaxy, concluding that an interaction with an intergalactic gas cloud is most likely the explanation for the structure of NGC 4694, although an interaction with VCC 2062 or another galaxy is possible. Hogg et al. (1998) discuss other galaxies classified as amorphous which show evidence for tidal interactions with a faint companion.

The *isolated* ST galaxy, NGC 4984, has a compact star-forming disk with active star formation distributed in an incomplete nuclear ring. The galaxy has a high C30 and is classified as Sa and a starburst (Devereux 1989; Kewley et al. 2001). The kinematics of the ionized gas show an outflow due to the starburst, but are otherwise regular, with a rapidly rising rotation curve to a maximum $v_{\text{sin}(i)} = 127$ km/s (Koopmann et al. 2003, in prep). Thus some types of truncated $H\alpha$ disks can occur in isolated galaxies, perhaps triggered by minor mergers or tidal interactions with low surface brightness companions.

7.5. Galaxies with enhanced outer disks?

An additional class might be that of galaxies with significantly enhanced outer disks. Such a morphology might be expected due to ICM/ISM induced star formation in a galaxy, particularly a galaxy entering the hot ICM for the first time. However, only 3 Virgo Cluster galaxies show evidence for enhanced star formation in the $0.5\text{--}0.7 r_{24}$ (NGC 4519, NGC 4713) or $0.7\text{--}1.0 r_{24}$ bin (NGC 4532). As discussed in Section 7.3, the star formation properties of these galaxies are most likely influenced by tidal interactions or gas accretion.

There is suggestive evidence in several cases of locally enhanced emission in the outer disk, which is not significant enough to influence the star formation rate over the whole radial bin. Several galaxies have arcs of star formation or areas of bright HII regions near the truncation radius. For example, NGC 4178, NGC 4189, and NGC 4654 show asymmetric, enhanced regions of star formation near the outer edge of the $H\alpha$ disk (Figure 29). NGC 4298 and NGC 4647, both members of apparent pairs (shown in Figure 30), and NGC 4380 (shown in Figure 27) show outer asymmetric arcs of star formation. These types of enhancements are different from the symmetric nature of the $H\alpha$ morphology of galaxies such as NGC 4580 and IC 3392.

7.6. Pairs in the Virgo Cluster

Several apparent pairs were noticed in the Virgo Cluster sample.

NGC 4567 and NGC 4568 overlap in projection, with almost identical line-of-sight velocities of 2274 km/s and 2255 km/s. NGC 4567 has disturbed outer kinematics (Rubin et al. 1999). Otherwise there are no indications of an ongoing interaction, e.g., tidal tails.

NGC 4298 and NGC 4302 also have almost identical line-of-sight velocities of 1135 km/s and 1149 km/s, with a nucleus-nucleus separation of $2.4'' = 11$ kpc. NGC 4298 appears asymmetric in both R and $H\alpha$, with an apparent extension towards NGC 4302. In $H\alpha$, a ridge of HII regions rings the outer edges of the star-forming disk, on the side nearest NGC 4302. Its rotation curve is disturbed (Rubin et al. 1999). NGC 4302 is an edge-on galaxy with a small bulge. $H\alpha$ emission extends over much of the optical disk.

NGC 4647 has a nuclear separation of $2.7'' = 12.4$ kpc from the S0/E galaxy NGC 4649 and the two galaxies have almost identical line-of-sight velocities of 1422 and 1413 km/s. NGC 4647 is also asymmetric in R and $H\alpha$, with an enhancement in HII regions in the outer disk toward NGC 4649.

NGC 4294 and NGC 4299, another close pair of similar mass galaxies with similar line-of-sight velocities, were discussed in section 7.3.

All of these galaxies have at least mildly truncated $H\alpha$ disks. Since tidal interactions affect both stars and gas, it is likely that ICM-ISM interactions

and not tidal interactions are responsible for the truncated gas disks in these Virgo pair galaxies. This is consistent with the location of these pairs, all of which are projected within 3.2 degrees from M87. Thus, these galaxies have likely experienced both ICM-ISM and tidal interactions. The presence of these pairs, but the absence of recent major mergers in the Virgo Cluster suggests that the most of the pairs may be disrupted by tidal interactions with other galaxies or the cluster before they can merge.

8. $H\alpha$ and HI Properties of Sample Galaxies

8.1. The Star Formation Rates of HI Deficient Galaxies

Virgo Cluster spiral galaxies have long been known to have less HI gas than field counterparts (Chamaraux et al 1980; Giovanelli & Haynes 1983). Previous studies (e.g., Chamaraux, Balkowski, & Fontanelli 1986; Solanes et al. 2001; see also Kenney 1990) concluded that the reduction in HI gas, quantified with an HI deficiency parameter (e.g. Giovanelli & Haynes 1983), has been more severe for early-type spiral galaxies. Based on this result, Chamaraux et al. (1986) and van Driel (1987) proposed that HI gas in early-type galaxies is more likely to be located in the outer disk, where it is easier to strip. Dressler (1986) suggested that HI deficient galaxies, which tend to have early-type classifications, are more likely to have radial orbits than HI rich galaxies, based on analysis of the velocity dispersions of HI rich and HI deficient galaxies in 9 clusters.

In light of the presence of a number of galaxies in the Virgo Cluster with misleading classifications, it is worth reexamining the relationship between HI deficiency and morphology. In Figure 31, we plot HI deficiency versus C30, marking the points according to Hubble type, for the isolated and Virgo Cluster samples. The Virgo Cluster sample has many HI deficient galaxies: there is a large population of galaxies with HI depleted by at least a factor of 5. It also has several galaxies with HI enhanced by a factor of a few. In the isolated sample, there is almost no correlation between C30 and HI or C30 and Hubble type (except that most of the galaxies with depleted HI are highly concentrated galaxies classified as S0 or

Sa). In the Virgo sample, there is also no correlation between HI deficiency and C30 for these sample galaxies. However, there is a stronger correlation between Hubble type and HI deficiency, in that many of the galaxies with HI deficiency greater than ~ 1 are classified as Sa, regardless of their central light concentration. Severely truncated galaxies, which are often assigned early-type classifications, also have large HI deficiencies, but intermediate C30. It is thus clear from this plot that *the correlation between HI deficiency and central concentration is much weaker than the correlation between HI deficiency and Hubble type.*

The correlation between Hubble type and HI deficiency is really a reflection of a correlation between star formation rates and HI deficiency in the Virgo Cluster. In Figure 32, the normalized $H\alpha$ fluxes are plotted versus the HI deficiency parameter, with symbols marked according to Hubble type. In the Virgo Cluster, there is a strong correlation between total normalized $H\alpha$ flux and HI deficiency, with the assignment of Hubble type tending in the same direction.

The stronger correlation between Hubble type and HI deficiency is one of the biases caused by forcing cluster galaxies into a one-dimensional classification system. Figures 31 and 32 together show that galaxies of any bulge-to-disk ratio can be strongly stripped of HI, suffer reduced star formation, and be classified as early type spirals. Therefore, the correlation between HI deficiency and Hubble type is no longer surprising, rather it is predominantly due to strongly stripped galaxies being classified as Sa's, rather than galaxies with large bulge-to-disk ratios being preferentially stripped. We therefore suggest that the reason for the previously observed systematic difference in spatial distributions and kinematics between early- and late-type Virgo spirals is at least partially due to the fact that stripped spirals, which are preferentially on radial orbits (Solanes et al 2001), tend to be misleadingly *classified* as early-types.

8.2. A comparison of $H\alpha$ and HI morphologies

In this section, we compare the $H\alpha$ radial morphologies as defined in Section 7 with HI radial morphologies. Cayatte et al. (1994) describe 4 types of HI profiles for 17 Virgo Cluster spi-

rals: Group I galaxies have normal HI distribution over most of disk compared to field spirals, Group II galaxies have lower inner HI densities and somewhat truncated outer distributions, Group III galaxies have severely truncated HI distributions, but similar central surface density to field spirals, and Group IV galaxies have a central HI hole and low surface density HI distributions.

We have eleven galaxies in common with the sample of Cayatte et al. Figure 33 shows the HI group designation of these galaxies in the $C30-F(H\alpha)/F(R)$ plot. There is a clear trend between HI radial morphology and star formation rates, with Group IV galaxies falling at lower star formation rates than Group I-II galaxies, although there is not a one-to-one matching.

Galaxies in Cayatte et al. Group I include 5 galaxies in our sample: NGC 4303 has enhanced star formation rates across the disk compared to isolated galaxies and therefore falls in our group C. NGC 4178, NGC 4192, NGC 4254, and NGC 4654 are members of our Category A, with star formation rates similar to isolated galaxies across the disk.

Four galaxies have Group II designations: NGC 4535 and NGC 4647 have star formation rates similar to the isolated sample over the whole disk and thus are members of Category A. NGC 4501 and 4689 have mildly truncated star-forming disks and therefore are members of Category D1.

We have only one Group III galaxy in common (out of three in Cayatte et al.'s sample). NGC 4569 has a normal inner disk star formation rate and a severely truncated $H\alpha$ disk (Category D1), matching the HI morphology.

Of the three Group IV galaxies in our sample, we find that NGC 4548 is anemic (our Category B). NGC 4450 has an anemic inner disk and a truncated outer disk (Category D2). NGC 4579 also has a truncated outer disk, but has inner disk star formation within the range of a typical isolated spiral, although it is on the low side, and thus is a member of Category D1.

Thus, we find an overall consistency but not one-to-one correspondence between HI and $H\alpha$ morphology: galaxies with more peculiar HI morphologies also tend to have peculiar $H\alpha$ morphologies. Galaxies with reduced or truncated HI tend to have reduced or truncated $H\alpha$.

8.3. The Relationship Between HI Content and Star Formation

The good correlation between global HI and $H\alpha$ properties helps explain some things about galaxy evolution and morphology in clusters, but is somewhat surprising from the point of view of understanding star formation. The correlation between HI and $H\alpha$ cannot be explained simply by a star formation rate which is proportional to the local amount of HI gas, since the radial distributions of HI and $H\alpha$ are generally very different. $H\alpha$ emission is peaked strongly toward the galaxy centers, whereas the HI radial distributions are much flatter and (for HI-normal galaxies) extend to larger radii. In Virgo spirals, the radial distributions of $H\alpha$ and other tracers of star formation are similar to those of the molecular gas (as traced by CO emission), and quite different from that of the HI (Kenney & Young 1989).

The correlation between HI and $H\alpha$ in Figure 32 appears somewhat better for Virgo than isolated galaxies, suggesting that the cluster environment improves the correlation. While we do not have a good understanding of this good correlation in Virgo, several factors may be relevant: (i) Gas stripping clearly removes reservoirs of star-forming gas. (ii) Any galaxy with a large gas reservoir intact (e.g., HI normal or HI-rich galaxies) might have any of a number of cluster interactions trigger star formation in this reservoir. (iii) Outer disk and low surface density HI, which is inefficient in producing massive stars (Kennicutt 1989) is easily stripped in most Virgo galaxies, but would not be stripped in isolated galaxies.

An illustration of this last point may be provided by NGC 4698, which has close to a normal HI content (HI deficiency = 0.25), but a low star formation rate. This galaxy is unusual in having a bulge in which stars rotate in a different plane than the outer disk (Bertola et al 1999). Most of the HI is located far outside the stellar disk (Warmels 1988) and is not experiencing any detectable massive star formation. The peculiar stellar kinematics indicate a merger, suggesting that the HI was accreted in the merger. Such HI accretion associated with mergers can occur inside and outside of clusters, and in some cases leave gas at large galactocentric radii, where star formation is inefficient. In many cluster galaxies, this

outer disk, non-star-forming gas can be stripped, which will improve correlations between global HI and H α properties. Outside of clusters, the outer disk, non-star-forming gas will tend to survive, contributing scatter to correlations between global HI and H α properties. In the outskirts of clusters, this gas may survive for ~ 1 Gyr, until the galaxy's orbit carries it into the cluster core. This may be the case for NGC 4698, which is 6° from M87, in the outskirts of the cluster (Figure 22).

9. The Effects of Extinction on H α Results

H α will underestimate the true massive star formation rate due to extinction by dust. Since we have done a comparative study of Virgo Cluster and isolated galaxies, our results will be affected only if there is a systematic difference in extinction between the two samples.

There could be a systemic difference, since stripped galaxies likely have less dust as well as less gas. There are likely radial gradients in extinction, with more in the centers than the outer disks (Giovanelli et al. 1994, 1995). Stripping and truncation selectively removes the low extinction part of the disks, i.e. the outer gas and dust disks. So the true difference in star formation rates between the stripped and unstripped galaxies may be less than is indicated in H α . Any difference should be less in the comparisons within distinct radial bins. The fact that we see large differences between the Virgo and isolated galaxies in the outer radial bins shows clearly that many outer Virgo disks are extremely deficient in H α . However, the outer disk contains a smaller fraction of the global star formation rate than is indicated by uncorrected H α , and the true global reduction in star formation rate may be less than is indicated by the H α results.

Tracers of SF which measure dust emission, such as FIR, will be subject to the opposite problem of overemphasizing the inner disk. An improved treatment should use information from both optical and FIR emission to estimate the true radial profile of star formation.

10. The Star Formation Rates of Barred Galaxies

From an examination of the H α images (e.g. Koopmann et al. 2001; Ryder & Dopita 1993),

it can be seen that many barred galaxies have a distinctive inner disk star formation morphology: weak star formation within the bar region, but strong circumnuclear star formation. Often there is a bright ring of star formation near the end of the bar. Not all barred galaxies show this morphology - some barred galaxies have star formation along the bar, a feature which is more common in late-type galaxies (Phillips 1993), but which may sometimes be an indicator of a relatively young bar (Martin & Roy 1995). Unbarred galaxies tend to have star formation distributed more smoothly over the inner disk, although unbarred galaxies also sometimes have bright rings of star formation.

Could differences in star formation distributions between barred and unbarred galaxies affect our analyses from the preceding sections? This is an important question for our study since the numbers of barred galaxies are different in the two samples. Table 4 gives the percentages of barred and unbarred galaxies in the isolated and Virgo samples for both the RSA and RC3 barred classifications. In both classification schemes, we find that the isolated sample has a higher occurrence of strong bars. This is not representative of the complete sample from which the isolated and Virgo Cluster galaxies were drawn, in which strong bars occur at similar frequency. In this section we examine whether the difference in numbers of barred galaxies in the observed samples is a possible bias for our study. We base our analysis on the RC3 bar classifications; however similar results are obtained for the RSA/BST bar classifications.

A comparison of the integrated inner and outer disk H α fluxes for barred and unbarred galaxies is shown in Figure 34. The high percentage of isolated barred galaxies, especially for lower C30 isolated galaxies, can be seen in the figure. However, the barred and unbarred galaxies in the Virgo sample have similar distributions throughout the plot. Galaxies with enhanced or reduced star formation show a variety of barred types. Similar results are obtained when the locations of barred and unbarred galaxies are examined in plots similar to Figure 14. and when relative H α concentration values are examined. These comparisons suggest that no serious bias has occurred in the comparisons in the previous two sections, which disregarded the presence of a bar.

To further check the differences between star

formation characteristics in the inner disks of barred and unbarred galaxies, we compared median profiles and overplotted individual $H\alpha$ profiles of barred and unbarred galaxies of different types and C30 (not shown). We find in the median that barred galaxies do have lower star formation rates within 0.2-0.3 r_{24} , but that these lower rates are often compensated by higher rates within 0.3-0.6 r_{24} . Based on the individual profiles, we find that Virgo and isolated barred galaxies have similar inner disk star formation, with no indication that Virgo barred galaxies have systematically less star formation than isolated counterparts within the truncation radius. Because of the smaller numbers of isolated unbarred galaxies, it is not possible to make as strong a conclusion about the comparative inner star formation rates of unbarred galaxies based only on overplotting of the individual profiles, although the few profiles we have lead to the same conclusion.

11. Discussion

11.1. General Comments on the Morphology of Virgo Cluster spirals

Classification is inherently subjective and as we and others have shown in the case of Virgo Cluster galaxies, can be dangerous and misleading. Objectives measures are generally preferable, but classification can have value, so here we offer some comments on an improved classification for large disk galaxies.

The standard Hubble classification scheme, as employed by Sandage and deVaucouleurs, uses both bulge-to-disk ratio and disk structure (closely related to disk star formation rate). This system cannot work for cluster galaxies because in Virgo the bulge-to-disk ratio is poorly correlated with the disk star formation rate. As pointed out by van den Bergh (1976), the Sa type has become a repository for galaxies with very different physical characteristics.

The van den Bergh (1976) RDDO system offers the important big step in a more correct approach, by completely separating the spatial distribution of the old stars (i.e. bulge-to-disk ratio) from the the spatial distribution of the new stars (as measured, for example, by $H\alpha$) in the classification system. For a galaxy of a given bulge-to-disk ratio, van den Bergh proposed 3 evolutionary stages

based on the amount of disk star formation: normal spiral, anemic, and lenticular.

These three stages are still not sufficient to describe the morphology of approximately half of the Virgo spirals in this sample, which have truncated profiles: a normal-enhanced inner disk star formation combined with weak-no outer disk star formation. Whereas many isolated and some Virgo galaxies might follow an evolutionary progression from normal spiral, through anemic, and then to lenticular, many cluster galaxies will not.

Van den Bergh et al. (1990) recognized the truncation phenomenon, calling such galaxies "Virgo types". The combination of weak outer disk star formation, but active inner disk star formation tends to make the outer disks look smooth, as described by van den Bergh et al. Our identification of such spirals is based on our quantitative comparison with isolated galaxies rather than visual classification. Therefore, our assignments and the van den Bergh et al. assignments differ for a number of galaxies. (Those identified by van den Bergh et al. have a broader range in star formation characteristics. We find that three van den Bergh Virgo-type galaxies, NGC 4527, NGC 4651, and NGC 4654, fit into the normal range of star formation defined by the isolated galaxies, and do not have severely truncated outer disks within r_{24} .) This morphology reflects the most frequently occurring type of environmental alteration in the Virgo Cluster; however since there are other peculiar morphologies in the Virgo Cluster, we have chosen not to use the term 'Virgo-type'.

We propose that an additional parallel branch could be added to the van den Bergh scheme, describing the truncated star formation morphology: STa - STb -STc, where the a-b-c division is based on the central light concentration or B/D. Galaxies with combination truncated/anemic profiles could possibly be symbolized as 'TA' in this scheme. However, we reemphasize that attempts to characterize galaxy morphologies should be founded on objective measurements rather than subjective visual classification whenever possible.

11.2. The Morphology of Virgo Galaxies Classified as S0 or Sa

Galaxies classified as S0 and Sa are likely to be the most environmentally damaged galaxies

in clusters, particularly since small bulge galaxies with reduced star formation are often assigned misleading early type spirals classifications. We summarize in this section the morphologies of the Virgo Cluster galaxies in our sample which were classified as either S0 or Sa.

10 galaxies in our sample are classified as Sa. Half of these galaxies have low-intermediate C30 and were classified as Sa because of their reduced star formation. Of these, NGC 4424 and NGC 4606 (Section 7.4.3) and NGC 4569 (Section 7.4.1) have truncated star formation with no outer disk star formation. Another of these galaxies is NGC 4380 (Section 7.4.2), which has an anemic inner disk, coupled with a truncated outer disk. The remaining low-intermediate C30 galaxy classified as Sa is NGC 4293, with a severely truncated star-forming disk consisting of only 1 HII region.

The larger-bulge galaxies classified as Sa include NGC 4450, NGC 4419, NGC 4698, NGC 4772, and NGC 4579. All of these galaxies have truncated/anemic profiles, except NGC 4698, which shows an anemic profile. Both NGC 4698 (Bertola et al. 1999) and NGC 4772 (Haynes et al. 2000) show evidence for a past minor merging event. NGC 4450 and NGC 4579 have disturbed kinematics (Rubin et al 1999). NGC 4419 has regular ionized gas kinematics (Rubin et al 1999), but a strongly asymmetric CO distribution (Kenney et al. 1990).

We have mostly discussed the Sa population in this paper, since our Virgo sample contains only three galaxies classified as S0. All three S0's, NGC 4429, NGC 4459, and NGC 4643, have high C30 and show no detectable HII regions. NGC 4459 appears featureless in R and the H α emission is centrally peaked. The R image of NGC 4429 (Koopmann et al. 2001) shows it to be a dusty galaxy, with a boxy, higher surface brightness feature within the central 5 kpc. The H α image shows faint central emission; it is possible that the continuum subtraction is affected by the dust and perhaps color changes across NGC 4429. NGC 4643 displays a bisymmetric linear stellar feature at large radii (e.g., Richter, Sackett, & Sparke 1994), which is possibly a polar ring observed near edge-on.

Given the large number of low-C30 galaxies classified as Sa, we expect that an equally sub-

stantial population of low-C30 galaxies classified as S0 could exist. Work by Boselli et al. (1997) reveals at least several low/intermediate C30 galaxies classified as S0 in the Virgo Cluster. Our work suggests that a significant fraction of fainter Virgo Cluster S0 galaxies should have low central concentration. These would be remnants of spiral galaxies which perhaps went through a truncated normal or anemic low C30 phase, but now have little or no massive star formation. Thus one reason for the decline in spirals and the corresponding increase in S0's as one looks at the distant universe compared to the local universe (Dressler et al. 1997) is likely to be the stripping of gas and consequent reduction in disk star formation, and subsequent, partly misleading, classification of such galaxies as early Hubble types.

11.3. Environmental Effects in the Virgo Cluster

What do these results indicate about the environmental interactions that are and have been at work in the Virgo Cluster? This work shows that both ICM-ISM and galaxy-galaxy interactions are important in evolution of Virgo Cluster galaxies.

11.3.1. ICM-ISM Interactions

The results of this survey provide strong evidence that ICM-ISM interactions play a significant role in the evolution of most Virgo Cluster spirals by stripping gas from their outer disks. The star formation of many Virgo Cluster galaxies has been reduced mostly in the outer disk, while inner star formation rates are normal to enhanced. The reduction in the star formation rate in the outer disks of galaxies with regular stellar isophotes is in all likelihood due to the systematic removal of gas from the outer disk in the Virgo environment. Star formation ceases once the gas is gone, or at least removed until its surface density is below a threshold determined by the local dynamics (Kennicutt 1989). The normal to enhanced star formation rates in the inner galaxy disks imply that ICM-ISM interactions have not had a strong effect on the inner regions of most Virgo (star-forming) galaxies. The inner star formation rates of even the severely HI deficient spirals are within the bounds of isolated spirals. This is consistent with the observation that the inner disks of galaxies are H $_2$ -dominated, and that CO luminosities

are close to normal for Virgo galaxies compared to field galaxies (Kenney & Young 1989). Apparently the total gas surface density in inner disks is still high enough to allow star formation.

It has been suggested that enhancements in star formation may also be caused by ICM-ISM interactions (e.g., Dressler & Gunn 1983). While a number of galaxies in our sample are observed to have global and inner star formation enhancements, these appear to be more strongly affected by processes other than ICM-ISM stripping, although local enhancements in some galaxies (Section 7.5) appear to be caused by ICM-ISM stripping.

If ICM-ISM stripping is an important effect in the Virgo Cluster, we would expect to see gas- and star-formation-poor galaxies with a continuum of bulge sizes. Our observations show that this is the case; in particular, we find significant numbers of small to intermediate bulge-to-disk ratio galaxies with truncated star forming disks. In addition, several of these ‘small bulge Virgo Sa’ and severely truncated galaxies are projected well away from M87 and have line-of-sight velocities consistent with large radial components in their orbits, which takes the galaxies close to the cluster center. As discussed in Koopmann & Kenney (1998) and this paper, it is the methods of classification of weakly star-forming galaxies which has partially led to the incorrect idea that it is large-bulge galaxies which are most affected by loss of gas and star formation.

Are there any ‘smoking guns’ for ICM-ISM stripping? Several elliptical galaxies have long been known to be undergoing ICM-ISM interactions, e.g. M86, which is probably within a merging subcluster (Forman et al. 1979; White et al. 1991; Schindler et al. 1999), and NGC 4472 (Irwin & Sarazin 1996), both located in the Virgo Cluster. Several spiral candidates have been more recently identified. The best spiral candidates in the Virgo Cluster to date include NGC 4654 (Phookun & Mundy 1995) and NGC 4522 (Kenney & Koopmann 1999; Kenney et al. 2002, in prep.).

Further identification of ICM-ISM induced morphologies relies on a better understanding of the physics of the ICM-ISM interaction. The key parameters of an ICM-ISM interaction are the ICM density, the velocity of the galaxy with respect to the ICM, and the disk angle with respect

to the ICM wind direction. All of these vary as a galaxy follows its orbital path within the cluster, and the present state of a galaxy depends on this orbital history. Of particular importance is the time since (until) maximum ram pressure. Since many HI-deficient galaxies in clusters have highly radial orbits (Dressler 1986; Solanes et al. 2001), the ram pressure can vary by factors of 20-100 during the orbit, and gas may even fall back into the galaxy after being pushed outwards (Vollmer et al. 2001). The interaction also depends on the properties of the galaxy and its ISM, particularly the total mass distribution and the ISM mass distribution. In addition, what we observe depends on the viewing angle between the vector of the galaxy’s motion through the ICM and the line-of-sight. A challenge for the future is to recognize the effects of these various parameters in particular galaxies, and to identify the evolutionary stages of the interactions.

Recent 3D simulations of ICM-ISM interactions (Abadi et al 1999; Quilis, Moore, & Bower 2000; Schulz & Struck 2001; Vollmer et al 2001) are able to produce truncated gas disks. The Schulz & Struck (2001) simulations show rings of enhanced gas surface density at the truncation radius. A couple of the Virgo galaxies (NGC 4580, IC 3392; see Figure 24) show rings of enhanced star formation at the truncation radius. These could be the features seen in the Schulz & Struck (2001) simulations, although it is presently unclear whether the enhanced H α emission observed is associated with an enhanced gas surface density.

While much remains to be learned about the physics of ICM-ISM interactions, the good agreement of our and other observations with ICM stripping predictions suggests that ICM-ISM interactions are important in the evolution of Virgo Cluster galaxies.

11.3.2. *Galaxy-Galaxy Interactions*

Gravitational interactions between galaxies vary from mergers and accretions to penetrating collisions to non-penetrating encounters. The variety in collision parameters, particularly mass ratio, impact parameter, and relative velocity, most likely results in a range of effects on the colliding galaxies. Simulations of merging galaxies of similar mass show that extensive tidal tails containing stars and gas are produced (e.g., Toomre

& Toomre 1972; see also Hibbard 1995). However, such tails would be harder to detect in a cluster of galaxies, since they are quickly destroyed by cluster tidal fields. There are no obvious candidates for an ongoing equal-mass merger in the Virgo Cluster; however, there is at least one clear case in the Coma Cluster (Bravo-Alfaro et al. 2002) and merger galaxies are frequently seen in higher- z clusters (e.g., van Dokkum et al. 1999).

There is evidence for older or unequal-mass-ratio mergers in a number of Virgo galaxies. Many of the large ellipticals in Virgo may have formed long ago via mergers. This appears to be the case for NGC 4365, an E3 galaxy which has a kinematically distinct core with a similar star formation history as the main body (Davies et al. 2001). The Virgo S0 NGC 4382 exhibits shells suggesting a recent (possibly minor) merger (Schweizer & Seitzer 1988). The cospatial counter-rotating stellar disks in the Virgo S0 NGC 4550 are likely due to a major merger or gas accretion event several Gyr ago (Rubin, Graham, & Kenney 1992; Rix et al 1992). van Driel and van Woerden (1991) find the SB0 galaxy NGC 4262 to have an outer HI ring and an unusually large M/L compared to galaxies of similar morphological type. These characteristics are possibly explained by an external accretion or merger. The morphological and kinematic peculiarities of NGC 4424 (Section 7.4.3) are likely due to an intermediate mass ratio merger (Kenney et al. 1996). The bulge and disk of NGC 4698, a high C30 galaxy classified as Sa, appear to be oriented orthogonally to each other, indicating a merger or major gas accretion event (Bertola et al. 1999). The ionized gas velocities in NGC 4772, also a high C30 galaxy classified as Sa, are steeply rising along the minor axis and decoupled from the stellar velocities along the major axis, suggesting a misaligned embedded disk or bar caused by a minor merger event (Haynes et al. 2000). The nearly face-on SO NGC 4643 has a bisymmetric linear stellar feature at large radii (e.g., Richter et al. 1994), which is possibly formed from accreted material. The Virgo Sc NGC 4651, which appears as a relatively normal Sc within r_{24} , has a peculiar linear feature and several shell-like features at large radii (Schneider & Corbelli 1993; Malin 1994), suggesting a minor merger. This information on Virgo mergers is somewhat incidental. While it is unlikely that there are many more

recent major mergers yet to be discovered in Virgo, the cases cited here are surely only a lower limit on the true number of minor mergers (of any age) and old major mergers.

Non-merging tidal encounters are common in clusters, and multiple, fast tidal encounters may strongly influence a galaxy's morphology over a Hubble time (Miller 1988; Moore et al. 1998). An extreme example of a recent, high-velocity tidal encounter is the Virgo Cluster galaxy NGC 4438, which may have experienced a direct collision (Kenney et al. 1995). Rubin et al. (1999) find disturbed kinematics in $\sim 50\%$ of Virgo galaxies, suggesting that tidal encounters are frequent in the Virgo Cluster. Deep imaging of Virgo Cluster galaxies shows some galaxies with low surface brightness tails (Malin 1993), which have likely been caused by some type of gravitational interaction.

Several apparent pairs of galaxies in the Virgo Cluster were described in Section 7.6. Several of these galaxies have mildly enhanced star formation rates over at least part of their disks and/or asymmetric arcs or other peculiar features perhaps associated with a tidal interaction. The existence of bound pairs and the absence of major mergers suggests that most pairs may be disrupted by tidal interactions (with other galaxies or the cluster) before they can merge.

11.3.3. *Gravitational and ICM-ISM Stripping?*

It is to be expected that many Virgo galaxies would be affected by multiple types of interaction, since we find that a large fraction of spirals show evidence of stripping, and Rubin et al. (1999) find that a large fraction of Virgo spirals have disturbed rotation curves indicative of tidal interactions. Strong tidal interactions typically drive inner gas inwards and outer gas outwards in tidal tails, depleting the gas at intermediate radii (e.g., Barnes & Hernquist 1991). Gas driven outward and low surface density gas at intermediate radii would be particularly susceptible to ICM-ISM stripping. Thus a tidal interaction could facilitate the stripping of the ISM by the ICM.

11.4. Comparison between Previous Work on the Virgo Cluster and Other Clusters

11.4.1. Star Formation Properties

It is clear that the star formation activity in the Virgo Cluster spans a large range. We find, in agreement with a number of previous multiwavelength studies of Virgo (Kennicutt 1983a; Kodaira et al. 1990), that the global star formation activity has been reduced in the median. The amount of reduction is a lower limit, since our study includes mostly spirals with at least some ongoing star formation activity. The selection of sample galaxies using the Hubble type may lead us to underestimate the reduction in star formation, since small-bulge galaxies which have ceased star formation are likely classified as S0's.

The result that a number of Virgo Cluster spirals have enhanced star formation is relatively new for studies of the Virgo Cluster. This may be partly due to previous comparison samples. The Kennicutt & Kent (1983) study of H α emission in Virgo cluster galaxies, for example, used a comparison sample of field galaxies, which included systems in groups, and in particular some starbursts (e.g., M82). Thus their study was not especially sensitive to rates of star formation enhanced above those found in isolated galaxies, which we are better able to quantify.

The observation of a significant percentage of Virgo Cluster galaxies with enhanced star formation is also due to the inclusion of a lower luminosity population. All except one of the Virgo Cluster galaxies with enhanced star formation have absolute magnitudes between -18.2 and -19. This result is probably related to the observation that 'k+a' and emission-line galaxies in the Coma Cluster tend to be fainter than 'k+a' counterparts at larger redshifts (Poggianti 2002).

Most previous studies of cluster galaxies have been limited to measurements of global star formation. Results for comparisons vary between studies, as documented in the introduction. There are relatively few previous spatial results for galaxies in clusters. We find that most galaxies with reduced star formation in the Virgo Cluster have truncated star-forming disks, but normal-to-enhanced inner rates. In the galaxies with the most severely truncated disks, the star formation

is distributed either in ring-like or in compact, linear, asymmetric morphologies.

There is evidence that similar star formation morphologies exist or existed in the Coma Cluster. Caldwell et al. (1996) identified a population of starburst and poststarburst spirals in Coma, most of which have centrally concentrated star formation, typically within 1-2 kpc (Caldwell et al. 1999). Similar morphology galaxies are found in Pegasus I (Rose et al. 2001). These poststarburst galaxies were initially classified as E or S0, and yet all are spirals and about half have small-intermediate B/D. In a study of the S0's in Coma, Poggianti et al. (2001) found that 40% show spectroscopic evidence for central star formation within the last 5 Gyr. Moss & Whittle (2000) find evidence of circumnuclear starbursts in a number of cluster galaxies.

Studies of the spatial characteristics of star formation in the Virgo and other clusters are especially important because of the clues they provide in investigating the dominant environmental effects on galaxy evolution in clusters.

11.4.2. Environmental Effects

The results of our spatial studies of star formation in the Virgo Cluster show that both ICM-ISM stripping and tidal interactions have had a major influence on the morphology and star formation histories of spirals in the Virgo Cluster. In this section, we briefly review and compare our results to other recent studies of nearby and distant cluster galaxies.

Results from recent studies can be roughly divided into three categories: (i) those which suggest that the major influence on spirals in clusters is ICM-ISM stripping, which reduces star formation mainly by simple truncation, although modest bursts may happen in at least some galaxies (e.g., Abraham et al. 1996; Bravo-Alfaro et al. 2000, 2001; Jones et al. 2000; Couch et al 1998; Balogh et al. 1999), (ii) those which suggest that starbursts caused by tidal interactions with the cluster or other galaxies have had a major effect on the evolution of a significant number of galaxies (e.g., Moss & Whittle 2000; Caldwell et al. 1996; Henrikson & Byrd 1996; van Dokkum et al. 1999; Rose et al. 2001), and (iii) those which suggest that both ICM-ISM stripping and tidal interac-

tions are necessary to explain observed star formation properties (e.g., Poggianti et al. 1999). It is interesting that different studies disagree about the main environmental effects even when analyzing the same cluster!

The HI and optical studies of Coma cluster galaxies strongly suggest that ICM-ISM interactions are a major driver of galaxy evolution in that cluster (Bravo-Alfaro et al 2000, 2001). However, the poststarburst galaxies detected in Coma (Caldwell et al. 1996) have centrally concentrated star formation, and spectral studies suggest that the last star formation was burstlike. This suggests a tidal origin rather than ICM stripping events alone. Poggianti et al. (2001) have also found evidence that the last star formation in more than 40% of S0 galaxies in the Coma Cluster occurred in their central regions within the last 5 Gyr.

Rose et al. (2001) find 2 out of 4 early-type spirals with active star formation similar to the Coma poststarburst galaxies in the Pegasus I cluster, which is a less massive cluster without substantial ICM.

Moss & Whittle (2000) find a high percentage of starbursting late-type spirals in 8 nearby Abell clusters. The percentages of starbursting spirals were highest in the 2 richest clusters, Coma and Abell 1367, both post-merger systems. They suggest that the starbursts are induced by the tidal forces caused by the cluster merger (both cluster potential and local tidal effects, with the former the most important). However, it is important to note that their survey was not sensitive to reductions in star formation activity because the survey has a rather high lower limit of $EW(H\alpha) \simeq 20\text{\AA}$ on the strength of $H\alpha$. (Most of the galaxies in our sample have $EW(H\alpha)$ below 20\AA .) This means Moss & Whittle cannot detect differences between normal and reduced amounts of star formation, and they cannot determine whether the overall star formation rate in their clusters is higher or lower than non-cluster samples.

Studies of more distant clusters have also produced a variety of results (see also O'Connell 1999 for a review). Balogh et al. (1999) conclude based on an analysis of galaxies from the CNOC1 sample that cluster galaxies have not experienced starbursts at an enhanced level compared to field environments and that they have more likely been

subject to the removal of a gas halo over long timescales by the cluster environment. Balogh et al. (2000) developed this idea, first suggested by Larson et al. (1980), into a 'strangulation' model for cluster evolution, and find that the model fits observations of Abell 2390 (Balogh & Morris 2000). Abraham et al. (1996) also find that the evolution of the galaxies in Abell 2390 can best be modeled by truncation in star formation rather than starbursts. Couch et al. (1998), in an optical HST study of 3 rich clusters at $z=0.3$, found that, while there are many tidal interactions and mergers in these rich clusters, ICM-ISM stripping of spirals is the likely explanation for the formation of lenticular-like galaxies with undisturbed stellar disks lacking star formation. Jones et al. (2000) suggest, based on analysis of three $z=0.31$ clusters and nine $z=0.37-0.56$ clusters and the results of Poggianti et al (1999) and Caldwell et al. (1996), that the best explanation for the development of the larger proportion of S0 galaxies since $z=0.5$ is truncated star formation in early-type spirals after a possible final, modest burst of star formation. In an optical spectroscopic and morphological study of 10 rich clusters from $0.37 < z < 0.56$, Poggianti et al. (1999), concluded that there are 2 different timescales and/or processes responsible for most of the spectral and morphological transformation of galaxies in clusters. One of these processes is probably ICM-ISM interactions, and the other is probably tidal encounters. van Dokkum et al. (1999) find that 17% of galaxies in a luminous X-ray cluster at $z=0.83$ are ongoing mergers.

Some of these studies have relied on the Hubble classification to distinguish between galaxies. We reemphasize that comparisons based on Hubble classifications can produce misleading and even erroneous results. In particular, gas-poor spirals with small B/D, probably stripped Sc's, are often misleadingly classified as Sa's. In order to judge the environmental impact on cluster Sc's, one should include the stripped Sc's with the non-stripped Sc's, and in using the Hubble classification one does not do this, but assigns the stripped Sc's to the Sa or other earlier type category. In some cases, E, S0, and S0/a galaxies, as well as those of indeterminate type, are excluded from samples (e.g., Moss & Whittle 2000). Some of these galaxies, particularly those classified as S0/a or indeterminate, may be environmentally mod-

ified systems relevant for understanding galaxy evolution in clusters.

The variety of results in these studies seems to indicate that more than one process is important in clusters, and that different clusters may be dominated by different processes, perhaps at different times in their evolution. Our results suggest strongly that ICM-ISM stripping is important in clusters as least as rich as Virgo. While tidal interactions are clearly an important process driving cluster galaxy evolution, it is doubtful that tidal interactions alone could be responsible for the spiral-S0 transformation. Two effects of tidal interactions help transform spirals towards a lenticular state. They drive gas toward the center, some of which then forms stars, yielding a galaxy with a higher central concentration of stars (although not necessarily a bulge.) They also cause an increase in the SFR, thereby causing the galaxy to consume its gas faster than it would in an isolated environment. However, tidal interactions will not clean out the outer disk of star-forming gas, and this is probably required for a galaxy to be classified as lenticular. ICM-ISM stripping seems to be required for the disk cleaning, although tidal interactions can make a galaxy more susceptible to ICM-ISM stripping by driving some of the outer disk gas outwards.

12. Conclusions

The results of this survey of star formation rates and morphologies of Virgo Cluster spirals compared to isolated spirals include the following:

1. $H\alpha$ -based estimates of the total massive star formation rates of Virgo Cluster galaxies span a range from strongly reduced (up to 10 times) to enhanced (up to 2.5 times) compared to the isolated sample. In the median, Virgo total star formation rates are reduced by factors up to 2.5 for different Hubble types and concentrations.
2. The reduction in star formation rates of Virgo Cluster spirals has caused the misleading classification of some small-intermediate B/D spirals as Sa. Half of our Virgo 'Sa' galaxies have central R light concentrations, and therefore B/D, smaller than any isolated Sa galaxy. Thus the Hubble Classification is inadequate for galaxies in clusters and should not be used blindly in comparisons of field and cluster spirals.
3. For most Virgo Cluster galaxies with reduced total star formation, it is truncation rather than anemia (low $H\alpha$ surface brightness across the disk) which causes the reduced total star formation rates. Median inner rates are similar or enhanced up to a factor of 1.7, while outer star formation rates are reduced in the median by factors of 1.6 - 7.1. In the outermost parts of the optical disks, star formation of all types and concentrations of galaxies are reduced by factors greater than 2.8 times. Reduction in individual galaxies range to factors greater than 100. No galaxies have star formation rates in the outer half of the disk enhanced above isolated rates, however, several galaxies show asymmetric, local enhancements at the outer edge of the star-forming disk. Thus, most galaxies with reduced total star formation have inner star formation rates which are similar to or enhanced with respect to isolated galaxies of similar central light concentration or Hubble type. In some cases, enhanced inner disk star formation has combined with reduced outer disk formation to produce a total star formation rate which is only mildly reduced. Virgo Cluster galaxies have more concentrated star forming disks than isolated counterparts, largely due to truncation.
4. Star formation morphologies in the Virgo Cluster are dominated by truncation of the star-forming disk, with 52% of spirals truncated within r_{24} . Only 3 spirals show disk-wide reduction in star formation, i.e., anemia. An additional 5 combine truncated star-forming disks with anemic inner disks. 8 galaxies show enhanced inner and global star formation rates. 14 galaxies have normal star formation rates within r_{24} compared to isolated galaxies.
5. At least two types of galaxies with severely truncated star-forming disks are identified. The most common type shows 'simple truncation', in which the inner disk star formation rates are similar to those in low C30 isolated galaxies, but there is no star formation beyond $0.3-0.4 r_{24}$. This peculiar morphology has resulted in several cases in the assignment of a mixed Hubble type such as Sc/Sa. In other cases, these galaxies have simply been assigned early-Hubble types. The morphology of these galaxies is most likely due to ICM-ISM interactions. The other type of severely truncated galaxies shows compact, asymmetric, circumnuclear star formation. These properties are more

likely due to gravitational interactions. In the case of NGC 4424 and NGC 4064, this star formation morphology, combined with their disturbed stellar morphologies and/or kinematics, suggest a merger origin (Kenney et al. 1996, Cortes & Kenney, in prep.).

6. The larger mean HI deficiency of Virgo cluster Sa's as compared to cluster Sb and Sc's's (Solanes et al 2001) is predominantly due to strongly stripped galaxies being classified as Sa's, rather than galaxies with large bulge-to-disk ratios being preferentially stripped. One reason for the previously observed systematic difference in spatial distributions and kinematics between early- and late-type Virgo spirals (Dressler 1986) is that stripped spirals, which are preferentially on radial orbits (Solanes et al 2001), tend to be misleadingly *classified* as early-types. Likewise, the excess of Sa galaxies in the Virgo cluster, and perhaps by extension other clusters, is in large part due to strongly stripped galaxies being classified as Sa's, and is not simply an excess of spiral galaxies with large bulge-to-disk ratios.

7. We have identified 3 Virgo galaxies experiencing global starbursts, with NMSFRs 2-4 times higher than any isolated sample galaxy, and 5 Virgo galaxies with more modest NMSFR enhancements of 1.2-2 times higher than any isolated sample galaxy. All of the starbursts and all but one of the near-starbursts are intermediate mass galaxies with $-18.2 > M_B > -19$. Some of them are in apparent binary pairs, which suggests that low-velocity tidal interactions play a role in the enhancement in SFR. All those galaxies with enhanced NMSFRs are HI normal to HI rich. A few of these galaxies in the cluster outskirts are not only HI rich, but are associated with large, extended clouds of HI, suggesting that HI accretion, perhaps combined with tidal forces, plays a role in the enhancement in SFR. One of the 3 Virgo starbursts (NGC 4299) has an H α morphology suggestive of ICM pressure, although it is also in a binary pair, and the relative roles of tidal and ICM-ISM interactions in the enhanced SFR of NGC 4294 cannot be easily determined. There is evidence, based on H α morphologies together with cluster location, that ICM-ISM interactions enhance the SFR of some Virgo galaxies, but only modestly and locally.

These results support evidence that many of

the lenticulars in $z=0$ rich clusters may indeed be stripped spirals, by demonstrating an intermediate population of small bulge spirals which are partially stripped, and misleadingly classified as Sa's. Spirals which are stripped more severely and completely, as is likely in clusters with denser ICMs and higher velocity dispersions than in Virgo, would naturally be classified as lenticulars.

In saying this we do not wish to imply that ICM-ISM stripping is the only mechanism driving lenticular formation in clusters. Some of the galaxies in Virgo with truncated H α disks are clearly much more peculiar than could be produced by ICM-ISM stripping, and have likely experienced tidal encounters or mergers. Nonetheless, these peculiar systems are very HI-deficient and exhibit no detectable outer disk star formation, and have likely been stripped by the ICM in addition to experiencing a tidal encounter. In Virgo these are less common than the purely ISM-stripped spirals, but the ratio could well be different in other clusters.

The funding for the research on the Virgo cluster and isolated spiral galaxies was provided by NSF grant AST-9322779. We thank Judy Young, Vera Rubin, Yasuhiro Hashimoto, and Shardha Jogee for valuable discussions. This research has made use of the NASA/IPAC Extragalactic Database (NED) which is operated by the Jet Propulsion Laboratory, California Institute of Technology, under contract with the National Aeronautics and Space Administration.

REFERENCES

- Abadi, M. G., Moore, B., & Bower, R. G. 1999, MNRAS, 308, 947
- Abraham, R. G., Valdes, F., Yee, H. K. C., & van den Bergh, S. 1994, ApJ, 432, 75
- Abraham, R. G., Smecker-Hane, T. A., Hutchings, J. B., Carlberg, R. G., Yee, H. K. C., Ellingson, E., Morris, S., Oke, J. B., & Rigler, M. 1996, ApJ, 471, 694
- Balogh, M. L. & Morris, S. L. 2000, MNRAS, 318, 703
- Balogh, M. L., Schade, D., Morris, S., Yee, H. K. C., Carlberg, R. G., & Ellingson, E. 1998, ApJ, 504, 75
- Balogh M. L., Morris, S. L., Yee, H. K. C., Carlberg, R. G., & Ellingson, E. 1999, 527, 54
- Balogh, M. L., Navarro, J. F., & Morris, S. L. 2000, ApJ, 540, 113

- Barnes, J. E. & Hernquist, L. 1991, ApJ, 370, L65
- Barth, A. & Shields, J. C. 2000, PASP, 112, 753
- Bennett, S.M. & Moss, C. 1998, A&A, 132, 55
- Bertola, F., Corsini, E. M., Vega Beltran, J. C., Pizzella, A., Sarzi, M., Cappellari, M., & Funes, J. G. S. J. 1999, ApJ, 519, L127
- Bicay, M. D. & Giovanelli, R. 1987, ApJ, 321, 645
- Binggeli, B., Sandage, A., & Tammann, G. A. 1985, AJ, 90, 1681 (BST)
- Boselli, A., Tuffs, R. J., Gavazzi, G., Hippelein, H. & Pierini, D. 1997, A&AS, 121, 507
- Bothun, G. D. 1982, PASP, 94, 774
- Bothun, G. D. & Sullivan, W. T. III 1980, ApJ, 242, 903
- Bravo-Alfaro, H., Cayatte, V., van Gorkom, J. H., & Balkowski, C. 2000, AJ, 119, 580
- Bravo-Alfaro, H., Cayatte, V., van Gorkom, J. H., & Balkowski, C. 2001, A&A, 379, 347
- Bravo-Alfaro, H., Cayatte, V., van Gorkom, J. H., & Balkowski, C. 2002, A&A, in press
- Butcher, H. & Oemler, A., Jr. 1978, ApJ, 219, 18
- Byrd, G. & Valtonen, M. 1990, ApJ, 350, 89
- Caldwell, N., Rose, J. A., Franx, M., & Leonardi, A. 1996, AJ, 111, 78
- Caldwell, N., Rose, J. A., & Dendy, K. 1999, AJ, 117, 140
- Cayatte, V., van Gorkom, J. H., Balkowski, C., & Kotanyi, C. 1990, AJ, 100, 604
- Cayatte, V., Kotanyi, C., Balkowski, C., & van Gorkom, J.H. 1994, AJ, 197, 1003
- Chamaraux, P., Balkowski, C., & Gérard, E. 1980, A&A, 83, 38
- Chamaraux, P., Balkowski, C., & Fontanelli, P. 1986, A&A, 165, 15
- Couch, W. J., Barger, A. J., Smail, I., Ellis, R. S., & Sharples, R. M., 1998, ApJ 497, 188
- Davies, R. L. et al. 2001, ApJ, 548, 33
- deVaucouleurs, G., deVaucouleurs, A., Corwin, H. G., Buta, R. J., Paturel, G., Fouqué, P. 1991, *Third Reference Catalog of Bright Galaxies*, (New York: Springer-Verlag)
- Devereux, N. A. 1989, ApJ, 346, 126
- Donas, J., Buat, V., Milliard, B., & Laget, M. 1990, A&A, 235, 60
- Dressler, A. 1980, ApJ, 236, 351
- Dressler, A. 1986, ApJ, 301, 35
- Dressler, A. & Gunn, J. E. 1983, ApJ, 270, 7
- Dressler, A., Oemler, A., Couch, W. J., Smail, I., Ellis, R. S., Barger, A., Butcher, H., Poggianti, B. M., & Sharples, R. M. 1997, ApJ, 490, 577
- Elmegreen, D. M., Sundin, M., Sundelius, B., & Elmegreen, B. 1991, AA, 244, 52
- Forman, W., Schwarz, J., Jones, C., Liller, W., Fabian, A. C. 1979, ApJ, 234, 27
- Gavazzi, G., Boselli, A., & Kennicutt, R. 1991, AJ, 101, 1207
- Gavazzi, G., Catinella, B., Carrasco, L., Boselli, A., Contursi, A. 1998, AJ, 115, 174
- Giovanelli, R. & Haynes, M. P. 1983, AJ, 88, 881
- Giovanelli, R., Haynes, M. P., Salzer, J. J., Wegner, G., Da Costa, L. N., & Freudling, W. 1994, AJ, 107, 2036
- Giovanelli, R., Haynes, M. P., Salzer, J. J., Wegner, G., Da Costa, L. N., & Freudling, W. 1995, AJ, 110, 1059
- González-Delgado, R. M., Pérez, E., Tadhunter, C., Vilchez, J. M., Rodríguez-Espinosa, J. M. 1997, ApJS, 108, 155
- Gourgoulhon, E., Chamaraux, P., & Fouqué, P. 1992, A&A, 255,69
- Graham, A. W. 2001, AJ, 121, 820
- Gunn, J. E. & Gott, J. R. 1972, ApJ, 176, 1
- Hameed, S. & Devereux, N. 1999, AJ, 118, 730
- Hashimoto, Y., Oemler, A., Lin, H., & Tucker, D. L. 1998, ApJ, 499, 589
- Haynes, M. P., Jore, K. P., Barrett, E. A., Broeils, A. H., & Murray, B. M. 2000, AJ, 120, 703
- Henriksen, M. J. & Byrd, G. 1996, ApJ, 459, 82
- Hernquist, L. 1992, ApJ, 400, 460
- Hernquist, L. 1993, ApJ, 409, 548
- Hernquist, L. & Quinn, P.J. 1988, ApJ, 331, 682
- Hibbard, J. E. 1995, PhD thesis, Columbia University
- Hoffman, G. L., Lu, N. Y., Salpeter, E. E., Farhat, B., Lamphier, C., & Roos, T. 1993, AJ, 106, 39
- Hoffman, G. L., Lu, N. Y., Salpeter, E. E., & Connell, B. M. 1999, AJ, 117, 811
- Hoffman, G. L., Salpeter, E. E., Farhat, B., Roos T., Williams, H. & Helou, G. 1996, ApJS, 105, 269
- Ho, L. C., Filippenko, A. V. & Sargent, W. L. 1997, ApJS, 112, 315
- Hogg, D. E., Roberts, M. S., Schulman, E., & Knezek, P. M. 1998, AJ, 115, 502

- Hubble, E. & Humason, M. L. 1931, ApJ, 74, 43
- Irwin, J. A. & Sarazin, C. L. 1996, ApJ, 471, 683
- Jogee, S. 1999, Ph.D. Thesis, Yale University
- Jones, L., Smail, I., & Couch, W.J. 2000, ApJ, 528, 118
- Keel, W. C. 1996, PASP, 108, 917
- Kenney, J. D. P. 1990, in *The Interstellar Medium in Galaxies*, H. A. Thronson & Shull, J.M. (eds.) (Dordrecht: Kluwer), p. 151
- Kenney, J. D. P., Koopmann, R. A., Rubin, V.C., & Young, J. S. 1996, AJ, 111, 152
- Kenney, J. D. P. & Koopmann, R. A. 1999, 117, 181
- Kenney, J. D. P., Rubin, V. C., Planesas, P., & Young, J. S. 1995, ApJ, 438, 135
- Kenney, J.D.P. & Young, J. 1989, ApJ, 344,171
- Kenney, J.D.P., Young, J.S. Hasegawa, T., & Nakai, N. 1990, ApJ, 353,460
- Kennicutt, R. C. 1983a, AJ, 88, 483
- Kennicutt, R. C. 1983b, ApJ, 272, 54
- Kennicutt, R. C. 1989, ApJ, 344, 685
- Kennicutt, R. C. 1998, ARA&A, 36, 189
- Kennicutt, R. C., Bothun, G. D., & Schommer, R. A. 1984, AJ, 89, 179
- Kennicutt, R. C. & Kent, S. M. 1983, AJ, 88, 1094
- Kent, S. M. 1985, ApJS, 59, 115
- Kewley, L. J., Heisler, C. A., Dopita, M. A., Lumsden, S. 2001, ApJS, 132, 37
- Kodaira, K., Watanabe, T., Onaka, T., & Tanaka, W. 1990, ApJ, 363, 422
- Koopmann, R.A. & Kenney, J.D.P. 1998, ApJ, 497, L75
- Koopmann, R. A., Kenney, J. D. P., Young, J. 2001, ApJ Supp, 135, 125
- Kristen H. & Jörsäter, S. 1996, in *Barred Galaxies, IAU Colloquium 157*, R. Buta, D. A. Crocker, and B. G. Elmegreen (eds.) (San Francisco: ASP), p. 236
- Larson, R. B., Tinsley, B. M., & Caldwell, C. N. 1980, ApJ, 237, 692
- Malin, D. 1993, *A View of the Universe* (Cambridge: Sky Publishing Corp.)
- Malin, D. 1994, in "Astronomy from Wide Field Imaging: Proceedings of IAU Symposium 161", ed. MacGillivray et al (Kluwer: Dordrecht), p. 567.
- Malkan, M. A., Gorjian, V., & Tam, R. 1998, ApJS, 177, 25
- Martin, P. & Roy, J.-R. 1995, ApJ, 445, 161
- Miller, R. H. 1988, Comm.Astrop. 13, 1
- Massey, P., Strobel, K., Barnes, J. V., & Anderson, E. 1988, ApJ, 328, 315
- Moore, B., Lake, G., & Katz, N. 1998, ApJ, 495, 139
- Moss, C. & Whittle, M. 1993, ApJ, 407, L17
- Moss, C., & Whittle, M. 2000, MNRAS, 317, 667
- Nulsen, P. E. J. 1982, MNRAS, 198, 1007
- O'Connell, R. W. 1999, Ap&SS, 267, 329
- Oemler, A. 1974, ApJ, 194, 1
- Oemler, A., Jr. 1992 in *Clusters and Superclusters of Galaxies*, A.C. Fabian (ed.) (Dordrecht: Kluwer), p. 29
- Phookun, B. & Mundy, L. G. 1995, ApJ, 453, 154
- Phillips, A.C. 1993, Ph.D. thesis
- Poggianti, B. M., Smail, I., Dressler, A., Couch, W. J., Barger, A. J., Butcher, H., Ellis, R. S., & Oemler, A., Jr. 1999, ApJ, 518, 576
- Poggianti, et al. 2001, ApJ, 563, 118
- Poggianti, B. M. 2002, preprint (astro-ph/0208181)
- Postman, M. & Geller, M. J. 1984, ApJ, 281, 95
- Quilis, V., Moore, B., & Bower, R. 2000, Science, 288, 1617
- Richter, O.-G., Sackett, P. D., & Sparke, L. S. 1994, AJ, 107, 99
- Rix, H-W, Franx, M., Fisher, D., & Illingworth, G. 1992, ApJ, 400, 5
- Rose, J. A., Gaba, A. E., Caldwell, N., & Chaboyer, B. 2001, AJ 121, 793
- Rubin, V. C., Graham, J. A., & Kenney, J. D. P. 1992, ApJ, 394, 9
- Rubin, V. C., Kenney, J. D. P., & Young, J. S. 1997, AJ, 113,1250
- Rubin, V.C., Waterman, A.H., & Kenney, J.D.P. 1999, AJ, 118,236
- Ryder, S. D. & Dopita, M. A. 1993, ApJS, 88, 415
- Sandage, A. & Bedke, J. 1994, *The Carnegie Atlas of Galaxies*, (Washington: Carnegie)
- Sandage, A. & Tammann, G. A. 1987, *A Revised Shapley-Ames Catalog of Bright Galaxies*,(Washington: Carnegie)
- Schindler, S., Binggeli, B., Böhringer, H. 1999, A&A, 343, 420
- Schneider, S. E., & Corbelli, E. 1993, ApJ, 414, 500
- Schulz, S., & Struck, C. 2001, MNRAS, 328, 185

Schweizer, F. & Seitzer, P. 1988, *ApJ*, 328, 88

Solanes, J. M., Manrique, A., Garcia-Gomez, C., Gonzalez-Casado, G., Giovanelli, R., & Haynes, M. P. 2001, *ApJ*, 548, 97

Struck, C. 1999, *Physics Reports*, 321, 1

Tschoke, D., Bomans, D. J., Hensler, G., & Junkes, N. 2001, *A&A*, 380, 40

Toomre, A. & Toomre, J. 1972, *ApJ*, 178, 623

Tully, R. B., & Shaya, E. J. 1984, *ApJ*, 281, 31

Tully, R. B. 1987, *Nearby Galaxies Catalog*, (Cambridge: Cambridge University Press)

Valluri, M. & Jog, C. J. 1990, *ApJ*, 357, 367

van den Bergh, S. 1976, *ApJ*, 206, 883

van den Bergh, S., Pierce, M.J., & Tully, R. B. 1990, *ApJ*, 359, 4

van Dokkum, P. G., Franx, M., Fabricant, D., Kelson, D. D., Illingworth, G. D. 1999, 520, 95

van Driel, W., 1987, PhD thesis, Groningen

van Driel, W. & van Woerden, H. 1989, *A&A*, 225, 317

van Driel, W. & van Woerden, H. 1991, *A&A*, 243, 71

Vollmer, B., Cayatte, V., Balkowski, C., & Duschl, W. J. 2001, *ApJ*, 561, 708

Warmels, R. H. 1988, *A&A Supp.*, 72, 19

White, D. A., Fabian, A. C., Forman, W., Jones, C., Stern, C. 1991, *ApJ*, 375, 35

Young, J.S., Allen, L., Kenney, J.D.P., Lesser, A., & Rownd, B. 1996, *AJ*, 112, 1903

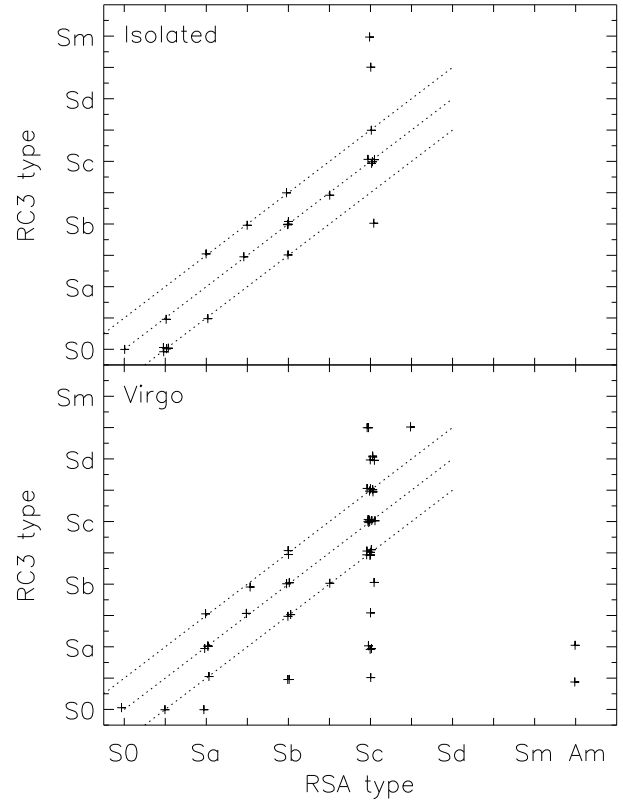


Fig. 1.— Comparison of BST/RSA/CA (x-axis) and RC3 (y-axis) Hubble types for sample galaxies. Points have been shifted a small random amount to illustrate the distribution. The lines indicate the bounds of a difference of half a type between classifications. 30% of Virgo Cluster galaxies vary in Hubble type by more than half a type between the two systems, with much of the discrepancy caused by early- versus late-type classifications.

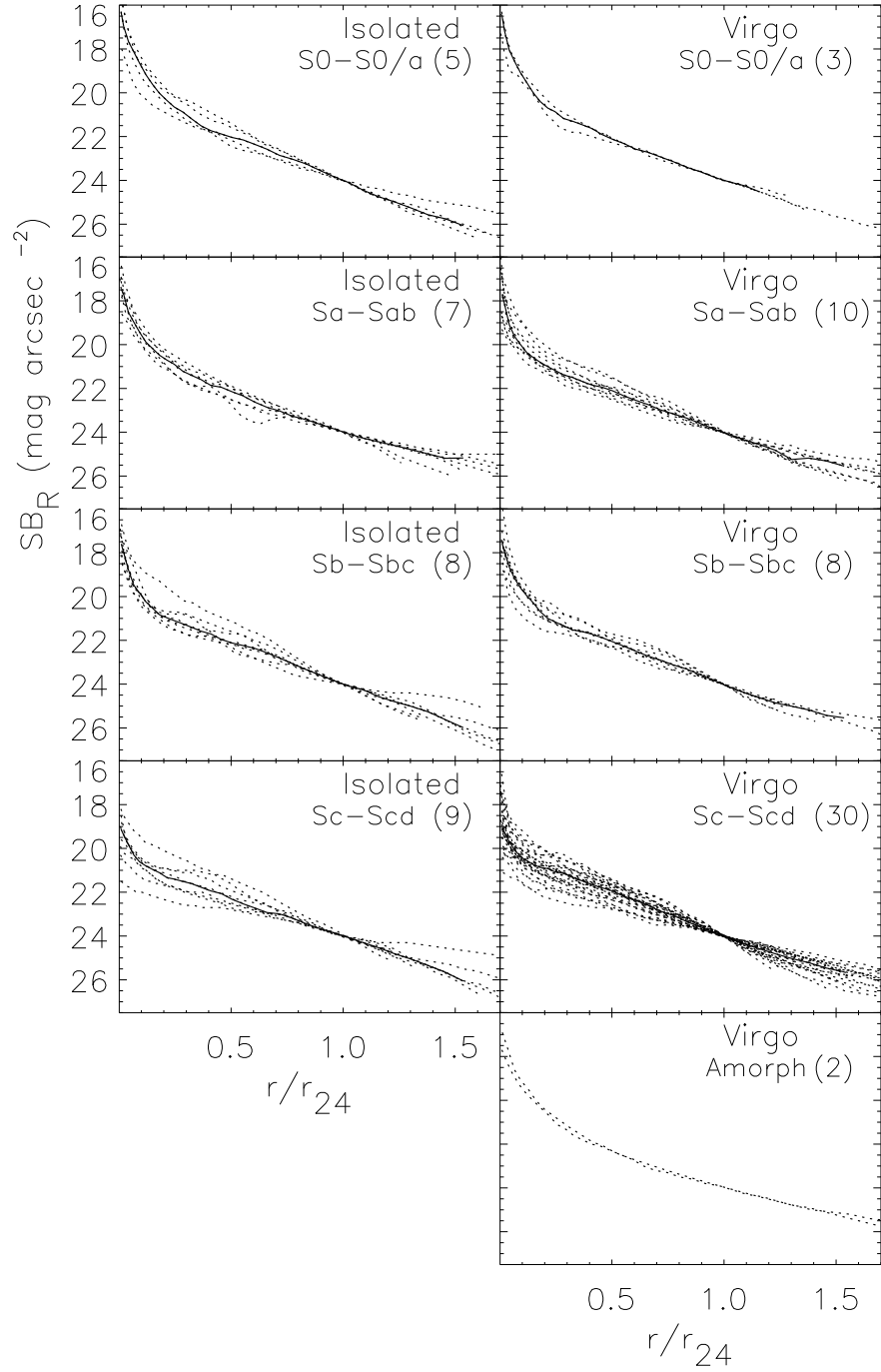


Fig. 2.— Radial R profiles normalized by r_{24} , plotted as a function of morphological type and environment. Isolated (I) profiles appear to the left, Virgo (V) to the right. The median profile for each bin is plotted as a solid line.

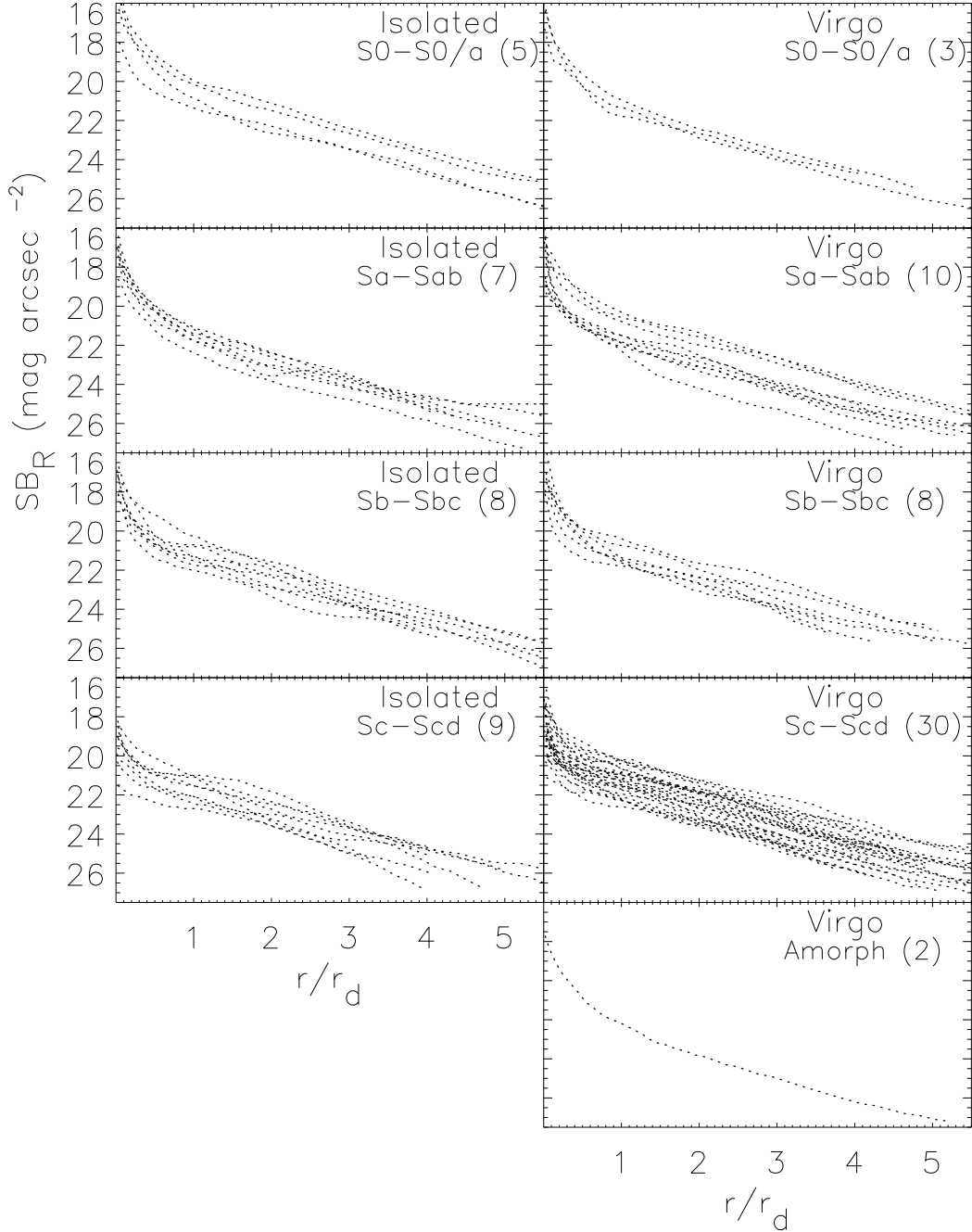


Fig. 3.— Radial R profiles normalized by disk scalelength, plotted as a function of Hubble type and environment. Isolated (I) profiles appear to the left, Virgo (V) to the right. The disk surface brightnesses of sample galaxies varies by factors up to 16 in the Hubble type bins. As a function of Hubble type, galaxies in the two different environments span similar ranges in disk surface brightness.

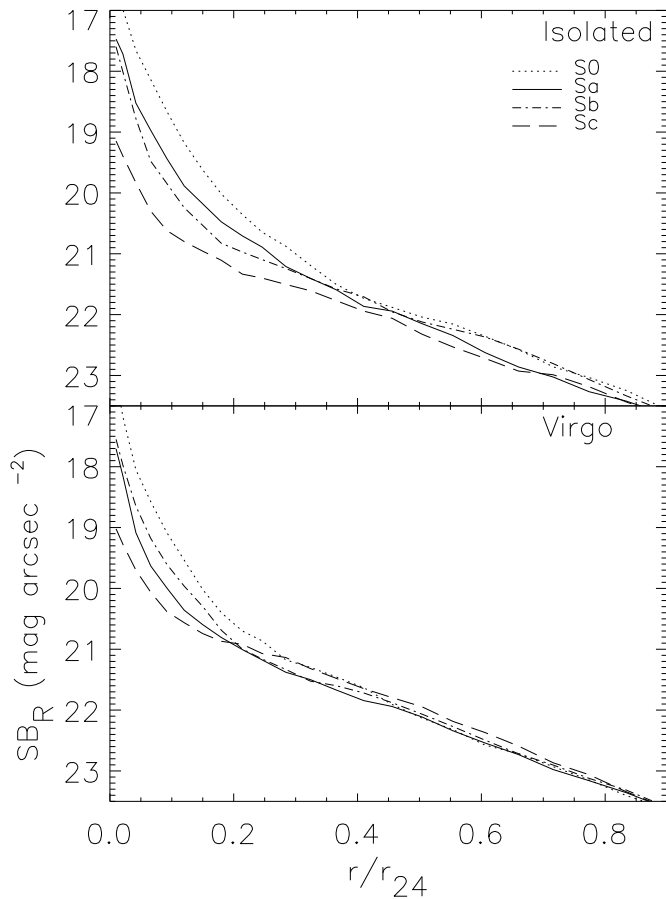


Fig. 4.— Median R profiles for isolated (a) and Virgo (b) sample galaxies. Types are indicated by line patterns. In the isolated sample, relative B/D increases from Sc to S0 types. In the Virgo sample, Sa galaxies have smaller relative B/D than Sb!

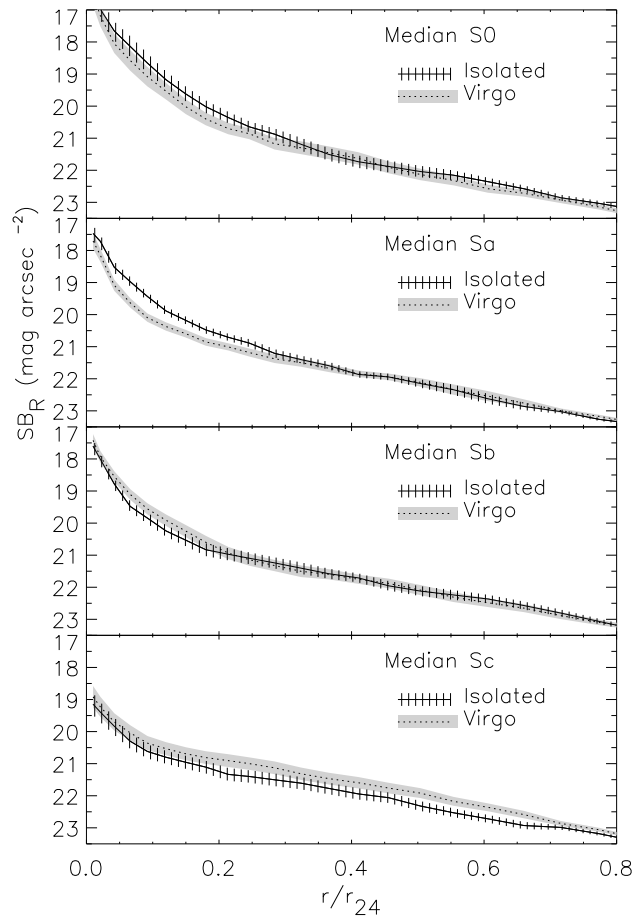


Fig. 5.— Median R profiles overplotted by type for isolated (solid) and Virgo (dotted) sample. The range between the 1st and 3rd quartiles is shown by vertical lines for the isolated sample and shading for the Virgo sample. The Virgo Sa median profile is less centrally concentrated than the isolated Sa median profile. The smaller central concentration of Virgo S0 galaxies is suggestive, but is based on only three Virgo S0 galaxies. Virgo Sc galaxies tend to have a higher surface brightness in the median.

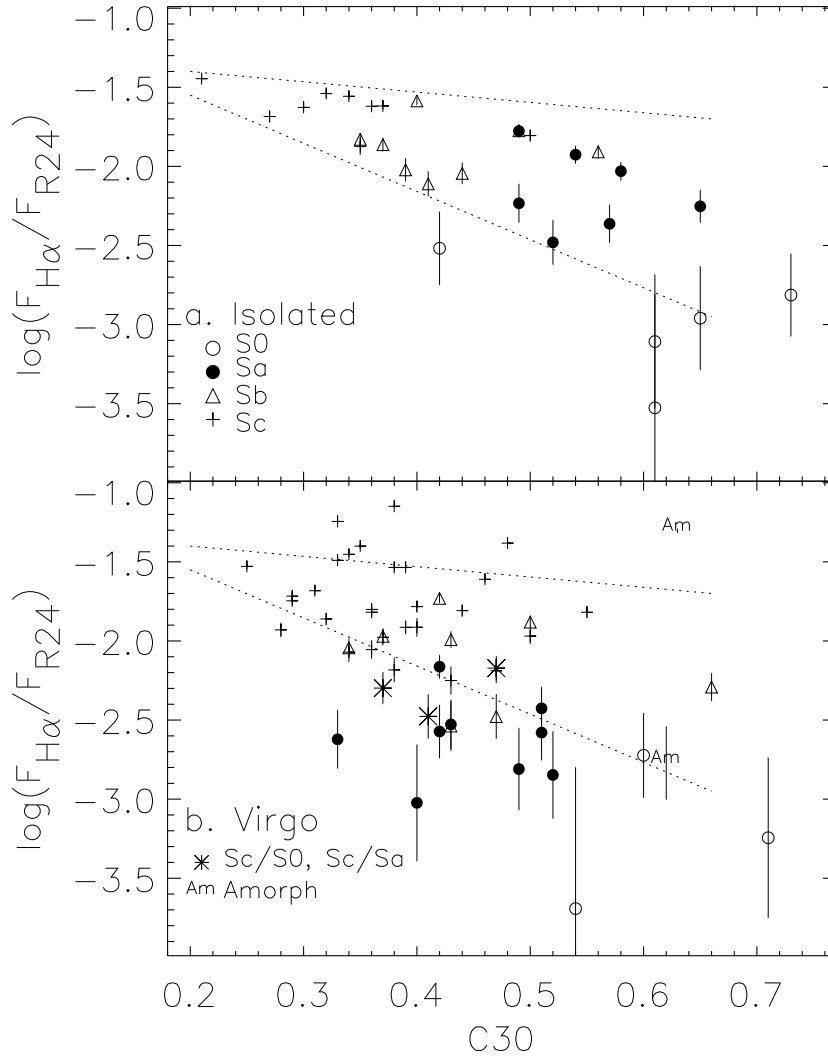


Fig. 6.— Total NMSFR’s as a function of $C30$. Symbols indicate Hubble type. Three galaxies with classifications of Sc/Sa or Sc/S0 are labeled with asterisks. Error bars are derived from the random sky error combined in quadrature with an estimated 3% continuum subtraction error. Where no error bars appear, the error bar is smaller than the symbol size. The dotted lines indicate the approximate bounds of isolated Sa-Sc galaxies. 32% of Virgo Cluster galaxies have NMSFR’s below the boundary of isolated galaxies. Many of these galaxies have been assigned early-type classifications regardless of their central concentrations. Several Virgo Cluster galaxies have enhancements in their star formation rates by factors up to 2.5.

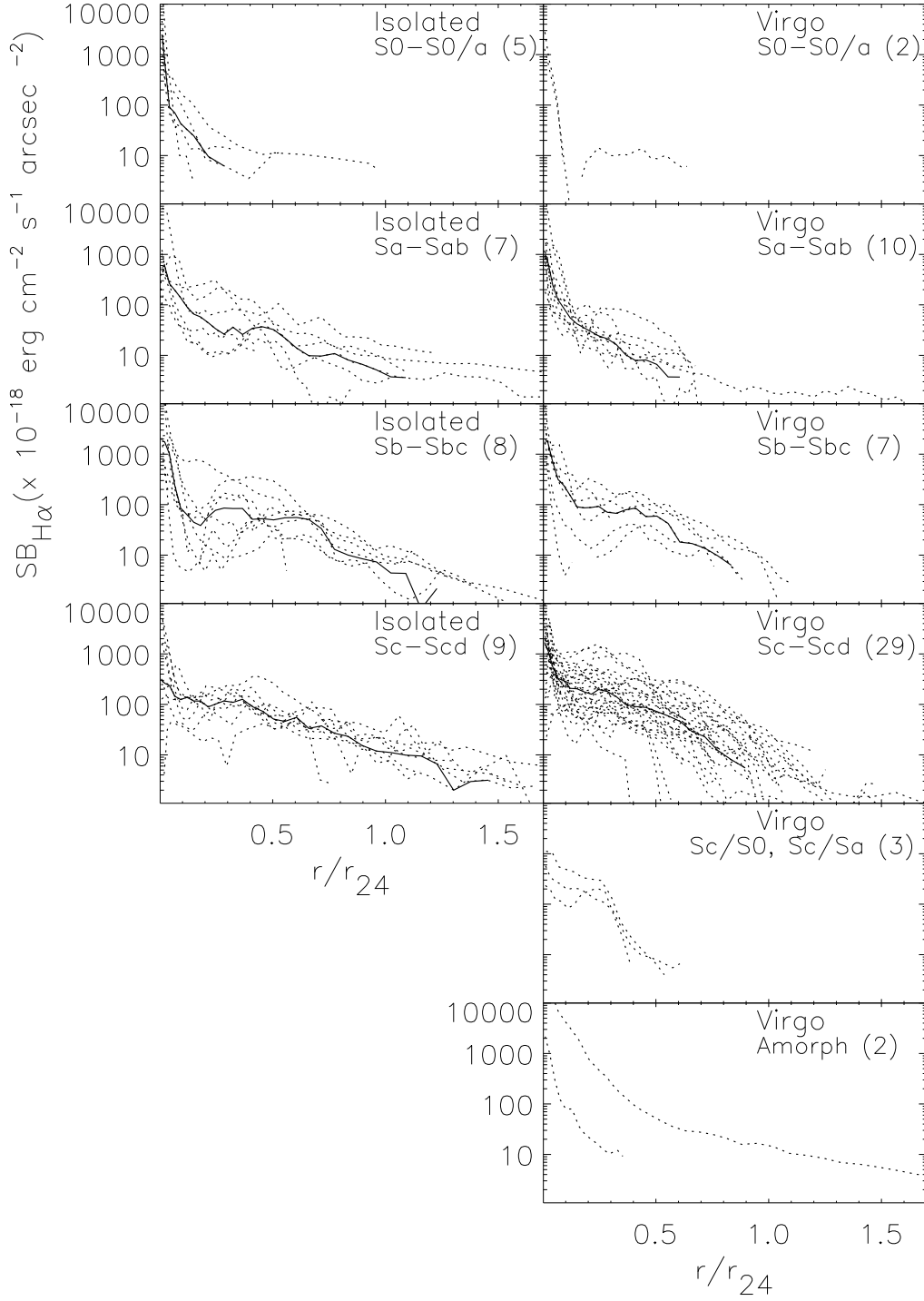


Fig. 7.— Radial $H\alpha$ profiles of sample galaxies, normalized by r_{24} . The profiles extend to the radius of the last visible HII region. The median radial profile for each bin is shown as a solid line.

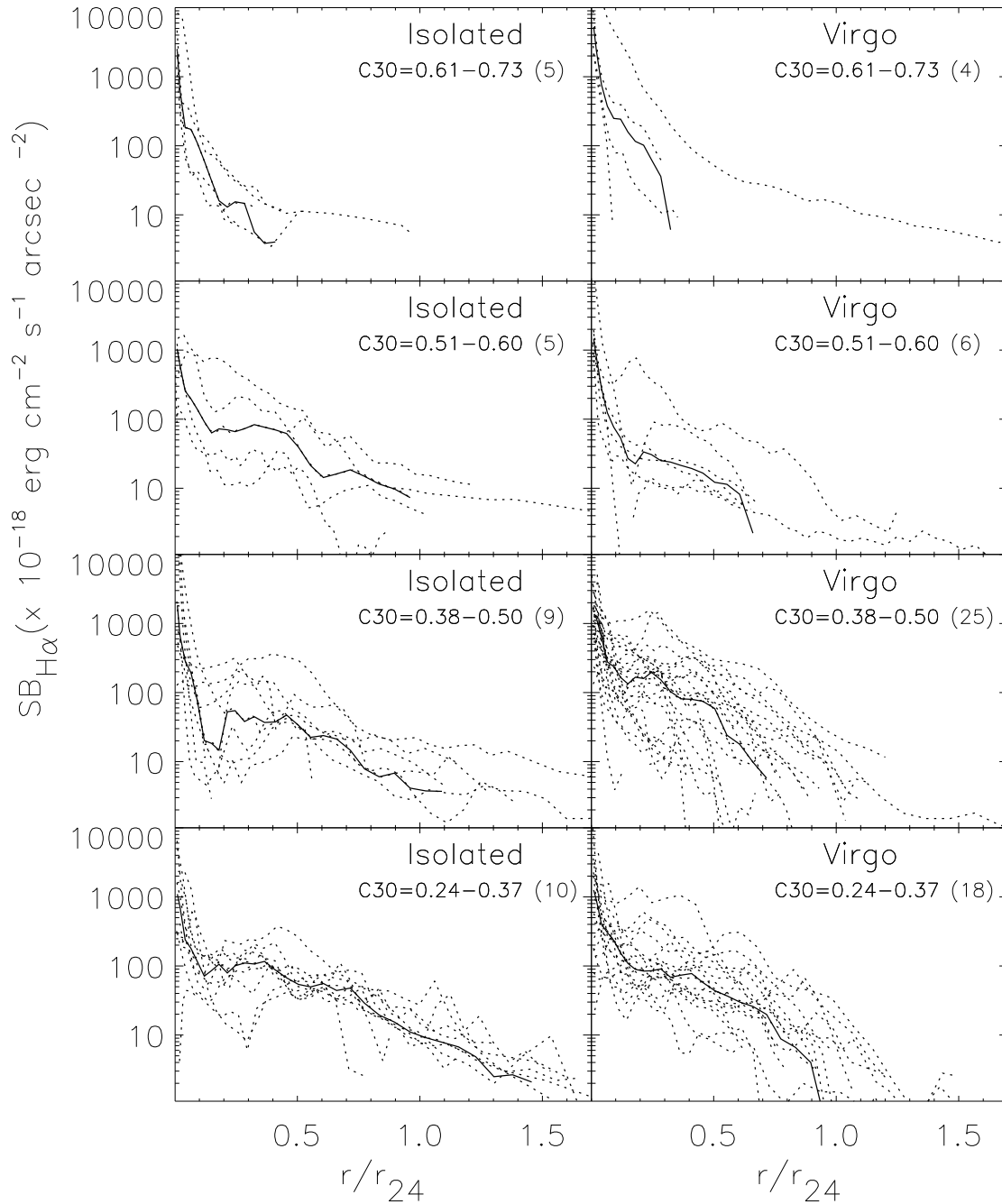


Fig. 8.— Radial H α profiles grouped by central R light concentration of the indicated ranges. The median radial profile line for each bin is shown as a solid line.

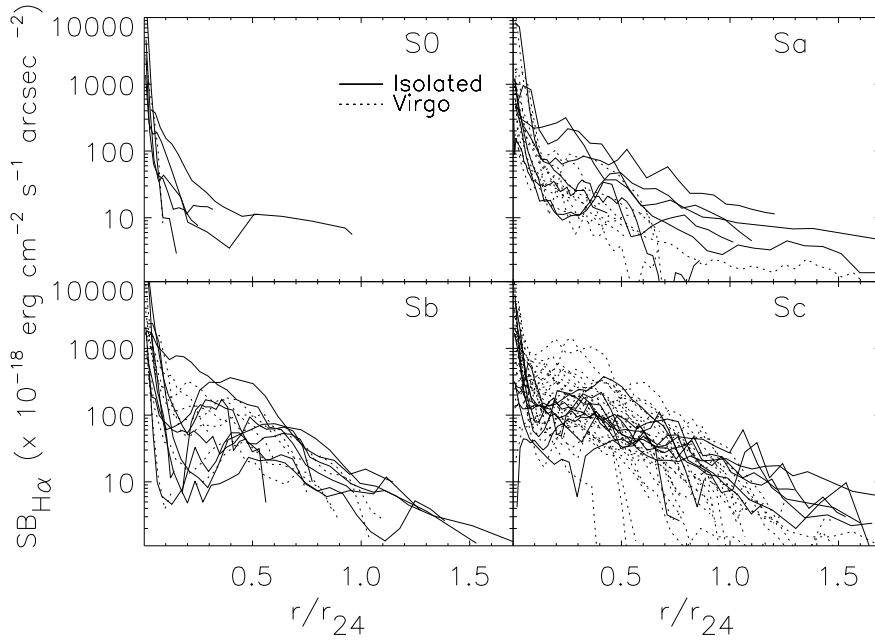


Fig. 9.— $H\alpha$ profiles, normalized by r_{24} , overplotted for the two environments. Virgo galaxies, represented by dotted lines, tend to have truncated $H\alpha$ disks with sharply declining outer profiles. Several Sc galaxies have emission in the inner $0.5r_{24}$ which is enhanced compared to isolated Sc's.

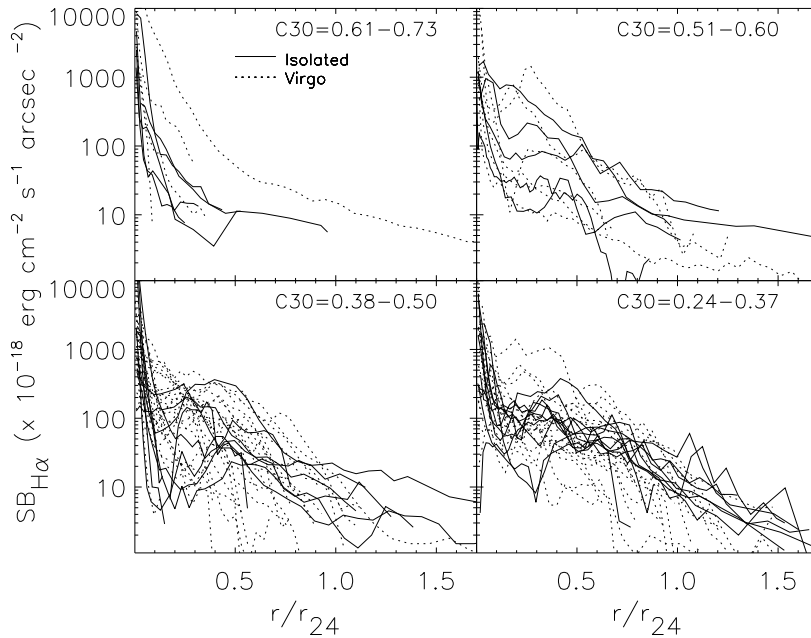


Fig. 10.— Radial $H\alpha$ profiles grouped by central R light concentration of the indicated ranges and overplotted for the two environments. Virgo galaxies, represented by dotted lines, show truncated $H\alpha$ disks compared to isolated galaxies of similar R light concentration. Galaxies classified as Sc with enhanced inner emission (see Figure 9) are spread over the 0.51-0.60, 0.38-0.50, and 0.24-0.37 bins.

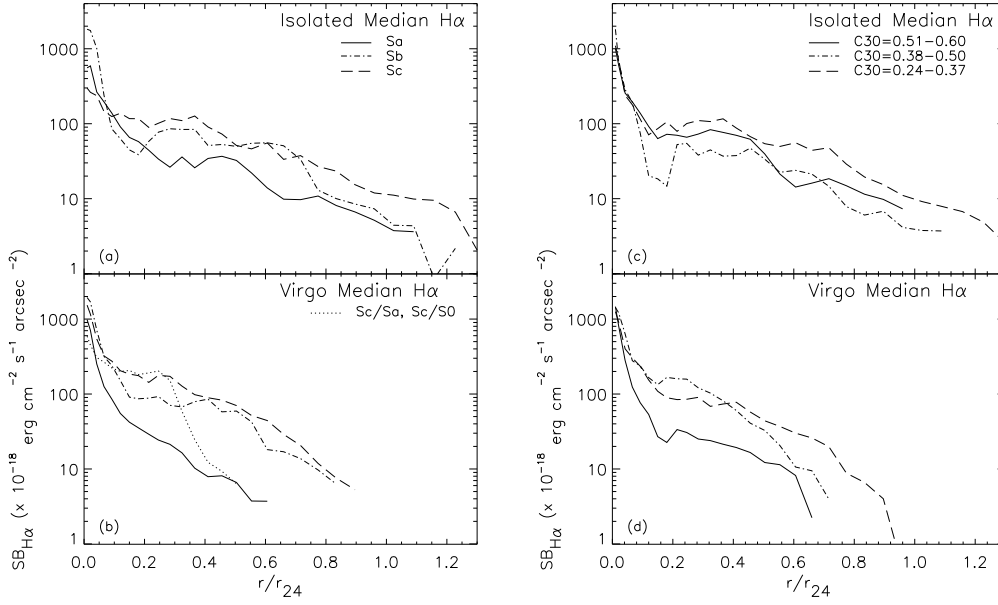


Fig. 11.— Median H α radial profiles for isolated and Virgo galaxies as a function of Hubble type (a,b) and C30 (c,d). Despite the scatter by factors of 10-100 in the individual profiles, isolated median profiles for different Hubble types or different C30 agree to within a factor of 3 over most of the galaxy disk. Virgo Cluster median profiles show the effect of truncation in the H α disks.

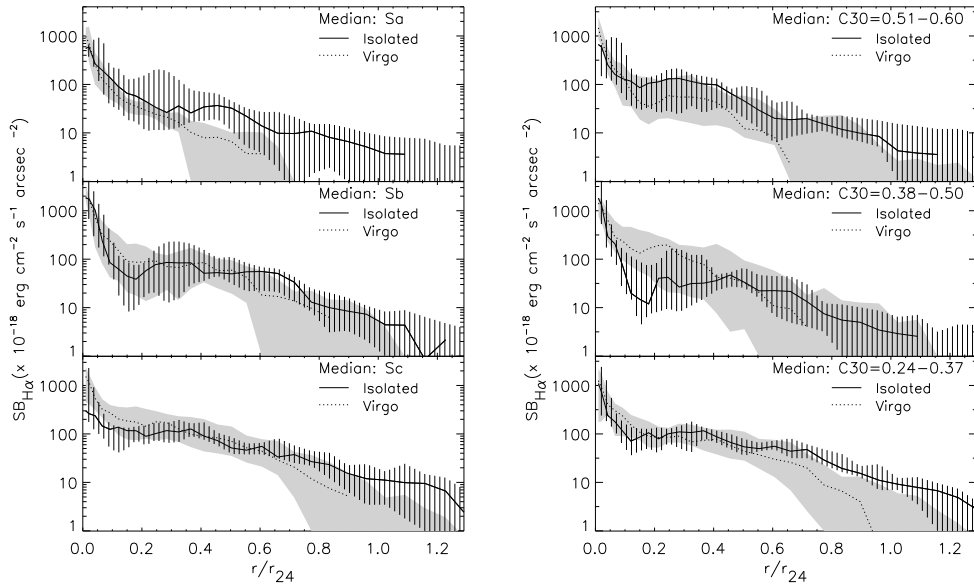


Fig. 12.— Median H α radial profiles for isolated (solid) and Virgo (dotted) galaxies as a function of Hubble type (left) and C30 (right). The range between the first and third quartiles is shown as vertical lines for the isolated galaxies and shading for the Virgo Cluster galaxies. The Virgo Cluster galaxies have truncated star-forming disks in all bins. The inner regions of Virgo spirals have normal to enhanced NMSFR's in most bins.

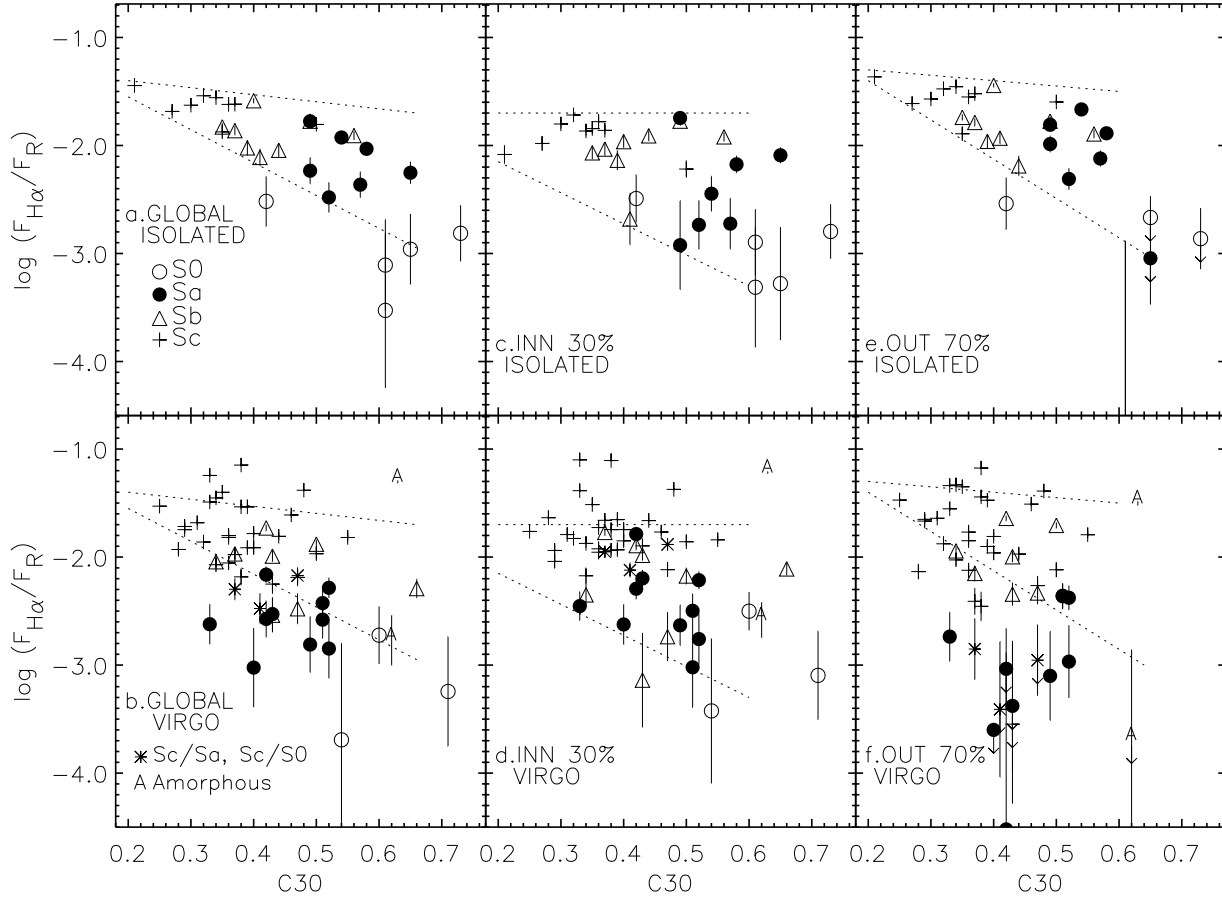


Fig. 13.— Normalized NMSFR's as a function of C30. The values for the total star formation disk are given in a (isolated) and b (Virgo), the values for the inner 30% of the optical disk in c (isolated) and d (Virgo), and the values for the outer 70% of the disk in e (isolated) and f (Virgo). Error bars are derived from the random sky error combined in quadrature with an estimate of the continuum subtraction error. Where no error bars appear, the error bar is smaller than the symbol size. The lines indicate the approximate bounds of isolated Sa-Sc galaxies. Typically, Virgo spirals with reduced star formation have reduced outer star formation, but similar or enhanced inner star formation compared to isolated galaxies. Thus the main cause of the reduction of star formation is truncation of the star-forming disk. (A similar figure appeared in Koopmann & Kenney 1998.)

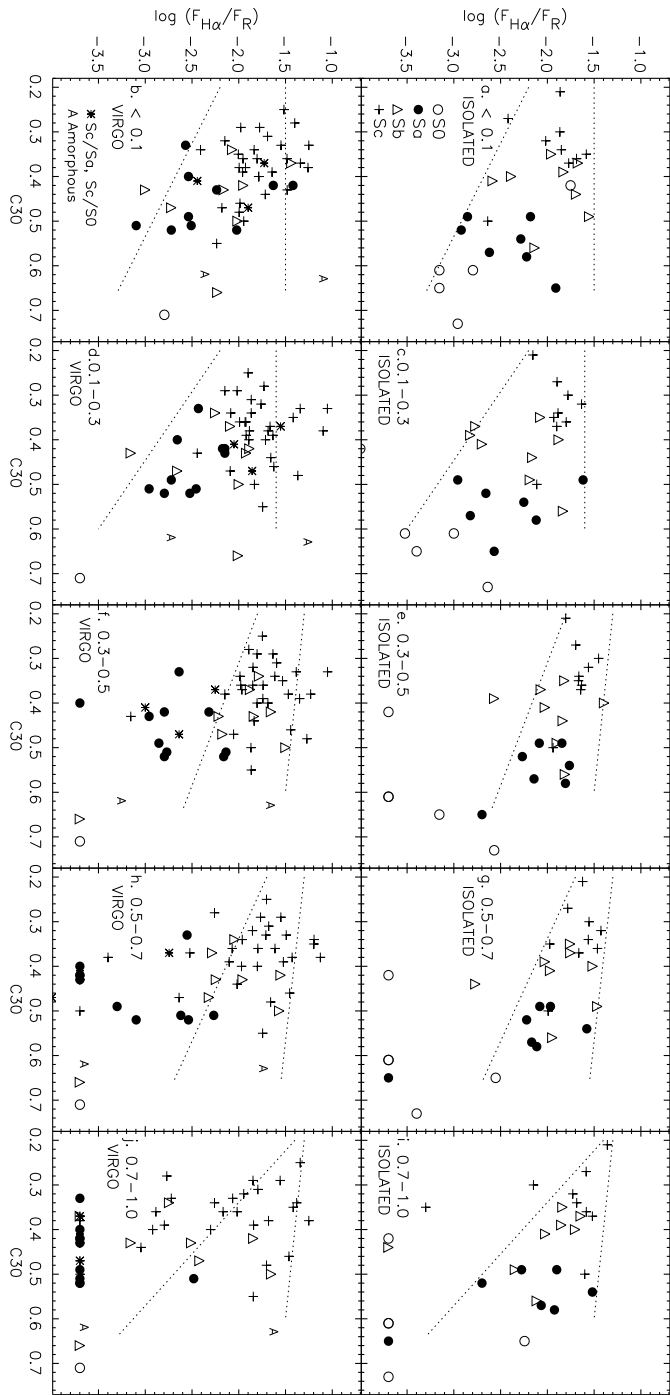


Fig. 14.— Normalized NMSFR's as a function of C30 for the indicated bins. Symbols which lie at the base of the plot represent values which are below the lower y limit of the plot. The lines indicate the approximate bounds of isolated Sa-Sc galaxies. Within 10% of the optical disk and between 10 and 30% of the optical disk, Virgo galaxies have normal to enhanced normalized H α fluxes. Between 30 and 50% of the optical disk, 15 of the Virgo galaxies have reduced star formation. Note that most of the Virgo galaxies classified as Sa have reduced star formation in this radial bin. The numbers of Virgo galaxies with star formation rates less than their isolated counterparts progressively increases as larger radius radial bins are examined. Even many of the Sc galaxies have truncated outer disks. Notice the lack of earlier-type galaxies with similar NMSFR's to isolated in the outer bins.

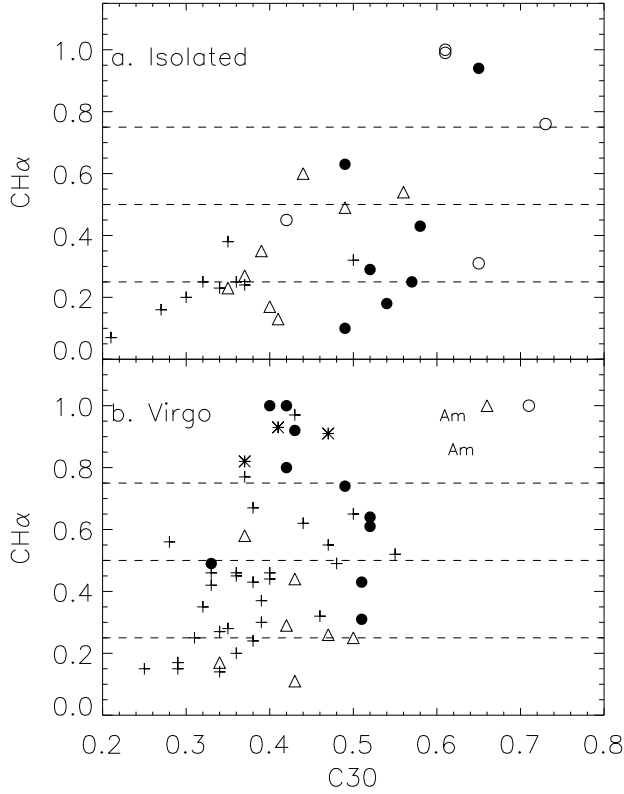


Fig. 15.— The central R light concentration versus the H α concentration for the isolated (a) and Virgo (b) samples. The dashed lines indicate the boundaries of galaxies with all, half, and one-quarter of their emission within $0.3 r_{24}$. Symbols indicate Hubble type, with coding the same as in Figure 13. Virgo Cluster galaxies tend to have a larger percentage of their star formation within $0.3r_{24}$. About 25% of Virgo Cluster galaxies have more than three-quarters of their star formation within $0.3r_{24}$ compared to only 4% of isolated galaxies. Note that no isolated low C30 ($C30 \leq 0.5$) galaxy has more than 65% of its star formation within $0.3r_{24}$, but that about 25% of low C30 Virgo Cluster galaxies do. This is largely due to the truncated outer star forming disks in Virgo Cluster galaxies.

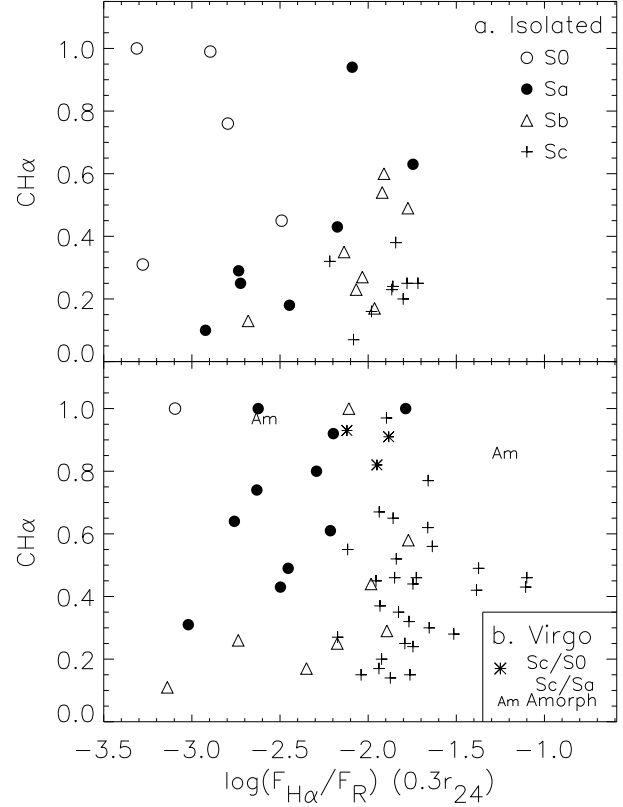


Fig. 16.— H α concentration vs the inner normalized H α flux for the isolated (a) and Virgo (b) samples. Symbols indicate Hubble type. The inner star formation rates of Virgo Cluster spirals are similar to those of isolated spirals, but Virgo Cluster galaxies tend to have higher CH α . Thus Virgo spirals tend to have normal-enhanced inner star formation combined with truncated outer disks.

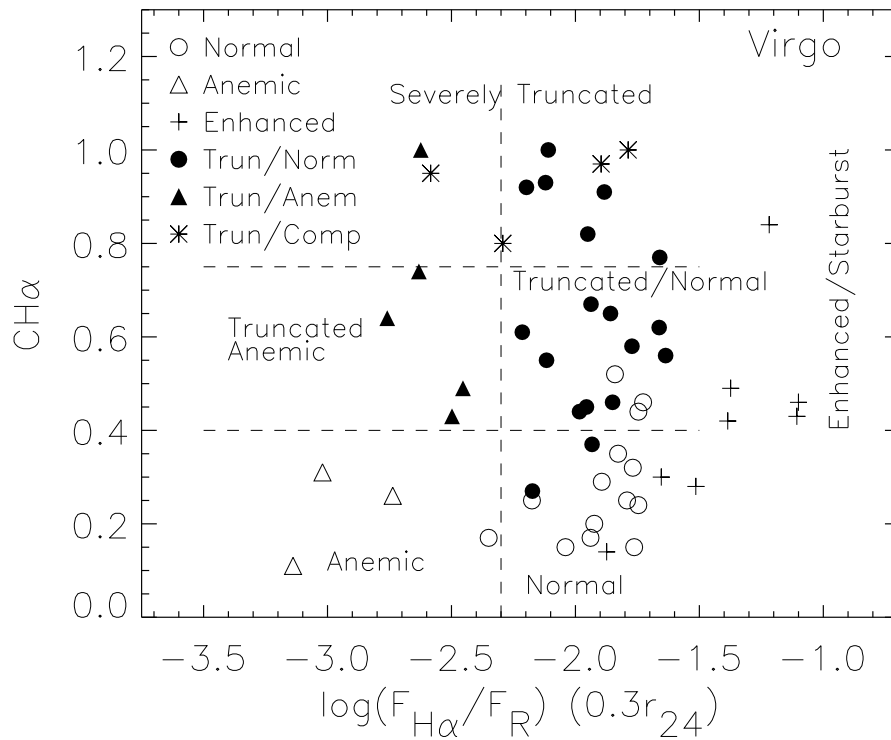


Fig. 17.— H α concentration vs the inner normalized H α flux for the Virgo sample. The symbols indicate the H α morphology type, which were defined by the radial distribution of star formation (Section 7). The lines indicate the approximate boundaries of the classes in terms of H α concentration and inner star formation rates.

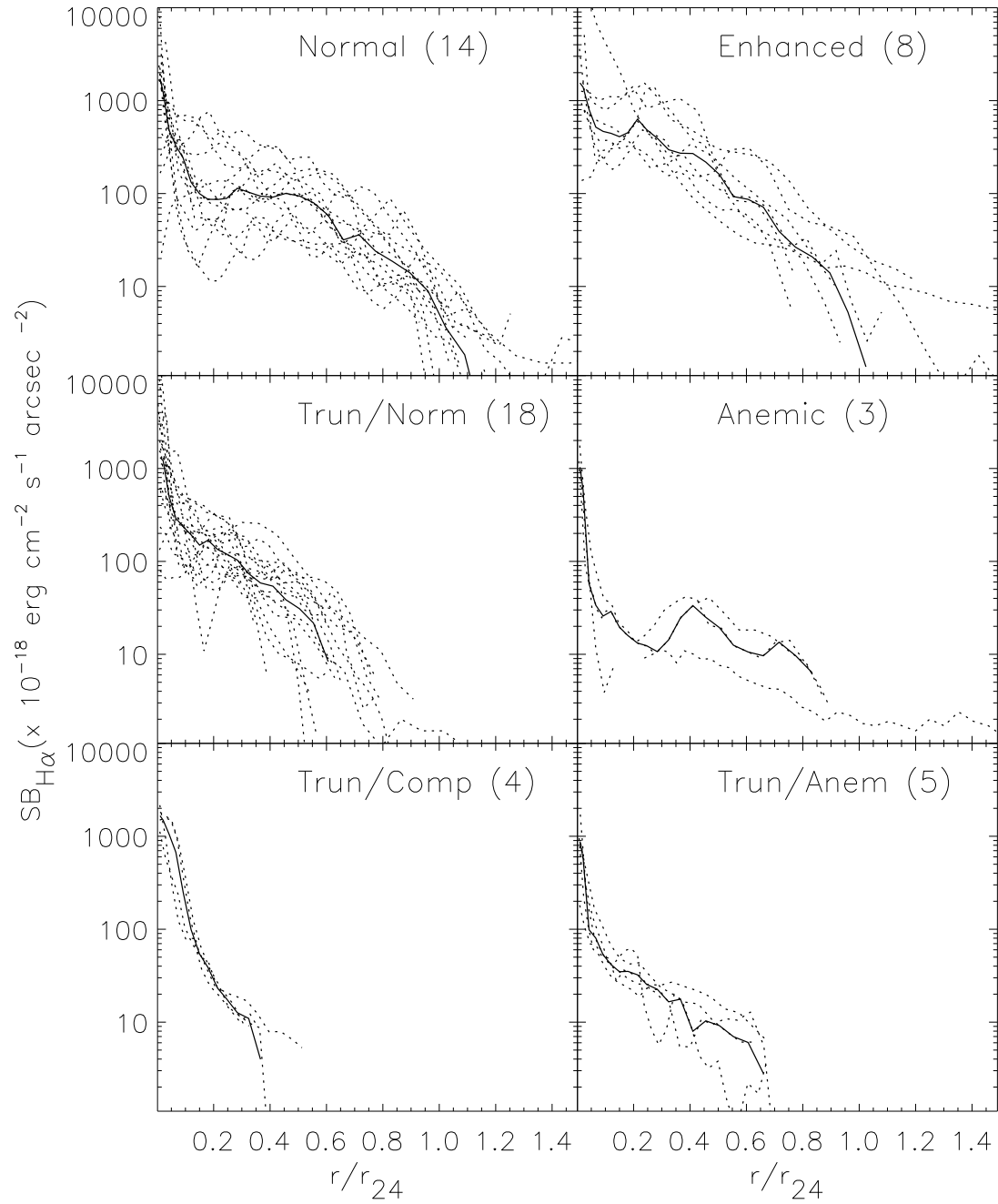


Fig. 18.— H α radial profiles as a function of the star formation categories defined in section 7. The median of each category is overplotted as a solid line.

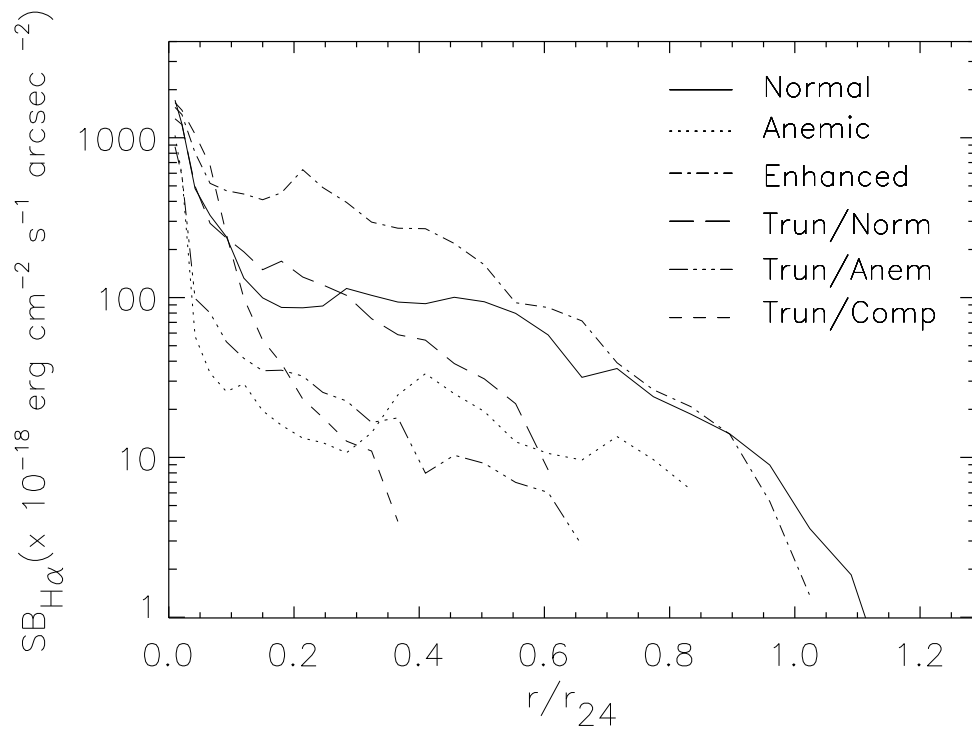


Fig. 19.— Median H α radial profiles for each star formation morphology category, as defined in Section 7.

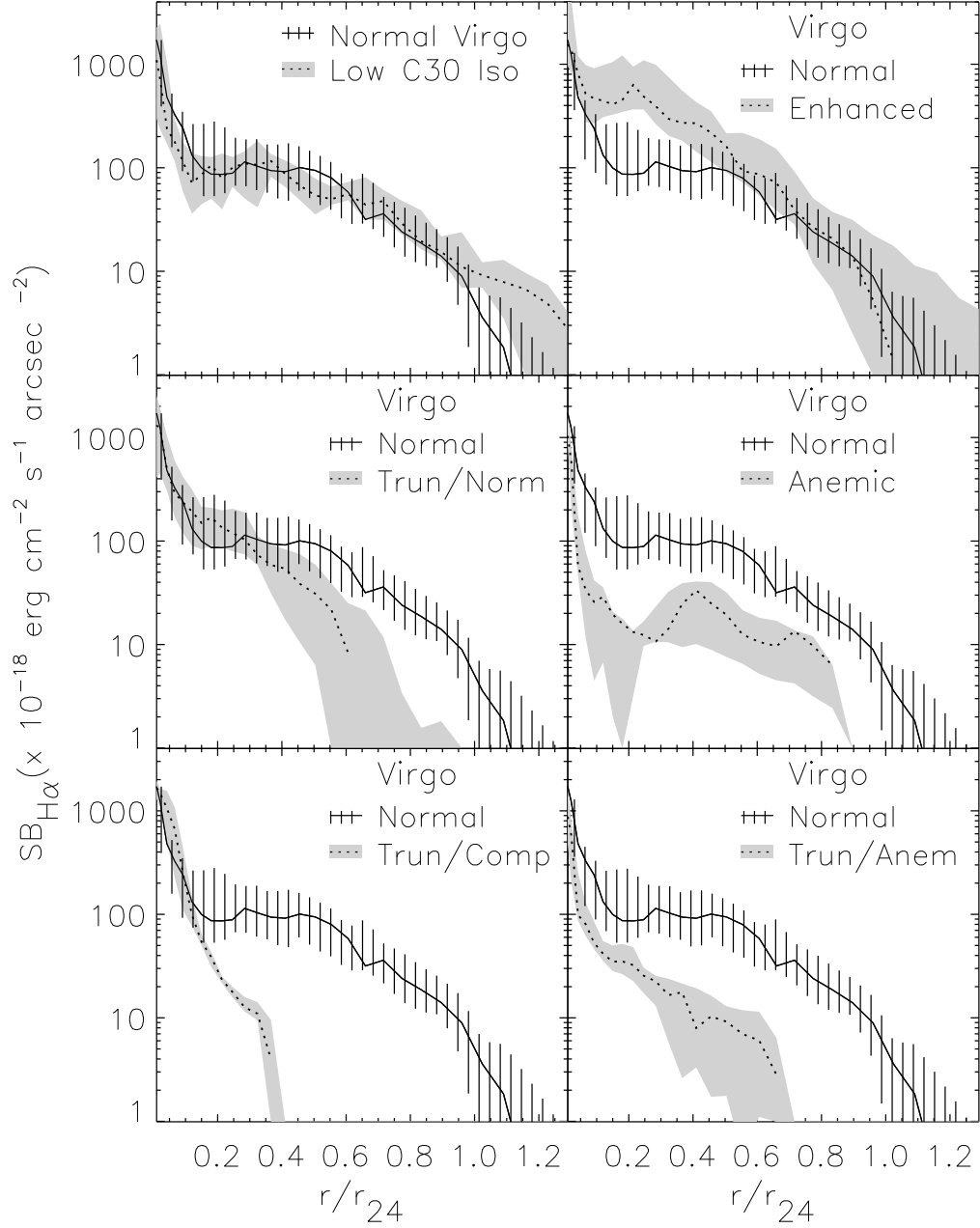


Fig. 20.— Median $H\alpha$ radial profiles for each star formation morphology category plotted with the 1st and 3rd quartile range. In each panel, the normal Virgo spiral category is compared with the indicated category. The upper left panel shows a comparison between the normal Virgo spiral median and the low-C30 isolated spiral median.

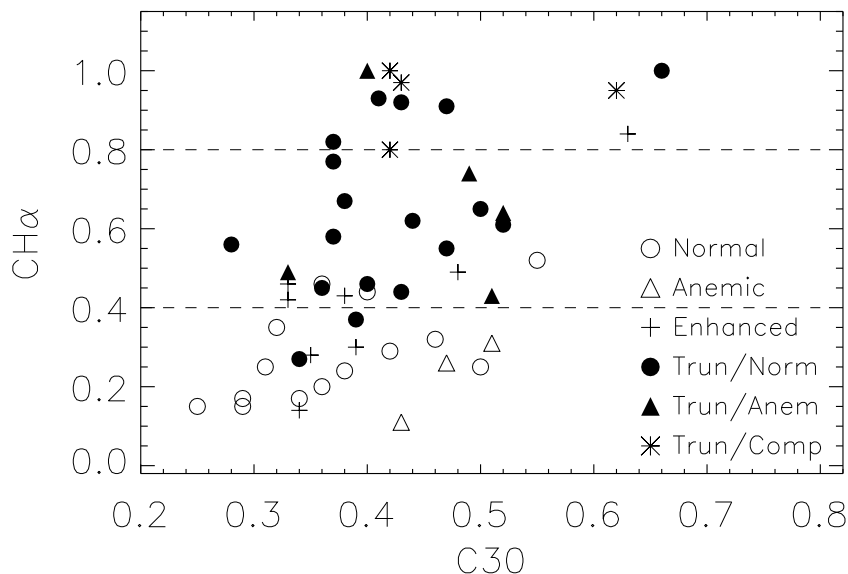


Fig. 21.— The location of different star formation morphologies as a function of C30 and $\text{CH}\alpha$, showing little correlation between C30 and the star formation morphology.

Fig. 22.— Properities of three Virgo Cluster galaxies with anemic star formation: NGC 4394, NGC 4548, and NGC 4698. These galaxies have reduced star formation rates across the disk. In this and the following figures, the R and $\text{H}\alpha$ images and surface photometry profiles are given for each galaxy. The images are displayed on a log scale, with north up and east to the left. The RSA/BST and RC3 morphological types are indicated. In the surface photometry plots, the R (solid) and $\text{H}\alpha$ (dotted) profiles are plotted as a function of radius in arc seconds. The $\text{H}\alpha$ profiles were superposed using an arbitrary zeropoint of 18.945. The isophotal radius at $24 \text{ mag arcsec}^{-2}$, r_{24} , is indicated with an arrow and an error bar. The $\text{H}\alpha$ profile is cut at the radius of the outermost HII region. Diamonds on the $\text{H}\alpha$ profile indicate annuli for which the sky uncertainty was greater than the azimuthally averaged signal. At lower left, the locations of these galaxies in the C30-NMSFR plot are indicated by large circles. Note how the indicated galaxies fall at low star formation rates globally, in the inner 30% of the disk, and in the outer 70% of the disk. At lower right the galaxy positions are shown with respect to the other members in the Virgo Cluster sample.

Fig. 23.— The Virgo Cluster galaxies NGC 4299, NGC 4532, and NGC 4383 have the highest $\text{H}\alpha$ emission in the Virgo sample, with global values enhanced by 2-3 times above those of isolated spirals. There is evidence for tidal forces and/or gas accretion in all three cases. NGC 4299 may plausibly be experiencing an ICM-ISM interaction. The locations of these galaxies are indicated in the C30-NMSFR plot by the large open circles and in the position plots by large font lettering. An additional 5 galaxies have normalized massive star formation rates 20-50% higher than galaxies in the isolated sample. These galaxies are: NGC 4294, NGC 4303, NGC 4519, NGC 4561, and NGC 4713. The locations of these galaxies are indicated in the C30-NMSFR by the smaller open circles and in the position plot by the smaller font lettering. Note the relatively high position of all of the enhanced galaxies in the C30-NMSFR diagram and that these galaxies tend to be located in the cluster outskirts. All of these galaxies except NGC 4303 have $-18.2 > M_B > -19$.

Fig. 24.— Three Virgo Cluster galaxies with severely truncated star-forming disks (within $0.3-0.4r_{24}$): NGC 4580, IC 3392, and NGC 4405. These galaxies have regular stellar disks. Their $H\alpha$ morphologies show symmetric rings of star formation near the truncation radius. The positions of these galaxies and their line-of-sight velocities are consistent with orbits with a large radial component. These galaxies have likely been stripped by the ICM.

Fig. 25.— Three Virgo Cluster galaxies with star forming disk truncated within $0.4r_{24}$, but normal inner star formation rates: NGC 4351, NGC 4457, and NGC 4569. The $H\alpha$ emission in NGC 4351 is offset from the apparent center in R. NGC 4457 shows a regular R morphology combined with an asymmetric $H\alpha$ spiral arm morphology. NGC 4569 has a ring of star formation at about $0.3r_{24}$ and a detached arm of HII regions.

Fig. 26.— Three Virgo Cluster galaxies with truncated star forming disks, but normal star formation within the truncation radius: NGC 4689, NGC 4413, and NGC 4571. In addition, the locations of the remaining 7 truncated/normal galaxies are indicated in the C30-NMSFR plot with smaller circles and in the position plot with smaller fonts. Most of these galaxies are located within a 5 degree radius from M87.

Fig. 27.— Three Truncated/Anemic Virgo Cluster galaxies: NGC 4380, NGC 4293, and NGC 4450. These galaxies have truncated star-forming disks and anemic inner star formation rates. NGC 4380 and NGC 4293 are classified as Sa galaxies, but both have a small central light concentration.

Fig. 28.— Three Truncated/Compact Virgo spirals: NGC 4424, NGC 4064, and NGC 4606. These galaxies have severely truncated star-forming disks. Star formation is located in several circumnuclear HII complexes, which have a non-axisymmetric distribution. The $H\alpha$ surface brightnesses of NGC 4424 and NGC 4064 within $0.1r_{24} \sim 0.8$ kpc are among the highest in the Virgo and isolated samples. The gas in these galaxies has low line-of-sight velocities (Rubin et al. 1999). NGC 4424 also displays shell-like features and banana-shaped isophotes. These galaxies are likely to be products of a merger or close tidal interaction.

Fig. 29.— Three Virgo Cluster galaxies which show locally enhanced $H\alpha$ emission in asymmetric arcs near the edge of the star-forming disk: NGC 4178, NGC 4189 and NGC 4654. NGC 4380 (Figure 27) and pair galaxies NGC 4298 and NGC 4647 (Figure 7.6) also show similar outer arcs of star formation. However this local enhancement is not significant enough to increase the NMSFR over the whole radial bin, as shown at lower left. (Note that, unlike preceding figures, the plot at lower left depicts the NMSFR's within three smaller radial bins outside $0.3r_{24}$.)

Fig. 30.— Three apparent pairs in the Virgo Cluster: NGC 4298/4302, NGC 4647/4649 and NGC 4567/4568. These galaxies appear close in projection and have similar line-of-sight velocities. Another apparent pair is NGC 4294/4299 (see Figure 23). The locations of the 4 pairs are shown in the C30-NMSFR and position plots. Note that a few galaxies are enhanced globally (NGC 4294 and NGC 4299) and all have substantial inner star formation.

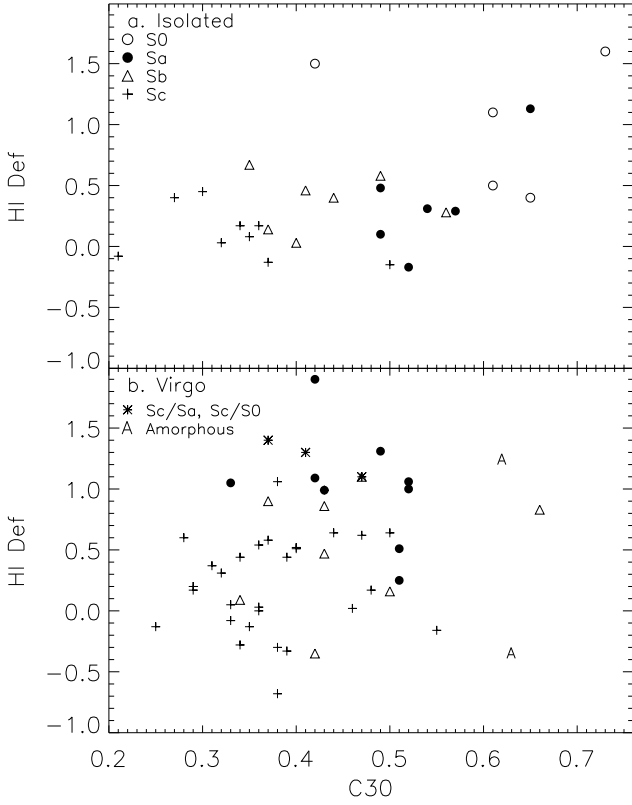


Fig. 31.— HI deficiency as a function of C30 for the isolated (top) and Virgo (bottom) galaxies. The HI deficiency values are taken from Koopmann et al. (2001) and Koopmann & Kenney (2001) and were calculated following the prescription set out in Giovanelli & Haynes (1983). On this scale, a galaxy with normal HI content has an HI deficiency value of 0, while a galaxy which is depleted by a factor of 10 has an HI deficiency value of 1.0.

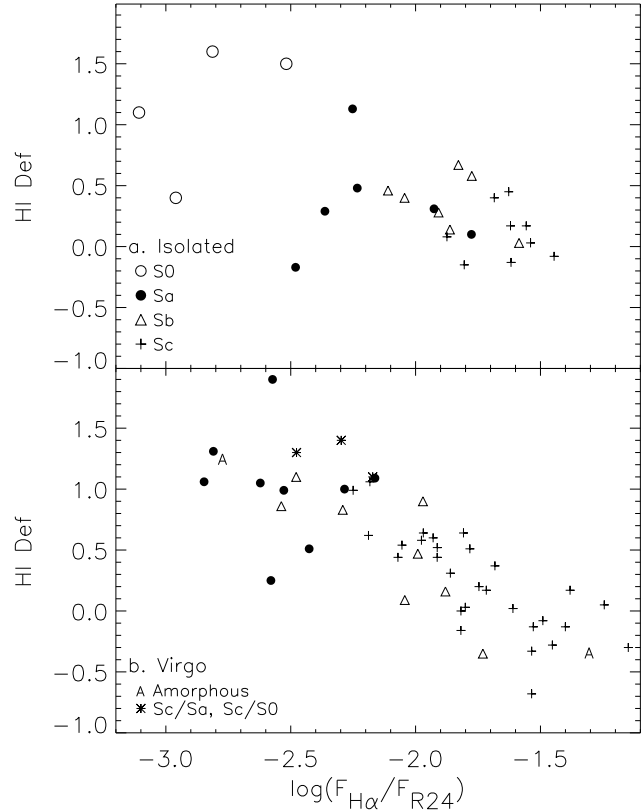


Fig. 32.— HI deficiency as a function of total normalized star formation rates for the isolated (top) and Virgo (bottom) galaxies. There is a correlation between total normalized H α fluxes and HI deficiencies in the Virgo sample, markedly stronger than that between C30 and HI deficiency. This suggests that gas-poor galaxies with reduced gas tend to be classified as early-type spirals.

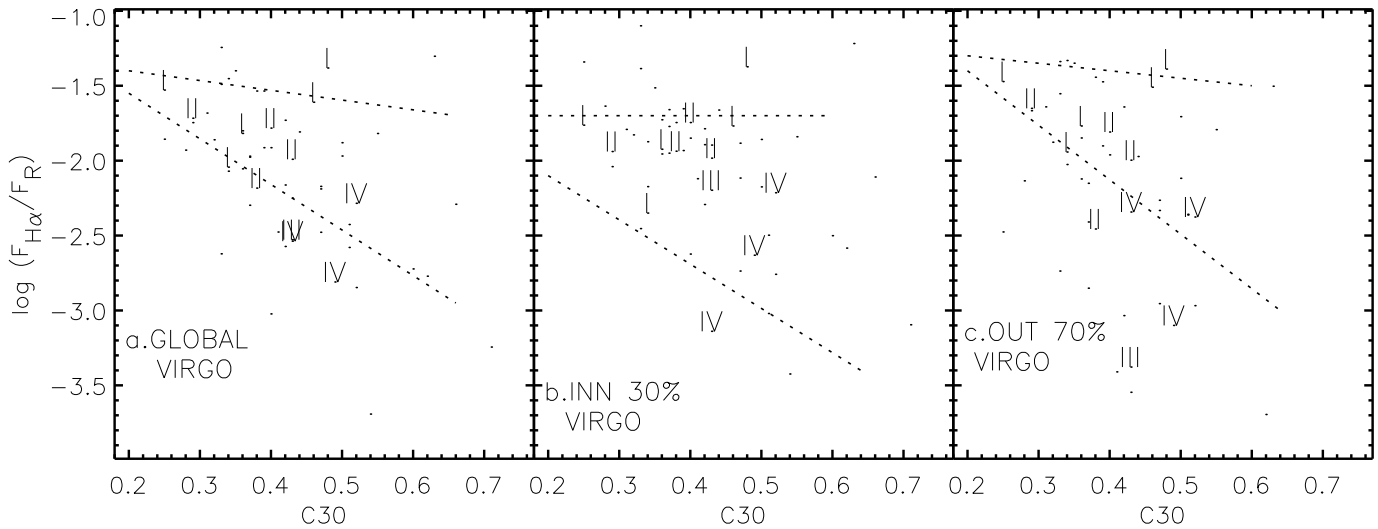


Fig. 33.— Figure 13 replotted to show locations of galaxies in Cayatte et al. Groups I, II, III, IV.

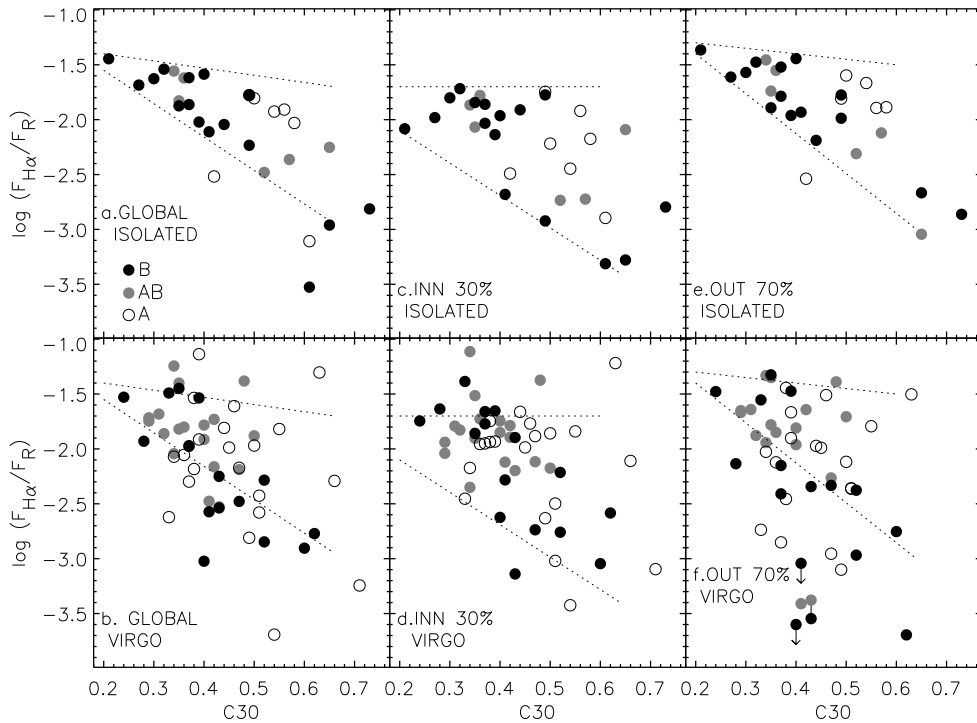


Fig. 34.— Same as Figure 13, but with symbols indicating whether the galaxy is strongly barred (black filled circles), weakly barred (grey-filled circles), or not barred (open circles), according to classifications in RC3. These plots show no strong correlation between placement of the galaxies in C30-NMSFR space and the presence of a bar.

TABLE 1
 MEDIAN NORMALIZED MASSIVE STAR FORMATION RATES

Type	Isolated (#) $\frac{F_{H\alpha}}{F_{R24}}$	Virgo(#) $\frac{F_{H\alpha}}{F_{R24}}$	$\frac{\text{Isolated}}{\text{Virgo}}$
Total			
S0-S0/a	-2.96 ± 0.29 (5)	-3.24 ± 0.49 (3)	-
Sa-Sab	-2.21 ± 0.27 (7)	-2.53 ± 0.24 (10)	2.1* (0.8)
Sb-Sbc	-1.87 ± 0.15 (8)	-2.02 ± 0.21 (8)	1.4 (0.4)
Sc-Scd	-1.62 ± 0.10 (9)	-1.78 ± 0.30 (29)	1.4 (0.3)
Sc-Scd < 6°		-1.81 ± 0.28 (22)	1.5
.61 ≤ C30 < 0.73	-2.96 ± 0.48 (5)	-2.47 ± 0.96 (4)	-
.51 ≤ C30 ≤ 0.60	-2.01 ± 0.16 (5)	-2.41 ± 0.40 (5)	2.5 (1.7)
.38 ≤ C30 ≤ 0.50	-2.00 ± 0.24 (9)	-1.99 ± 0.40 (25)	1.0 (0.4)
.24 ≤ C30 ≤ 0.37	-1.62 ± 0.11 (10)	-1.80 ± 0.28 (19)	1.5 (0.3)
Inner 30%			
Sa-Sab	-2.44 ± 0.43	-2.47 ± 0.43	1.1 (0.9)
Sb-Sbc	-2.00 ± 0.14	-2.06 ± 0.21	1.1 (0.3)
Sc-Scd	-1.86 ± 0.12	-1.78 ± 0.33	0.8 (0.2)
Sc-Scd < 6°	-	-1.83 ± 0.28	1.1
.61 ≤ C30 < 0.73	-2.89 ± 0.54	-2.29 ± 0.86	-
.51 ≤ C30 ≤ 0.60	-2.44 ± 0.37	-2.48 ± 0.44	1.1 (1.0)
.38 ≤ C30 ≤ 0.50	-2.13 ± 0.26	-1.91 ± 0.34	0.6 (0.2)
.24 ≤ C30 ≤ 0.37	-1.87 ± 0.11	-1.81 ± 0.34	0.9 (0.2)
Outer 70%			
Sa-Sab	-2.00 ± 0.21	-2.85 ± 0.37	7.1* (3.8)
Sb-Sbc	-1.84 ± 0.20	-2.06 ± 0.33	1.7 (0.8)
Sc-Scd	-1.55 ± 0.11	-1.78 ± 0.30	1.7* (0.4)
Sc-Scd < 6°	-	-1.83 ± 0.28	1.9
.61 ≤ C30 < 0.73	-3.04 ± 0.31	-4.00 ± 2.2	-
.51 ≤ C30 ≤ 0.60	-1.89 ± 0.18	-2.34 ± 0.36	2.8 (1.8)
.38 ≤ C30 ≤ 0.50	-1.91 ± 0.27	-2.11 ± 0.52	1.6* (0.9)
.24 ≤ C30 ≤ 0.37	-1.55 ± 0.12	-1.83 ± 0.31	1.9 (0.5)

NOTE.—Median and standard deviation (median) of $\log \frac{F_{H\alpha}}{F_{R24}}$, as a function of environment, Hubble type, and central R light concentration for the isolated and Virgo samples. The number of galaxies in each bin is given in parenthesis after the flux. Note the larger spread in the Virgo distribution relative to the isolated distribution. The ratio of isolated to Virgo rates is given in the 4th column, with the standard deviation in the median given in parentheses. A number greater than 1 indicates a reduction for Virgo galaxies, while a number less than 1 indicates an enhancement. An asterisk indicates that the difference in the distributions is significant at better than 99% according to a Mann-Whitney ranked-sum test. Virgo Cluster galaxies have reduced total and outer disk star formation rates in the median for all Hubble type and C30 bins. However, the inner disk rates for Virgo Cluster galaxies are similar to mildly enhanced compared to isolated counterparts.

TABLE 2
 VIRGO STAR FORMATION RATES RELATIVE TO ISOLATED

Type or C30	$\frac{\text{Isolated}}{\text{Virgo}}$ Flux Ratio in each radial bin				
	$r < 0.1r_{24}$	$0.1r_{24} < r < 0.3r_{24}$	$0.3r_{24} < r < 0.5r_{24}$	$0.5r_{24} < r < 0.7r_{24}$	$0.7r_{24} < r < 1.0r_{24}$
Sa-Sab	0.9 (1.4)	0.8 (1.1)	5.0 (3.0)	> 5	> 5
Sb-Sbc	1.6 (1.0)	0.7 (0.2)	1.0 (0.4)	2.0 (1.2)	> 5
Sc-Scd	0.9 (0.2)	0.8 (0.2)	1.2 (0.3)	1.4 (0.3)	2.8 (1.1)
$.51 \leq \text{C30} \leq 0.60$	0.8 (0.6)	1.4 (1.8)	1.9 (0.7)	> 3	> 3
$.38 \leq \text{C30} \leq 0.50$	0.6 (0.4)	0.5 (0.3)	0.9 (0.4)	2 (1)	> 5
$.24 \leq \text{C30} \leq 0.37$	0.8 (0.2)	1.0 (0.4)	1.4 (0.4)	1.4 (.4)	3.2 (1.8)

NOTE.—The ratio of isolated to Virgo $\text{H}\alpha$ median fluxes in the indicated radial bins as a function of Hubble type, and central R light concentration. In parentheses is given the standard deviation in the median. Lower limits were calculated based on the background sky error in each image. Virgo Cluster galaxies have larger median reductions in NMSFR's at progressively larger radii for all Hubble type and C30 bins. In the inner disk, ratios show that Virgo and isolated spirals have similar or enhanced NMSFR's. Enhancements are present at a significant level in the $r < 0.1r_{24}$ and $0.1r_{24} < r < 0.3r_{24}$ bins for spirals with intermediate C30 (0.38 - 0.50).

TABLE 3
 PROPERTIES OF SEVERELY TRUNCATED GALAXIES

(1) Name	(2) RSA/BST	(3) RC3	(4) B_T^O	(5) v_{he} (km/s)	(6) D_{87} ($^\circ$)	(7) HI Def	(8) $\log \frac{F_{H\alpha}}{F_{R24}}$ global	(9) $\log \frac{F_{H\alpha}}{F_{R24}}$ inner $0.3r_{24}$	(10) C30	(11) CH α
Truncated/Normal										
NGC 4351	Sc(s)II.3	SB(rs)ab:pec	13.04	2310	1.7	.58	-1.93	-1.55	0.29	0.77
NGC 4405	Sc/S0	SA(rs)0/a	12.99	1747	4.0	1.1	-2.17	-1.87	0.47	0.91
IC 3392	Sc/Sa	SAb:	13.30	1687	2.7	1.4	-2.30	-1.60	0.37	0.82
NGC 4457	RSb(rs)II	(R)SAB(s)0/a	11.76	882	8.8	.83	-2.29	-2.12	0.66	1.00
NGC 4569	Sab(s)I-II	SABab	10.25	-235	1.7	.99	-2.53	-2.18	0.43	0.92
NGC 4580	Sc/Sa	SABa?	12.49	1034	2.5	1.3	-2.47	-2.11	0.41	0.93
Truncated/Compact										
NGC 4064	SBc(s):	SB(s)a:pec	12.30	913	8.8	.99	-2.25	-1.91	0.43	0.97
NGC 4424	Sa pec	SAB0p	12.32	439	3.1	1.1	-2.16	-1.77	0.42	1.00
NGC 4606	Sa pec	SBa:	12.69	1664	2.5	>1	-2.57	-2.27	0.41	0.80
NGC 4694	Amorph	SB0 pec	12.19	1175	4.5	1.2	-2.77	-2.57	0.62	0.95

NOTE.— (1) Name of galaxy, (2) Hubble types from BST or Sandage & Tammann (1987) or Sandage & Bedke (1994), (3) Hubble type from deVaucouleurs et al. (1991), (4) the total, face-on blue magnitude (B_T^O) from deVaucouleurs et al. (1991), (5) the heliocentric radial velocity, (6) the projected angular distance in degrees of the galaxy from M87, (7) the HI deficiency parameter, which was calculated following the prescription of Giovanelli & Haynes (1983), (8) the normalized star formation rate, $\log \frac{F_{H\alpha}}{F_{R24}}$, over the whole disk, (9) the normalized star formation rate, $\log \frac{F_{H\alpha}}{F_{R24}}$, over the inner $0.3r_{24}$ disk, (10) the central R light concentration, and (11) the central H α concentration.

TABLE 4
 PERCENTAGES OF BARRED SAMPLE GALAXIES

Bar Class	Isolated	Virgo
RSA/BST barred designations		
B	70%	40%
no B	30%	60%
RC3 barred designations		
B	55% (16)	29% (16)
AB	21% (6)	32% (18)
A	24% (7)	39% (22)
B & AB	76%	61%

This figure "f22.jpg" is available in "jpg" format from:

<http://arxiv.org/ps/astro-ph/0209547v1>

This figure "f23.jpg" is available in "jpg" format from:

<http://arxiv.org/ps/astro-ph/0209547v1>

This figure "f24.jpg" is available in "jpg" format from:

<http://arxiv.org/ps/astro-ph/0209547v1>

This figure "f25.jpg" is available in "jpg" format from:

<http://arxiv.org/ps/astro-ph/0209547v1>

This figure "f26.jpg" is available in "jpg" format from:

<http://arxiv.org/ps/astro-ph/0209547v1>

This figure "f27.jpg" is available in "jpg" format from:

<http://arxiv.org/ps/astro-ph/0209547v1>

This figure "f28.jpg" is available in "jpg" format from:

<http://arxiv.org/ps/astro-ph/0209547v1>

This figure "f29.jpg" is available in "jpg" format from:

<http://arxiv.org/ps/astro-ph/0209547v1>

This figure "f30.jpg" is available in "jpg" format from:

<http://arxiv.org/ps/astro-ph/0209547v1>